THE ROLE OF ADENOSINE RECEPTORS AND AMPK IN MOUSE FDB MUSCLES DURING FATIGUE

By

Callum McRae

A thesis submitted to the University of Ottawa
In partial fulfillment of the requirements of the
Degree of **Master of Science**

Department of Cellular and Molecular Medicine
Faculty of Medicine
University of Ottawa

ABSTRACT

Muscle fatigue is an intrinsic myoprotective process that prevents damaging ATP depletion during intense or prolonged exercise by limiting ATP demand when ATP production becomes insufficient. One mechanism of fatigue involves a reduction in membrane excitability with the opening of ATP-sensitive K^+ (K_{ATP}) and ClC-1 Cl^- channels, resulting in submaximal sarcoplasmic reticulum Ca^{2+} release and reduced force generation, but the intracellular signalling pathways for this process is unknown. As a first step toward understanding this process, the objective of this study was to test the hypothesis that adenosine receptors (ARs) and AMPK trigger fatigue when a metabolic stress occurs during muscular activity. Compared to control conditions, a pan-activation of ARs with 10 µM adenosine and NECA initially reduced the fatigue rate during the first 60 s of a 3 min fatigue bout triggered with 1 tetanic contraction every s. An activation of the A1 adenosine receptor (A1R) with 10 and 20 µM ENBA resulted in faster rate of fatigue; an effect blocked by 5 µM DPCPX, an A1R antagonist. At 10 and 20 µM, adenosine, NECA, and ENBA activated AMPK via an increased in T172 phosphorylation. At 10 µM, MK8722, an AMPK agonist, initially caused a reduction in fatigue rate during the first 60 s followed by an increased fatigue rate during the last 2 min of the fatigue bout. Co-activation of ARs and AMPK did not give rise to either an additive or synergistic effect. FDB from AMPK $\alpha1^{-/-}$ and $\alpha2^{-/-}$ mice had faster fatigue rate and greater increased in unstimulated force compared to FDB from AMPK $\alpha1^{+/+}$ and $\alpha2^{+/+}$ mice. It is suggested that ARs and AMPK play a role in the mechanism of fatigue when a metabolic stress develops during muscle activity.

TABLE OF CONTENTS

LIST OF FIGURES

LIST OF ABBREVIATIONS

$[]_e$	Extracellular ion concentration
$[]_i$	Intracellular ion concentration
$[]_{int}$	Interstitial ion concentration
$[K^+]_{crit}$	Critical potassium concentration
5-Br-cAMP	5-bromo-cyclic adenosine monophosphate
5'-NT	5'-nucleotidase
8-PT	8-phenyltheophylline
ACC	Acetyl-CoA carboxylase
Ach	Acetylcholine
ADO	Adenosine
ADP	Adenosine diphosphate
AICAR	5-aminoimidazole-4-carboxamide-1-β-D-ribofuranoside
AMP	Adenosine monophosphate
AMPK	AMP-dependent protein kinase
ANOVA	Analysis of variance
AP	Action potential
AR	Adenosine receptor
A1R	A1 adenosine receptor
A2AR	A2A adenosine receptor
A2BR	A2B adenosine receptor
A3R	A3 adenosine receptor
ATP	Adenosine triphosphate
β2-AR	β2 adrenergic receptor
bp	Base pairs

BSA	Bovine serum albumin
Ca^{2+}	Calcium ion
CAMKKβ	Calcium/calmodulin-dependent protein kinase kinase β
cAMP	Cyclic adenosine monophosphate
CGS	CGS-15943
Cl^-	Chloride ion
ClC1	Voltage-dependent chloride channel 1
Cr	Creatine
DHPR	Dihydropyridine receptor
DMSO	Dimethyl sulfoxide
DPCPX	8-cyclopentyl-1,3-dipropylxanthine
EDL	Extensor Digitorum Longus/i
E_M	Membrane potential
ENBA	5'-chloro-5'-deoxy-(±)-ENBA
FBS	Fetal bovine serum
FDB	Flexor Digitorum Brevis/i
G1P	Glucose-1-phosphate
G6P	Glucose-6-phosphate
G_{Cl}	Chloride conductance
G_K	Potassium conductance
GLUT4	Glucose transporter type 4
G_M	Membrane conductance
GPCR	G-protein coupled receptor
H^+	Hydrogen ion
HEK	Human embryonic kidney
HyperKPP	Hyperkalemic Periodic Paralysis
IMP	Inosine monophosphate

indKO	Induced knockout
INSERM	Institut National de la Santé et de la Recherche Médicale
IP3	Inositol triphosphate
K^+	Potassium ion
K_{ATP}	ATP-sensitive potassium channel
K_D	Dissociation constant
K_i	Inhibition constant
K_{ir}	Inward-rectifier potassium channel
KO	Knockout
LK	Liver kinase
LSD	Least square differences
mdKO	Muscle-specific double knockout
MEM	Minimum essential medium
MgADP	Magnesium-adenosine diphosphate
MHC	Myosin heavy chain
min	Minutes
M.O.M	Mouse-on-mouse
Na^+	Sodium ion
NECA	5'-*N*-ethylcarboxamidoadenosine
PAMPK	Phospho-threonine 172 AMPKα
PanX1	Pannexin
PBS	Phosphate-buffered saline
PBST	Phosphate-buffered saline, 0.1% tween20
PCr	Phosphocreatine
PCR	Polymerase chain reaction
PGC	Peroxisome proliferator-activated receptor gamma coactivator
P_i	Inorganic phosphate

PKA	Protein kinase A
PKC	Protein kinase C
PSB	PSB-0777
PTX	Pertussis toxin
ROS	Reactive oxygen species
RyR1	Ryanodine receptor 1
s	Seconds
S.E.	Standard error
siRNA	Small interfering RNA
SIRT	Sirtuin 3
SR	Sarcoplasmic reticulum
SURA2	Sulfonylurea receptor A2
tAMPK	Total AMPKα
TBS	Tris-buffered saline
TBST	Tris-buffered saline, 0.1% tween20
Thr	Threonine
T-Tubule	Transverse tubule
WT	Wild type
ZM	ZM-241385

ACKNOWLEDGEMENTS

I'd like to thank my supervisor, Dr. Jean-Marc Renaud, for sharing his guidance and support throughout the last several years. Despite the many unexpected roadblocks we encountered over these years, from the initial COVID-19 lockdowns to having to re-evaluate and troubleshoot my initial hypotheses, your mentorship has been invaluable to this entire project and I am deeply grateful and honoured to have been your final student. I hope you continue to enjoy a fulfilling retirement. I would also like to thank my thesis advisory committee, Dr. Mary-Ellen Harper and Dr. Nadine Wiper-Bergeron for your guidance and assistance in making this project a reality. Thank you to my lab mates Tarek, Mohamed, and Hind, you helped make my time in the Renaud Lab so rewarding and I hope your future endeavors go well. I'd also like to thank our undergraduate Honours student Arvin, your enthusiasm and creativity made getting to mentor you a pleasure, and I look forward to seeing your successful career in medicine and research.

Finally, I'd like to thank Dr. Benoit Viollet from the Institut National de la Santé et de la Recherche Médicale (INSERM), Unité (U)1016, Institut Cochin, Paris, France, for providing the AMPK KO mouse model used in this study and the University of Ottawa CBIA core facility for the use of their microscopy equipment and the help with troubleshooting they provided over the course of this study.

CHAPTER 1: INTRODUCTION

Within the human body, skeletal muscle tissue is unique in the extent to which its energy needs change over time, between periods of activity and rest. During periods of sudden contraction, this can manifest in an over 100-fold increase in ATP demand over the course of a few milliseconds[1]. Although muscle tissues have the capacity to rapidly increase ATP production in response to sudden or prolonged activity (e.g. using stored glycogen, creatine phosphate, and myokinases), such demand will inevitably and eventually outstrip supply, resulting in damaging ATP depletion and even muscle fiber death. To prevent this outcome, skeletal muscle tissues must instead reduce this ATP demand during prolonged or intense activity, which is achieved via the innate cellular process of muscle fatigue.

Muscle fatigue is defined as a transient decline of contractile performance and the ability of muscles to do work, which recovers after a period of rest. This process is connected to the energy state of muscle fibers, where it serves to reduce ATP demand by reducing membrane excitability and calcium release in response to motor neuron stimulation, maintaining ATP homeostasis within muscle fibers[2,3] Although this process has been known as long as humans have exercised, and though some effectors which actively reduce membrane excitability and calcium release have been identified, how this is achieved and the intracellular signalling pathways involved are not fully understood. The overall objective of this thesis is to elucidate the potential role of adenosine receptors (ARs) and AMP-activated protein kinase (AMPK) in triggering fatigue.

SKELETAL MUSCLE ACTIVITY AND METABOLISM

Muscle Fiber Excitation to Contraction

The events leading from neural stimulation to muscle excitation, contraction, and relaxation are well described[4,5]. Briefly, voluntary contractions are elicited when motor neurons release acetylcholine (Ach) at the motor end plates. Ach then crosses the synapse cleft and binds to muscle nicotinic acetylcholine receptors, which are ligand-gated cation channels. Ach binding causes these channels to open, allowing Na^+ and K^+ ions to flow through, resulting in membrane depolarization as more Na^+ enters the fibers than K^+ leaves them. Once this depolarization reaches a threshold of -55mV, voltage-gated Na^+ channels open, triggering an action potential (AP) that depolarizes the sarcolemma from a resting membrane potential (resting E_M) of -70 mV to +30mV. APs then propagate along the sarcolemma and into the t-tubules. Continued depolarization eventually results in the inactivation of these voltage-gated Na^+ channels and the opening of voltage-gated K^+ channels, causing K^+ efflux and repolarization, eventually returning the membrane potential back to the resting E_M. Throughout the action potential and at rest, the Na^+/K^+ ATPase continuously actively transports 3 Na^+ ions out of and 2 K^+ ions into the fibers, maintaining the electrochemical gradient of Na^+ and K^+.

Depolarization of t-tubular membranes causes the activation of voltage sensitive $Ca_V1.1$ Ca^{2+} channels also known as dihydropyridine receptors (DHPRs) or L-Type Ca^{2+} channels. This induces a conformational shift, which by physical contact activates nearby Ryanodine receptors (RyR1) in the sarcoplasmic reticulum (SR) membrane through an interfacing protein domain. RyR1 is a Ca^{2+} channel and its activation induces an efflux of Ca^{2+} from the SR into the myoplasm. From here, Ca^{2+} diffuses into the sarcomere where it binds to troponin, which displaces

tropomyosin, liberating the myosin binding sites on associated actin filaments. This displacement allows for myosin ATPase heads to bind to actin filaments, leading to the formation of myosin-actin cross bridges and associated cross bridge cycling, resulting in force generation and/or sarcomere shortening via the activity of the myosin ATPase. Muscle relaxation occurs when repolarization of the t-tubule membrane ends DHPR activation, resulting in the closing of RyR1 as well as Ca^{2+} being actively pumped back into the SR by Ca^{2+} ATPases in the SR membrane. The Ca^{2+} dissociation from troponin allows tropomyosin to re-block myosin binding sites on the actin filaments, preventing further contraction until the fiber is re-excited. During this process of excitation-contraction coupling, the activation of the three mentioned ATPases is responsible for the increase in ATP demand observed with activity: i) myosin ATPases for sarcomere shortening account for ~60% of this increase in ATP demand, ii) Ca^{2+} ATPases which actively transport Ca^{2+} back into the SR account for ~40%, and iii) Na^{+}/K^{+} ATPase which maintains the Na^{+}/K^{+} gradient accounts for ~1%[1,5].

ATP Metabolism during Activity

As the demand for ATP is dynamic within muscle fibers between periods of rest and activity, so too is ATP generation. ATP is generated via both aerobic and anaerobic pathways within muscle fibers, with the latter being faster, utilizing stored and extracellular carbohydrates and dominating during high-intensity activity, while the former utilizes carbohydrates and fats and dominates during extended submaximal exercise[6,7].

At the onset of exercise, the first anaerobic ATP source is creatine phosphate (PCr), which transfers its bound high energy inorganic phosphate (P_i) to ADP via creatine kinase to generate ATP and creatine (Cr):

$$PCr + ADP \leftrightarrow Cr + ATP$$

This is among the quickest methods of ATP generation used in skeletal muscles but is exhausted quickly within ~50 seconds of activity[8]. A second anaerobic pathway is the transfer of P_i between 2 ADP molecules, forming ATP and AMP, followed by AMP deamination to IMP in order to maintain equilibrium in favour of ATP generation during activity:

$$2\ ADP \leftrightarrow ATP + AMP$$

$$AMP\ \rightarrow IMP + NH_4$$

The next source of ATP is from glycolysis, which uses extracellular and glycogen-derived glucose (glucose-1-phosphate, G1P), respectively generating 2 and 3 ATP per glucose molecule:

$$Glucose + 2ADP + 2NAD^+ + 2P_i\ \rightarrow 2Pyruvate + 2ATP + 2NADH + 2H^+$$

$$G1P + 3ADP + 2NAD^+ + 3P_i\ \rightarrow 2Pyruvate + 3ATP + 2NADH + 2H^+$$

In the absence of oxygen or when O_2 levels fall during exercise, this is followed by the reduction of pyruvate to lactate in order to regenerate NAD^+ necessary for the glycolytic process:

$$Pyruvate + NADH + H^+ \rightarrow Lactate + NAD^+$$

The last pathway to generate ATP requires O_2, being an aerobic pathway. This pathway uses either pyruvate from glycolysis or acetyl CoA generated by the β-oxidation of fatty acids. It is a more efficient albeit slow pathway to generate ATP as a maximum of 36 ATP (30 ATP from the TCA cycle, 2 from glycolysis, and 4 from NADH produced during glycolysis) per glucose molecule and 106 ATP per palmitate can be formed:

$$Glucose + 36ADP + 36P_i + 6O_2 \rightarrow 36ATP + 6H_2O + 6CO_2$$

$$Palmitate + 106\ ADP + 106P_i + 24O_2 \rightarrow 106ATP + 24H_2O + 24CO_2$$

Metabolic Differences between Muscle Fibers

Skeletal muscle tissue is heterogenous as there are several fiber types. Muscle fibers are typed based on their Myosin Heavy Chain (MHC) isoforms[6]. This includes Type I, IIA, IIB, and IIX fibers, with a minority of fibers containing more than one MHC. Rodent skeletal muscles express all four fiber types, while humans do not express IIB[8]. Type I fibers are slow twitch oxidative fibers, with the lowest peak force and greatest time to peak force. Type IIA fibers are fast twitch oxidative fibers, generating greater force than type I fibers. Both fiber types are the most resistant to fatigue due to their reliance on more efficient aerobic ATP generation pathways. It should also be noted that even for oxidative fibers, anaerobic substrates (substrates not directly involved with oxidative phosphorylation such as glucose, PCr, and ADP via myokinase) are favoured for ATP generation at the onset of exercise and during maximal exercise, with greatest usage of aerobic substrates occurring during prolonged submaximal exercise around 60% intensity[7,9]. In contrast, Type IIB are fast twitch glycolytic fibers with the highest peak force and quickest time to maximum tetanus but are also the most fatigable because they rely primarily on anaerobic ATP generation during muscle activity. Type IIX fibers are intermediate between type IIA and IIB fibers in terms of peak force, fatigue resistance, and aerobic and anaerobic pathways. Overall, fatigue resistance between fiber types is on the order of Type I ~ IIA > IIX > IIB[10].

FATIGUE

The Mechanism of Muscle Fatigue

As mentioned earlier, muscle fatigue is defined as a transient decline of contractile force and/or work, which recovers after a period of rest. This process is well documented as peripheral to central homeostasis, and is intrinsic to muscle fibers[5,11–13]. Though earlier work studying fatigue focused on the accumulation of metabolites such as inorganic phosphate (P_i) and lactic acid, it was eventually realized that they have little effect on force generation. In fact, the force loss during fatigue is associated with a decrease in intracellular Ca^{2+} $[Ca^{2+}]_i$ during contraction resulting in submaximal activation of the contractile components. When caffeine was added at the end of the fatigue bout to cause supramaximal Ca^{2+} release by directly activating RyR1, the contractile components of fully fatigued fibers generate as much force as before the fatigue bout from electrical stimulations involving AP generation[3,14].

The next question is what causes this reduction in $[Ca^{2+}]_i$? There are four potential mechanisms to explain it: 1) a depletion of SR Ca^{2+} stores, which is unlikely considering that supramaximal $[Ca^{2+}]_i$ is achieved with a caffeine exposure [3,14]; 2) buffering of SR Ca^{2+} by P_i released by the hydrolysis of PCr, which enters the SR via anion channels that open during fatigue, reducing the releasable pool of Ca^{2+} [15–17]; 3) an inhibition of the DHPR-RyR1 complex when [ATP] decreases, as Ca^{2+} release is reduced when ATP dissociates from Cav1.1 and RyR1, a process that remains to be elucidated[18,19]; 4) a reduction in membrane excitability, i.e., the capacity to generate normal action potential, a process that involves the activation of ClC-1 Cl^- and K_{ATP} K^+ channels[20]. The latter has been extensively studied over the past few years and will be discussed in greater detail.

During muscle activity, membrane excitability and conductance (G_M) is regulated in a biphasic pattern, as shown by Pedersen, de Paoli, et al. (2009)[21]. Together, K^+ and Cl^- make up all passive membrane conductance of muscle fibers (G_M) at rest, with chloride conductance (G_{Cl}) through the ClC-1 channel contributing as much as 80-90%, and the remaining being the K^+ conductance (G_K)[22]. At the onset of muscle contractions, G_{Cl} is reduced by more than 50% as ClC-1 channels close; i.e., less Cl^- can diffuse through the sarcolemma. The reduction in ClC-1 activity occurs due to phosphorylation by Protein Kinase C (PKC), allowing AP amplitude to remain constant[21,23,24]; i.e., preventing a decrease in membrane excitability. This period of reduced G_{Cl} via ClC-1 activation is defined as phase 1. In EDL fast-twitch muscles, higher frequency stimulation brings an end to this phase, being slightly longer when muscles are stimulated at lower frequencies. Notably, phase 1 always ends after approximately 2500-3000 APs regardless of the stimulation frequency[21].

At the end of phase 1, G_{Cl} increases 4-fold due to the activation of ClC-1 channels. As more Cl^- can enter in the fiber, it counteracts Na^+-induced membrane depolarization, resulting in AP amplitude dropping from ~100mV to ~30mV; i.e., the increase in G_{Cl} reduces membrane excitability. This period is defined as Phase 2. Phase 2 is also associated with an increase in G_K via the activation of K_{ATP} channels, which occurs during metabolic stress, also contributing to a reduction in AP amplitude as an increase in K^+ efflux also counteracts the Na^+-induced depolarization[21]. The shift to phase 2 was found to be accelerated in conditions that enhance metabolic stress during activity. For example, Phase 2 starts after about 1500 APs when experiments were conducted in glucose-free solution, or glycogen breakdown was impaired via glycogen phosphorylase knockout[20,24]. Phase 2 was not observed when similar experiments were

conducted using fibers of the fatigue resistant slow-twitch soleus, with G_M remaining stable (i.e., Phase 1) over the course of 15000 APs[24]. Taken together, the authors suggested that Phase 2 occurs as a metabolic stress takes place, and that the increase in G_{Cl} and G_K through the activation of ClC-1 and K_{ATP} channels is a mechanism for the reduction of membrane excitability, resulting in lowered depolarization during the AP peak[24]. Ca^{2+} release rapidly drops as the AP peak becomes less than 0 mV, resulting in the reduction in contraction associated with fatigue[25]. The structure and regulation of ClC-1 and K_{ATP} channels as well as the physiological significance of changes in G_{Cl} and G_K will now be discussed.

CLC-1 Cl^- CHANNELS

Structure, regulation, and function

ClC-1 is a double-barreled Cl^- channel that accounts for 80-90% of membrane conductance at rest, made up of a homodimer with 2 Cl^- pores and 3 conductance states: zero conductance (i.e. closed), intermediate conductance (i.e., one channel open), and maximal conductance (i.e. both channels open)[26]. The channel is regulated by two protopore gates, one for each pore responsible for the intermediate and maximal states, and one common gate responsible for the fully closed state. At rest, one pore of the channel remains open, with the second opening upon membrane potential depolarization, increasing G_{Cl}[27,28].

Cl^- and ClC-1 play a key role in the maintenance of resting E_M. Cl^- equilibrium potential and E_M are the same, resulting in no net Cl^- flux through ClC-1 at rest[29]. Therefore, any disturbance to resting E_M via the action of Na^+ or K^+ during APs will result in a Cl^- current through ClC-1 channels that drives E_M back towards resting potential, stabilizing it during periods of

activity. As a result, there is a net Cl^- influx during both the depolarization and repolarization phases of an action potential, which can significantly reduce AP amplitude when ClC-1 channels are activated such as during Phase 2, linking G_{Cl} to overall membrane excitability during muscle activity.

Important in the context of fatigue, ATP binds to a regulatory cystathionine β-synthase domains in the C-terminal region of ClC-1, modulating the activity of the common gate in a pH-dependent manner[30,31]. ATP binding to ClC-1 reduces the open probability of ClC-1 channels, i.e., reductions in $[ATP]_i$ shift channel opening towards more negative E_M, and thus increases ClC-1 activity at resting E_M [32]. The binding K_i of ATP is about 1mM, an ATP concentration which has physiologically been found after 25s of intense exercise in fully fatigued fibers[33]. As such, ATP likely plays a role in ClC-1 regulation during muscle activity and especially fatigue where a decrease in ATP is likely to increase ClC-1 channel activity.

Modulation of the K^+ Effects on Contractile Force by Cl^-

K^+ has long been considered a major factor causing the decrease in force during fatigue. To understand how Cl^- modifies this effect, the mechanism of the K^+-induced force depression must first be described. Over the course of multiple APs, the repeated opening of voltage-gated Na^+ channels during depolarization and K^+ channels during repolarization causes increases in intracellular Na^+ ($[Na^+]_i$) and interstitial $[K^+]$ ($[K^+]_{int}$), with the latter increasing from 4-5mM at rest to as high as 10-13mM during intense as well as moderate exercise[34]. In vitro studies have shown that increases in $[K^+]_{int}$ depolarizes resting E_M. For example, in mouse wild type EDL muscles, an increase in $[K^+]_{int}$ from 4.7 to 12mM K^+ causes a resting E_M depolarization from -75mV to -65mV,

with another 10mV depolarization occurring between 12-14mM K^+ [35]. As a consequence of the depolarization, Na^+ channels become inactivated affecting membrane excitability as AP amplitude decreases and may render fibers completely unexcitable, both of which resulting in lower Ca^{2+} release and force generation[25,35,36].

The relationship between $[K^+]_{int}$ and force of mouse EDL for example follows an inverse sigmoidal pattern, with a 10% decrease in force occurring when $[K^+]_{int}$ increases from 4.7mM to 12mM, followed by 90% of force loss occurring over a 2-3mM range, as $[K^+]_{int}$ increases from 12-14mM becoming zero at 15 mM [35,36]. The $[K^+]_{int}$ where this sudden 90% drop in force begins is known as the critical $[K^+]$ ($[K^+]_{crit}$), being 12mM for mouse EDL and 9 mM for mouse soleus under physiological resting conditions at 37°C. Thus, the increase in $[K^+]_{int}$ during muscle contractions mentioned above is very close to the critical $[K^+]_{int}$, which may negatively affect muscle performance. However, $[K^+]_{crit}$ is affected by several factors, one of which is G_{Cl}. A 60% reduction in G_{Cl} in resting muscle increases $[K^+]_{crit}$ by 2-3mM. Thus, the decrease in G_{Cl} during Phase 1 prevents the K^+-induced action potential and force depression over multiple APs[37,38]. In fact, action potential amplitude remains constant during the entirety of Phase 1. It has been suggested that the reduction of G_{Cl} via ClC-1 inhibition at the onset of activity is crucial to allow normal contractile performance despite an increase in $[K^+]_e$. As mentioned above, Phase 2 starts when a metabolic stress occurs, which triggers fatigue to prevent deleterious ATP depletion. So far, there is no compound to activate ClC-1 channels. However, if a decrease in G_{Cl} increases $[K^+]_{crit}$, then one can assume that a 4-fold increase in G_{Cl} above resting levels reduces $[K^+]_{crit}$ to a point that K^+-force induced depression takes over, contributing to the failure of E-C coupling by rendering fibers less excitable or completely unexcitable. It has been suggested that the activation of ClC-

1 channels during Phase 2 is thus important in the fatigue process to lower membrane excitability and preserve ATP. However, the precise mechanism or intracellular signalling pathway behind the channel activation is still unclear beyond a direct ATP dissociation that increases channel activity.

K_{ATP} CHANNELS

In skeletal muscle, K_{ATP} is a hetero-octameric K^+ channel made up of 4 inwardly rectifying $K_{ir}6.2$ subunits providing 4 pores surrounded by 4 regulatory SUR2A subunits that contribute to G_K at rest with another K^+ channel ($K_{ir}2.1$)[39]. Each $K_{ir}6.2$ subunit contains an ATP binding site, which functions to close the channel on binding, as opposed to ClC-1 channels where ATP shifts the current-E_M relationship towards less negative values decreasing channel activity. The K_{ATP} channel's main function is to link cellular energy status to membrane excitability. In addition to being antagonized by ATP, there is evidence that K_{ATP} channel activity is stimulated by increases in ADP, MgADP, AMP, and reductions in pH[40]. As such, K_{ATP} is an energy sensor that reacts to the ratio of ADP/AMP to ATP. The importance of this link is further supported by the difference in K_{ATP} channel content between fiber types, as the fatigability and K_{ATP} channel contents are in the order of IIB>IIX>IIA>I[41]. Additionally, glycolytic fast-twitch EDL and FDB muscles were found to have a greater K_{ATP} content in the t-tubular membrane (where K_{ATP} has a greater effect on membrane excitability) vs. outer cell membrane compared to more oxidative soleus muscles[41].

When K_{ATP} opens during Phase 2 of activity, the resulting increase in G_K causes K^+ efflux during depolarization that counters the depolarizing Na^+ current, reducing AP amplitude in a similar manner to Cl^- influx through ClC-1 channels[22,42]. This in turn results in lower Ca^{2+} release

that reduces force and therefore ATP demand from myosin ATPase and Ca^{2+} ATPase[43]. This has been demonstrated pharmacologically using the K_{ATP} channel activator pinacidil, which increases the rate of fatigue in exposed muscles while also reducing the development of unstimulated force, defined as the force remaining between two contractions[44]. Unstimulated force increases when muscles fail to fully relax between contractions during fatigue and can be a sign of contractile dysfunction[44]. In this function, K_{ATP} channels are important in preventing damaging ATP depletion during exercise and abolishing its activity results in deleterious effects during fatigue. On the one hand, if activating K_{ATP} channels contributes to the decrease in force, then a lack of K_{ATP} channels should result in a slower fatigue rate. On the other hand, if K_{ATP} channels are crucial at preventing damaging ATP depletion, then muscle dysfunction may occur, resulting in a faster fatigue rate.

To test this, studies have tested the effects of a lack of K_{ATP} channel activity using two approaches: 1) pharmacologically by exposing FDB muscles to glibenclamide, a K_{ATP} blocker, and 2) genetically via $K_{ir}6.2$ knockout ($K_{ir}6.2^{-/-}$). Both of these methods gave rise to quantitatively similar results when comparing differences between control and K_{ATP} channel deficient muscles. Furthermore, glibenclamide exposure has no effect on $K_{ir}6.2^{-/-}$ muscles[45–47]. This suggests that the effects of glibenclamide exposure or the knockout are due to a lack of K_{ATP} channel activity rather than non-specific glibenclamide or knockout-related effects. Using both approaches, studies have demonstrated the occurrence of severe excitability, contractility, and metabolic dysfunctions in K_{ATP} channel deficient skeletal muscles during fatigue as follows.

In vitro, K_{ATP} deficiency causes severe membrane depolarization. Resting E_M typically depolarizes by <15mV during fatigue, which becomes 50mV in K_{ATP}-deficient muscles[45,48]. This

large depolarization is due to a lack of continuous K^+ efflux between contractions[45,46], and is enough to activate $Ca_V1.1$ channels resulting in large increases in unstimulated $[Ca^{2+}]_i$ and consequently in unstimulated force. In mouse FDB unattached single muscle fibers, unstimulated $[Ca^{2+}]_i$ increased to a greater extent in K_{ATP} channel-deficient fibers. The increase in unstimulated $[Ca^{2+}]_i$ was such that 55-58% of the tested K_{ATP}-deficient fibers supercontracted as opposed to no supercontraction in normal fibers[47]. In K_{ATP}-deficient FDB muscle bundles, the large increase in unstimulated $[Ca^{2+}]_i$ resulted in subsequent increase in unstimulated force up to 20% of the pre-fatigue tetanic force in the absence of the channel compared to only 1% in control FDB[46]. Thus, in the absence of K_{ATP} channel activity the ATP demand from myosin and Ca^{2+} ATPases increases drastically. A further contractile dysfunction in the absence of K_{ATP} activity is an impaired force generation because the large resting E_M depolarization also results in greater than normal Na^+ channel inactivation, resulting in a greater decrease in force compared to control muscles[43,47]. Finally, the capacity of force recovery following fatigue was impaired in K_{ATP} channel deficient muscles. Following fatigue, control FDB bundles recover 95% of the pre-fatigue force within 15 min of recovery while K_{ATP} channel deficient FDB only recover 69% of force after 30 min[45].

In vivo, Thabet et al., (2005)[49] found that $K_{ir}6.2^{-/-}$ mice fatigued 41% faster during treadmill running than wild type mice and had 65% less improvement in running distance with daily treadmill running. Furthermore, they showed severe fiber damage in hindlimb muscles with evidence of regeneration as observed by the presence of central nuclei. Central nuclei are generated when damaged fibers are repaired via the recruitment of satellite stem cells and remain centrally located in repaired muscle fibers rather than being just below the outer cell membrane. Five weeks of daily treadmill running did not result in internal nuclei in wild type

muscles, while 25% of Kir6.2$^{-/-}$ EDL fibers and 12% of Kir6.2$^{-/-}$ plantaris and tibialis fibers had internally located nuclei. K_{ATP}-deficient muscles also present less recovery of force after fatigue, likely due to fiber damage as well as metabolic dysfunction. Extensive fiber damage was also observed in Kir6.2$^{-/-}$ diaphragms, but with no sign of fiber regeneration. Thus, in the absence of K_{ATP} channels severe fiber damage occurs, which is repaired in hindlimb muscles but not in diaphragm.

Regarding metabolic dysfunction, Scott et al., (2016)[50] found that ATP levels decreased to greater extent in Kir6.2$^{-/-}$ FDB than in wild type. For both muscles, ATP level drops to 65% of initial levels within 60 s, then returns to 88% of initial ATP levels in wild type FDB over the next 60 s, being ~12.5µmol/g dry wt at 180 s[50]. In Kir6.2$^{-/-}$ FDB, ATP content continued to decrease reaching 38% of initial ATP content by 180 s, around 7µmol/g dry wt. Finally, there was a net loss of adenylates in Kir6.2$^{-/-}$ muscles, with total adenylates dropping from ~22µmol/g dry wt at 0 s to ~14µmol/g dry wt at 180 s while total adenylates increased in wild type muscles from ~18µmol/g dry wt to ~22µmol/g dry wt over the same time period.

The lack of ATP recovery during the 2nd min of the fatigue bout in Kir6.2$^{-/-}$ FDB is not surprising considering the large ATP demand by SR Ca^{2+} ATPase due to the large increase in unstimulated $[Ca^{2+}]_i$ as well as by myosin ATPase due to the large increase in unstimulated force. However, the lack of ATP recovery was also related to at least two metabolic dysfunctions. First, lower ATP should result in greater glycogen mobilization, but the reverse was observed. Kir6.2$^{-/-}$ FDB muscles had a lower glycogen mobilization than wild type during the last 120 s of a 3 min fatigue bout: 29µmol/g dry weight vs 39µmol/g dry weight, respectively[50]. Second, while in normal FDB muscles there was no increase in CO_2 production from glucose during the 3 min

fatigue bout, there was an increased CO_2 production during the first 60 s of activity in $K_{ir}6.2^{-/-}$ FDB. However, this CO_2 production did not increase further during the remaining 120s despite further decrease in ATP levels. This reduced CO_2 production is potentially due to the excessive increase in unstimulated $[Ca^{2+}]_{i,}$ which is known to suppress the activity of isolated mitochondria[51]. Thus, despite greater ATP demand in the absence of K_{ATP} channel activity, muscles are unable to generate sufficient ATP due to impaired glycogen mobilization and oxidative phosphorylation.

Similar to the ClC-1 channel, the mechanism by which K_{ATP} is activated during fatigue is not fully understood. Although ATP binding does reduce the activity of K_{ATP} channels, the K_i for ATP binding to $K_{ir}6.2$ is ~194 μM[52], much greater than physiological [ATP] which is greater than 1 mM even in fatigued muscles[53]. Although other metabolites also modulate channel activity, there is debate as to how K_{ATP} channels are activated during periods of metabolic stress such as fatigue. The question is whether there are intracellular pathways that activate both ClC-1 and K_{ATP} channels during Phase 2. There are actually two possibilities as both adenosine receptors[54,55] and AMPK[56,57] have been shown to activate K_{ATP} channels in cardiac muscle during metabolic stress, while in skeletal muscle one study reported an activation by the A1 adenosine receptor (A1R)[58]. These constituents will now be discussed.

PURINERGIC SIGNALLING DURING SKELETAL MUSCLE FATIGUE

It is well established that ATP is released by skeletal muscles during activity and can be converted to adenosine extracellularly[59,60]. Purinergic receptors are ATP and adenosine receptors, classified as P2 and P1 receptors respectively[61].

ATP Signalling

During muscle activity, ATP is transported out of fibers into the interstitial and t-tubular space via Pannexin-1 Hemichannels (PanX1), which are activated by increases in $[Ca^{2+}]_i$, membrane depolarization, and phosphorylation via the activation of extracellular P2Y receptors, and inhibited by acidification[59,62]. PanX1 is permeable to Ca^{2+} as well and is thought to play a role in the potentiation of twitch contraction at the onset of activity, releasing ATP and Ca^{2+} when energy levels are high then closing at the onset of fatigue[59,60]. Once in the extracellular space, ATP participates in autocrine signalling via P2X and P2Y receptors. P2X receptors are a family of ATP-gated Ca^{2+}, K^+, and Na^+ channels and P2Y receptors are ATP-activated G protein coupled receptors (GPCRs). In skeletal muscle, ATP binding to P2X4 aids with contraction via Ca^{2+} influx to activate sarcomeric motor proteins in slow-twitch muscles during sub-maximal stimulation[63]. Secreted ATP also binds to P2Y1: a G_0/G_{11}-coupled G-Protein Coupled Receptor (GPCR) that activates PKC contributing to PanX1 activation and continued ATP secretion[59,64]. This PKC activation may also be involved with the PKC-mediated inhibition of ClC-1 during Phase 1 of activity, contributing to the prevention of K^+-induced force depression[23].

Adenosine Signalling in Cardiac and Skeletal Muscles:

Paracrine and autocrine purinergic signalling in the interstitial space is further regulated by the action of membrane-bound ecto-NTPases that act on a variety of nucleotide phosphates, breaking down ATP to ADP, then AMP. Finally, ecto-5'-nucleotidase (ecto-5'-NT) metabolizes AMP into adenosine and inorganic phosphate[65]. As PanX1 activity begins to decrease at the onset of fatigue, the ratio of ATP:ADP then ADP:AMP begins to drop, leading to an accumulation of

AMP which is metabolized into adenosine by ecto-5'-NT[66]. This breakdown of extracellular ATP to AMP and eventually adenosine leads to an attenuation of pro-contractile ATP signalling and a shift towards adenosine-based signalling around the same time muscle fibers start to enter metabolic stress.

Over the course of muscle activity, adenosine accumulates in the interstitial space via export from membrane nucleoside transporters and the breakdown of extracellular AMP, which represent approximately 30% and 70% of this accumulation respectively[67]. Hellsten et al., (1998)[68] found that interstitial adenosine concentration in human *vastis lateralis* muscles increased from 220 ± 100 nmol/L at rest to 1140 ± 540 nmol/L after light (10 W) exercise, increasing to approximately 2000 nmol/L after moderate (50 W) exercise. This accumulation of adenosine is involved with paracrine signalling to induce vasodilation of nearby capillaries and increase blood flow to exercising muscles[69] as well as autocrine signalling via binding to skeletal muscle adenosine receptors (ARs), also known as P1 purinergic receptors.

ARs are GPCRs, with 4 isotypes found in skeletal muscle: A1R, A2AR, A2BR, and A3R[58,70]. Out of these, AR1 and A3R are G_i-linked while A2AR and A2BR are G_S-linked, the former inhibiting adenylate cyclase and downstream Protein Kinase A (PKA) and the latter activating it[71]. Though muscular adenosine is known to participate in paracrine signalling with nearby vasculature as previously described, its role in autocrine/paracrine signalling within muscle tissue itself remains unclear. However, the effect of such signalling pathways has been extensively studied in both cardiac muscle and neurons.

Within cardiac muscle, adenosine has a well-established acute cardioprotective effect against ischemia via the activation of all 4 receptor subtypes, playing an important role in ischemic preconditioning[54,55], defined as the protection conferred to ischemic myocardium by brief periods of sublethal ischemia separated by short bursts of reperfusion delivered before the ischemic insult[72]. This preconditioning effect has been shown to be dependent on K_{ATP} channel activation directly via interaction with G_i, leading to a similar loss of membrane excitability that preserves energy status as described above in skeletal muscle[73] . A1R has also been found to activate K_{ATP} in neurons via G_i-mediated activation of the PLC/IP3/PKC pathway leading to K_{ATP} phosphorylation[74]. Although such a pathway directly linking AR activation to K_{ATP} channel opening has not yet been found in active skeletal muscle, A1R has been found to activate K_{ATP} under patch clamp conditions, resulting in increased G_M[75]. A1R, A2AR, and A3R have also been found to have a cytoprotective effect in skeletal muscles in the context of ischemia and reperfusion injury, pointing towards a similar mechanism involving K_{ATP} channels as in cardiac tissues[58], and non-specific adenosine receptor blockade has been shown to increase resting [Ca^{2+}] similarly to K_{ATP} channel blockers[76]. A1R activation has also been shown to increase insulin sensitivity, playing a role in increasing glucose uptake in response to activity[77,78].

The potential role of A2A/BR in the activation of K_{ATP} and fatigue in cardiac and skeletal muscles is somewhat confounded by other G_S-mediated pathways that are involved with the potentiation of contraction. Paradoxically, activation of the β2-Adrenergic Receptor (β2-AR), another G_S -linked GPCR, by epinephrine causes a PKA-mediated activation of the RyR-DHPR complex that improves Ca^{2+} release during sub-maximal stimulation, increasing force[79]. However, recent research into GPCR nanodomains helps to resolve this contradiction: although

both β2-AR and A2A/BR activate adenylate cyclase and downstream PKA, the targets affected by PKA activation may differ based on compartmentalization of these PKAs and targets into separate nanodomains[80,81]. For example, in cardiac muscle both catecholamines and prostaglandins activate G_S-coupled receptors and PKA, but the former increases membrane excitability and sensitivity to ischemia while the latter reduces excitability and has a cardioprotective effect, similar to A2AR and A2BR adenosine receptor activation[82].

Catecholamine/cAMP/A1 & A3 Receptor Crosstalk

Although A1/A3R activation has not yet been found to play a role in the reduction of force during fatigue, Duarte et al. (2012) found that it reduces twitch force in mouse diaphragm muscles and attenuates β2-AR mediated twitch potentiation[83]. They showed that perfusion with the β2-AR agonist clenbuterol causes a 20% increase in twitch force followed by a rapid return to pre-exposure force in approximately 30 min. This return to baseline was prevented when diaphragm was co-exposed with clenbutarol and either PTX, a G_i-inhibiting toxin, CGS, a non-specific AR antagonist, DPCPX, an A1R-specific antagonist, or AMPCP, an ecto-5'-NT antagonist. Exposure to adenosine or cAMP (which can be degraded to AMP and adenosine), but not the non-metabolizable 5-Br-cAMP, caused a reduction in twitch force that was attenuated by the previously mentioned antagonists. Given these results, A1 activation by adenosine reduces twitch force as well as counteracting the catecholamine-induced twitch potentiation.

Taking all the studies described above, A1 adenosine receptors may well be one intracellular signalling pathway involved in the triggering of fatigue during metabolic stress, leading to the activation of K_{ATP} and ClC-1 channels during Phase 2.

AMPK SIGNALLING DURING FATIGUE

AMPK Structure and Function in Skeletal Muscles

AMP-dependent Protein Kinase (AMPK) is a heterotrimer consisting of a catalytic α subunit, and one regulatory β and γ subunit. These subunits include multiple isoforms including: α1, α2, β1, β2, γ1, γ2, and γ3, resulting in 12 possible heterotrimer combinations[84]. In human skeletal muscles, 3 overall AMPK isoforms have been identified: α2β2γ1 which constitutes 65% of the total pool of AMPK, α2β2γ3 which constitutes 20%, and α1β2γ1 which constitutes 15%[85,86]. Two additional isoforms have been identified in mouse skeletal muscles: α1β2γ1, and α1β1γ1[84]. Differences in isoform distribution have been found to correlate with fiber type, with the γ3-containing isoform expressed primarily in glycolytic Type II fibers, likely related to AMPK's role in glycogen metabolism, where it inhibits glycogen synthase via phosphorylation to increase ATP availability[87].

The α subunit contains a kinase domain, with activity dependent on phosphorylation of a Thr-172 residue by upstream activators, which is modulated allosterically by the γ subunit[84]. The γ subunit contains two adenosine nucleotide binding domains including ATP, ADP, and AMP, allowing it to function as a cellular energy sensor. The β subunit acts as a scaffold that holds the other 2 subunits together and can also bind to glycogen, which renders the complex inactive. As a result, the cellular pool of active AMPK increases as stored glycogen is metabolized. Additionally, autophosphorylation occurs at residue Thr-148 when glycogen levels are low, preventing glycogen binding and maintaining activity during exercise recovery. Activation of the AMPK complex occurs in 2 steps: allosteric activation via the binding of AMP/ADP to the γ subunit, which is inhibited by ATP binding, followed by the phosphorylation of Thr-172 of the α

subunit by upstream kinases, including LKB1 which has been implicated in activation during moderate- to high-intensity activity (i.e. during fatigue) and contraction-stimulated glucose uptake[88], and CaMKKβ for long term low-intensity activity, which plays a greater role in fatty acid oxidation[84]. AMPK is also activated by the production of Reactive Oxygen Species (ROS), which occurs in the mitochondria during periods of metabolic stress[89,90]. Because this activation is dependent on 1) AMPK to be released from storage with glycogen, 2) a low ratio of cellular [ATP]:[ADP]/[AMP], and 3) ROS production, AMPK forms a key sensor of cellular energy within skeletal muscles, activating during periods of metabolic stress.

AMPK acts on a wide variety of substrates that overall induces a shift in metabolism from anabolic to catabolic pathways to reduce ATP demand and increase ATP production. Experiments activating AMPK in skeletal muscle via AMP-analogue AICAR show greater glucose uptake via increased GLUT 4 translocation and fatty acid oxidation via Acetyl-CoA Carboxylase (ACC) activation, increasing the amount of substrate available for ATP production[91]. AMPK also inhibits glycogen synthesis via phosphorylation of glycogen synthase, priming muscle tissues for greater glycogen breakdown, though it should be noted that exposure to AICAR was also found to increase glycogen synthesis, likely as consequence of increased glucose uptake leading to higher Glucose-6-phosphate levels, which allosterically activates glycogen synthase[92]. Long-term activation of AMPK was found to increase mitochondrial biogenesis via the activation of the transcription factor PGC1a and downstream mitochondria deacetylase SIRT3, leading to a switch in MHC expression from more glycolytic types to oxidative, resulting in more efficient ATP generation and playing a role in long-term adaption to exercise[93].

Links between AMPK and Fatigue Activation

There is some evidence that AMPK plays a role in the activation of K_{ATP} in cardiomyocytes where it may have a similar role as adenosine in cardioprotection. AMPKα directly associates with cardiac K_{ATP} channels, phosphorylating a site on the SUR2A domain that induces K_{ATP} opening in an [AMP]-dependent manner[56]. Cardiac AMPK has also been found to be activated during ischemia due to metabolic stress, where it plays a key role in ischemic preconditioning, reducing infarct size as a result of the recruitment of K_{ATP} channels to the plasma membrane and subsequent K_{ATP} activation in a manner similar to A1 and A3 adenosine receptors[57]. This may suggest a potential synergistic effect between AMPK and adenosine receptors for the activation of K_{ATP}, but this link has yet to be investigated in skeletal muscle.

Although some muscle AMPK KO studies may point towards AMPK being implicated in skeletal muscle fatigue, tested knockout models also exhibit lower mitochondrial content and dysfunctional glycogen homeostasis, confounding analysis of AMPK's fatigue-related effects with respect to membrane excitability. Knockout of a single subunit isoform, i.e., $\alpha1^{-/-}$ or $\alpha2^{-/-}$, induces a greater expression of the remaining subunit, resulting in redundancy that prevents a single KO from affecting the contraction-activated effects of AMPK including GLUT4 translocation and changes in gene expression. However, AMPK$\alpha2^{-/-}$ mice manifested lower voluntary activity, as well as lower forced exercise capacity in a study by Mu et al. (2001)[94], likely caused by impaired cardiac metabolism and muscle mitochondrial content. Of greater relevance to this study, a muscle-specific AMPK α1/α2 double knockout (mdKO) model did produce similar results, causing significantly reduced exercise performance, force production, and fatigue resistance but without any reduction in mitochondrial number compared to wild type mice[95], suggesting that AMPK is

involved in more than just maintaining ATP production during activity. Also similar to K_{ATP} deficiency models, mdKO mice also had an increased proportion of myofibers with centralized nuclei after exercise, a marker of muscle tissue damage followed by repair via satellite cell recruitment. Although mdKO muscles do show exercise-related dysfunction and damage that is likely caused by ATP depletion, it is also possible that this has more to do with dysfunction in ATP generation, which triggers fatigue sooner.

Interaction between Adenosine and AMPK Signalling

Aside from adenosine receptors and AMPK playing a similar cardioprotective role in cardiac muscle during ischemia, there is no direct evidence for a synergistic crosstalk between these pathways. However, an inverse relationship has been uncovered between 5'-NT expression and AMPK activity that may constitute an indirect link. Kulkarni et al. (2011)[96] found that siRNA knockdown against soluble 5'-NT in mouse myotubes resulted in greater AMPK activation and downstream ACC phosphorylation. Since 5'-NT catalyzes the breakdown of AMP into adenosine, this relationship is likely due to an increase in cellular [AMP], allowing for greater AMPKα phosphorylation and subsequent complex activation. Similarly, Plaideau et al. (2012)[97] found that AMPK activity was reduced in HEK293T cells upon 5'-NT overexpression. However, this relationship may not be relevant to fatigue signalling as the pool of AMP that activates AMPK, and AMP that is broken down into adenosine to activate adenosine receptors are in two separate cellular compartments (cytosolic vs interstitial). As mentioned earlier, the link between AMPK and adenosine signalling is more concrete in cardiac muscles as both are implicated in ischemic preconditioning. In addition to this, the activation of AMPK via AICAR has been found to block

the reuptake of adenosine from cardiomyocytes during ischemia, which may lead to greater adenosine receptor activation and a synergistic effect between cardiac AMPK and A1R/A3R[98]. Given that AMPK is also important for the sensitization of skeletal and cardiac muscle to insulin however, this synergy may play a greater role in A1R's involvement in glucose uptake.

Given the state of the current research into muscle fatigue and ischemic cardioprotection, adenosine receptors and AMPK may be involved in the activation of fatigue upon skeletal muscles entering into metabolic stress during intense or extended activity, leading to a loss of membrane excitability that prevents damaging ATP depletion. Additionally, crosstalk may exist between adenosine and AMPK signalling during fatigue, with activation or inhibition of both constituents potentially leading to synergistic effects on the triggering of fatigue.

OBJECTIVES AND HYPOTHESIS

Based on the studies described above, I propose a mechanism wherein the activation of ARs and AMPK during metabolic stress increases the activity of K_{ATP} and ClC-1 channels, reducing membrane excitability and thereby triggering fatigue (Fig. 1.1). This proposal raises 2 questions: 1) Are ARs and AMPK involved in triggering skeletal muscle fatigue and 2) Does this occur via K_{ATP} and ClC-1? The overall objective of this thesis is to answer the first question and elucidate the potential role of ARs and AMPK in triggering fatigue. The overall hypothesis is that "ARs and AMPK trigger the fatigue process during muscular activity when a metabolic stress occurs". To test this hypothesis the following aims were pursued:

FIGURE 1.1

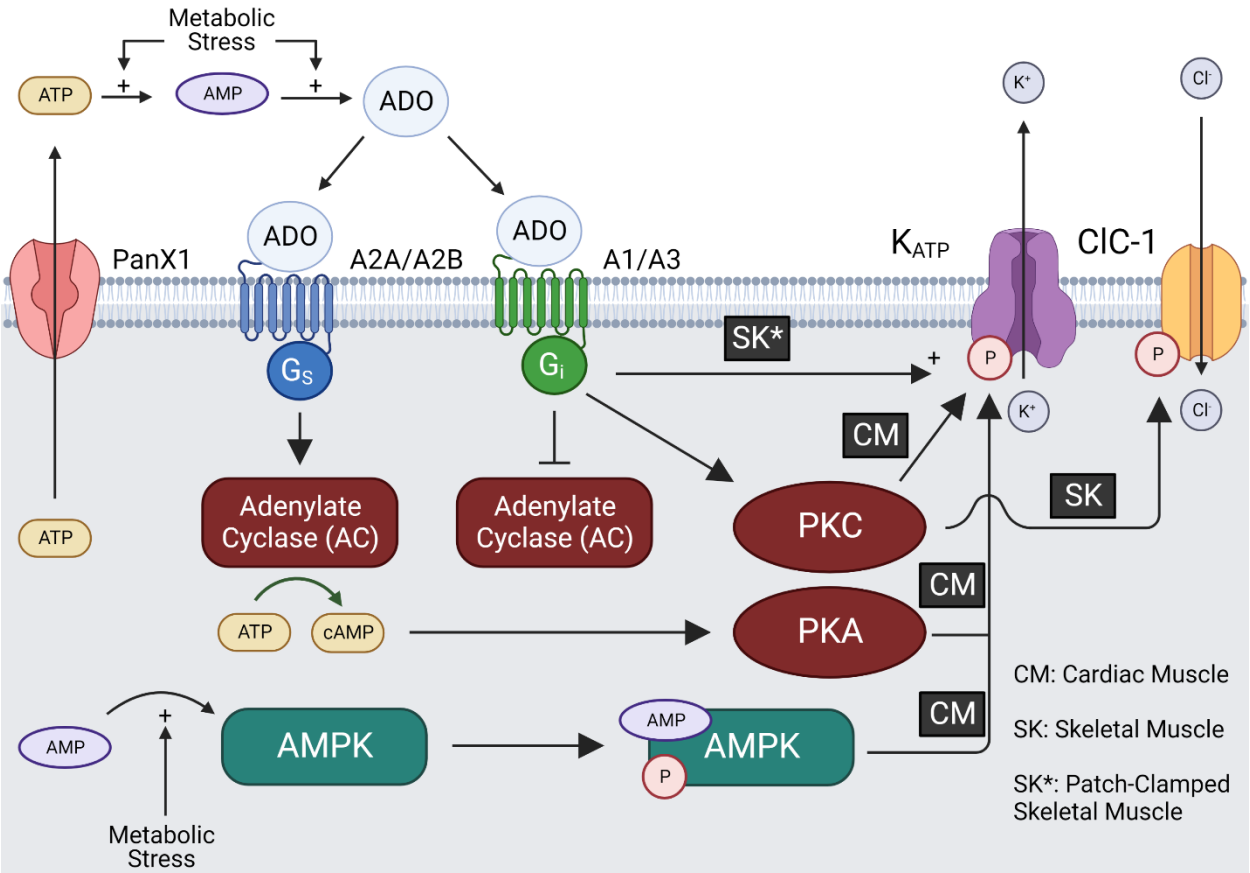

Figure 1.1: Proposed mechanism for the triggering of fatigue by ARs and AMPK. During metabolic stress, the accumulation of adenosine (ADO) causes the activation of G_s-linked A2A/BR and G_i-linked A1/3R, leading to an activation of PKA and PKC respectively and downstream phosphorylation of K_{ATP} and ClC1, increasing channel activity and reducing membrane excitability. G_i also activates K_{ATP} directly in a noncanonical signaling pathway. Metabolic stress also increases AMPK activation, leading to increased K_{ATP} activity via phosphorylation. These pathways are labelled with the conditions under which they have been observed, in contracting cardiac muscle (CM), skeletal muscle (SK), or patch-clamped skeletal muscle fibers (SK*). Figure created with Biorender.com.

Aim 1: Determine the role of adenosine signalling in skeletal muscle fatigue

There is evidence that both K_{ATP} and ClC-1 channels are activated during metabolic stress such as fatigue. Also, an activation of K_{ATP} channels increases the rate of fatigue, while in K_{ATP} channel deficient muscles large increases in unstimulated force and decreased capacity to recover force following fatigue occurs. If ARs are involved in triggering fatigue, especially via an activation of K_{ATP} and ClC-1 channels, then an AR activation will increase fatigue rate, which is defined as a faster decrease in tetanic force. Also, an inhibition will result in large increases in unstimulated force as well as consequent increase in the fatigue rate as has been shown for K_{ATP} channel deficient FDB.

Aim 2: Determine the role of AMPK signalling in skeletal muscle fatigue

Similar to the proposal for ARs, if AMPK is involved in triggering fatigue, then an AMPK activation will increase the fatigue rate while an acute AMPK knockout in skeletal muscles will result in large increases in unstimulated force and consequent increase in the fatigue rate.

Aim 3: Determine A1 receptor-AMPK signalling crosstalk in skeletal muscle fatigue

Results from aims 1 and 2 will demonstrate how individual modulations of ARs and AMPK activity affect the rate of fatigue. So, the third aim will be to determine if co-activation or co-inhibition of ARs and AMPK have an additive or synergistic effect during fatigue.

CHAPTER 2: MATERIALS AND METHODS

ANIMALS AND APPROVAL FOR ANIMAL STUDIES

All animal procedures were performed with mice 8-16 weeks in age. Female CD1 mice were purchased from Charles River and used as wild type mice for initial force measurement and histology experiments. AMPK IndKO mice were generated as described by Cokorinos et al. (2017)[99]. Transgenic female C57/Bl6 AMPK $\alpha1^{fl/fl}/\alpha2^{fl/fl}$ mice graciously donated by Dr. Benoit Viollet, Institut National de la Santé et de la Recherche Médicale (INSERM) Paris, France were crossed with male hemizygous mice expressing tamoxifen-inducible Cre recombinase driven by the human skeletal actin promoter (Tg(ACTA1-cre/Esr1*)2Kesr/J, Strain #: 025750), purchased from Jackson Laboratories (Bar Harbor, ME, USA)[95,100]. Deletion of AMPK α1/α2 was performed by intraperitoneal injections of tamoxifen (Sigma, St. Louis, MO, USA) dissolved in anhydrous ethanol and suspended in sunflower seed oil (Sigma, St. Louis, MO, USA) (3 x 100 mg/Kg body weight). Both indKO and control Cre-negative AMPK $\alpha1^{fl/fl}/\alpha2^{fl/fl}$ littermates underwent tamoxifen treatment and force measurement experiments were performed 3 weeks after the last injection. AMPK knockout was confirmed via Western Blot (see results section for Western Blots). Mice were fed ad libitum and housed according to the Canadian Council for Animal Care's guidelines. All experimental procedures and protocols were approved by the Animal Care Committee of the University of Ottawa. All animals were fed ad libitum and prior to muscle dissection, mice were anaesthetized via intraperitoneal injection of 65 mg ketamine/13 mg xylazine/2 mg acepromazine per kilogram body weight and sacrificed by cervical dislocation.

GENOTYPING

DNA extraction from mouse ear clippings was performed with a Nucleospin Tissue mini kit (Machery-Nagel, Düren, Germany) using the manufacturer's standard protocol for animal tissue[101]. PCR was then completed using DNA extract and the following primers: HSA-CRE FP (forward), 5'-CAGGTAGGGCAGGAGTTGG-3'; HSA-CRE RP (reverse), 5'-TTTGCCCCCTCCATATAACA-3'; AMPK a1 flox FP (forward), 5'-TATTGCCATGCTAC-3'; AMPK a1 flox RP (reverse), 5'-GACCTGACAGAATAGGATATGCCCAACCTC-3'; AMPK a2 flox FP (forward), 5'-GCTTAGCACGTTACCCTGGAT-3'; AMPK a2 flox RP (reverse), 5'-GTCTTCACTATACATAGCA-3'. DNA bands were then separated by electrophoresis on an agarose-ethidium bromide gel and visualized, with presence of Cre producing a strong band at 248 bp that was absent in WT mice. AMPK α1 and α2 floxed alleles produced bands at 682 and 310 bp respectively, while wild type alleles produced then at 586 and 260 bp.

PHYSIOLOGICAL SOLUTIONS

Physiological solutions were made as described by Uwera et al. (2020)[36]. Briefly, control solutions contained (in mM): 118.5 NaCl, 4.7 KCl, 2.4 $CaCl_2$, 3.1 $MgCl_2$, 25 $NaHCO_3$, 2 NaH_2PO_4, 1% (v/v) DMSO and 5.5 D-glucose (Fisher Scientific, Hampton, NH, USA). Several agonists and antagonists were used as shown in Table 2.1. When insoluble in water, drugs were first dissolved in DMSO (Fisher Scientific, Hampton, NH, USA) before being added to the physiological solutions, giving a final DMSO concentration of 1%. All solutions were continuously bubbled with 95% CO_2/5% O_2 to maintain a pH of 7.4.

RT-PCR MEASUREMENTS OF ADENOSINE RECEPTORS

Single Muscle Fiber Cell Culture

These measurements were carried out from isolated single soleus, EDL and FDB muscle fibers to avoid contamination from other cells present in muscles, such as those of blood vessels. Initial fiber cell isolation and culture was performed as described by Selvin et al. (2015)[102]. Briefly, muscles were treated with a collagenase digestion. FDB muscles were incubated 3 h at 37°C in high glucose MEM culture medium (Gibco, Burlington, ON, Canada) to which was added 0.2% (wt/vol) collagenase type I (Worthington, Lakewood, NJ), inactivated FBS (heat inactivated; Gibco) to a final 10% (v/v) concentration, 100 units/ml of penicillin and 100g/ml of streptomycin (Gibco). Fibers were separated by gentle trituration in 3 ml of collagenase-free culture medium and transferred to a 35mm culture dish (Fisher Scientific). Under an inverted microscope, 12 muscle fibers were then carefully picked up under a dissection microscope by suction using a glass microelectrode with a broken tip, avoiding any connective or vascular tissue.

RT-PCR Analysis

RNA was extracted from the isolated muscle fibers with a NucleoSpin RNA mini kit (Machery-Nagel) using the manufacturer's standard protocol for cultured cells and tissue [103]. RT-PCR was then performed as described by Dixon et al. (1996) [104] using the following primers for adenosine receptor mRNA detection: A1R FP (forward), 5'-ATCCCTCTCCGGTACAAGACAGT-3'; A1R RP (reverse), 5'-ACTCAGGTTGTTCCAGCCAAAC-3'; A2A FP (forward), 5'-CCCTTCATCTACGCCTACAGGAT-3'; A2A RP (reverse), 5'-CGTGGGTTCGGATGATCTTC-3'; A2B FP

TABLE 2.1

Drug	Concentrations Used (μM)	Effect
NECA	2, 10, 20	A1, A2A, A2B receptor-specific agonist
ENBA (aka CCPA)	2, 10, 20	A1 receptor-specific agonist
PSB 0777 (PSB)	2	A2A receptor-specific agonist
Adenosine (ADO)	10, 20	Pan-adenosine receptor agonist
8-Phenyltheophylline (8-PT)	2	A1, A2A receptor-specific antagonist
DPCPX	2, 5	A1 receptor-specific antagonist
ZM-241385 (ZM)	2	A2A receptor-specific agonist
MK-8722	5, 10, 20	AMPK allosteric activator

Table 2.1: Agonists and Antagonists used in force measurement experiments. NECA, 8-PT, DPCPX, and ZM-241385 were purchased from Tocris Bioscience (Bristol, UK). ENBA and PSB 0777 were purchased from R&D Systems (Minneapolis MN, USA). Adenosine was purchased from Milliporesigma (Burlington MA, USA). MK-8722 was purchased from Cedarlane Laboratories (Burlington ON, Canada).

(forward), 5’-TCTTCCTCGCCTGCTTCGT-3’; A2B RP (reverse), 5’-CCAGTGACCAAACCTTTATACCTGA-3’; A3R FP (forward), 5’-ACTTCTATGCCTGCCTTTTCATGT-3’; A3R RP (reverse), 5’-AACCGTTCTATATCTGACTGTCAGCTT-3’. Resulting DNA products were then separated by electrophoresis on an agarose-ethidium bromide gel and visualized.

FORCE MEASUREMENT

Ex vivo force measurement and fatigue experiments were performed as described by Uwera et al. (2020), using FDB bundles as described by Scott et al. (2016)[36,105]. Briefly, the FDB muscle is separated by fascia into fiber bundles, with each bundle controlling the movement of a digit. The bundle responsible for movement of the fourth digit was excised by cutting along the lateral fascia separating the fiber bundles for the third and fourth digits. FDB bundles were dissected in physiological solution and placed horizontally in a Plexiglas chamber. Chamber temperature was kept at 37^{o}C and the flow rate of physiological solution into each chamber was kept to 15 mL/minute, split into laminar flow just above and below the muscle to prevent a buildup of reactive oxygen species, which have a negative impact on muscle force generation at 37^{o}C [106]. One end of the muscle was fixed to a stationary hook while the other was attached to a force transducer (model 400A; Aurora Scientific Canada) using silk sutures #6. The transducer was connected to a KCP13104 data acquisition system (Keithley Instruments, USA) and data were recorded at 5 kHz. FDB bundles were stimulated by two platinum wires located on opposite sides near the muscle center, connected to a grass S88X stimulator and a Grass stimulation isolation unit (Grass Technologies/Astro-Med). Tetanic contractions were elicited with 200ms trains of 0.3ms, 10V pulses at a frequency of 200Hz. Muscle length was adjusted to give maximal force

while muscles were stimulated every 100 s. Once maximum force had been reached, muscles were either kept in control solutions or exposed to a drug-containing solutions for a 30-min equilibrium period. Fatigue was then elicited for three min by reducing the time interval between contractions to 1 sec. Fatigue traces were then analyzed to calculate the maximum tetanic and unstimulated force during each contraction (Fig. 2.1). After fatigue was complete, muscles were either flash-frozen in liquid nitrogen using pre-cooled clamps and stored at -80^{o}C for AMPK analysis or allowed a 20-minute recovery period during which three contractions were elicited every 100 sec before increasing the interval to 5 min.

MUSCLE PROTEIN EXTRACTION AND QUANTIFICATION

Frozen FDB muscle bundles were crushed with a liquid nitrogen-chilled mortar and pestle and added to MEU buffer (3M Urea, 2M Thiourea, 40mg/mL CHAPS, 8.5mg/mL Dithiothreitol (DTT), 12.5% Tris-HCl pH 6.8, ¼ tablet cOmplete™ Protease Inhibitor Cocktail, and ¼ tablet PhosSTOP™ (Millipore Sigma)). Muscle samples were then vortexed for 30 minutes at room temperature using 30 s pulses followed by a 10 s pause. Samples were then centrifuged at 20,000 g for 15 min at 4^{o}C and supernatants were transferred to fresh tubes and kept on ice for protein quantification assay.

G-Biosciences (St. Louis MI, USA) CB-X Protein Assay was used for sample clean-up and protein quantification, using the manufacturer's standard protocol[107]. One ml of -20^{o}C CB-X solvent was added to 40µL of protein extract, followed by centrifugation at 16,000 g for 5 min at 4^{o}C. Supernatants were discarded and pellets were resuspended in 100µL of CB-X solubilization

FIGURE 2.1

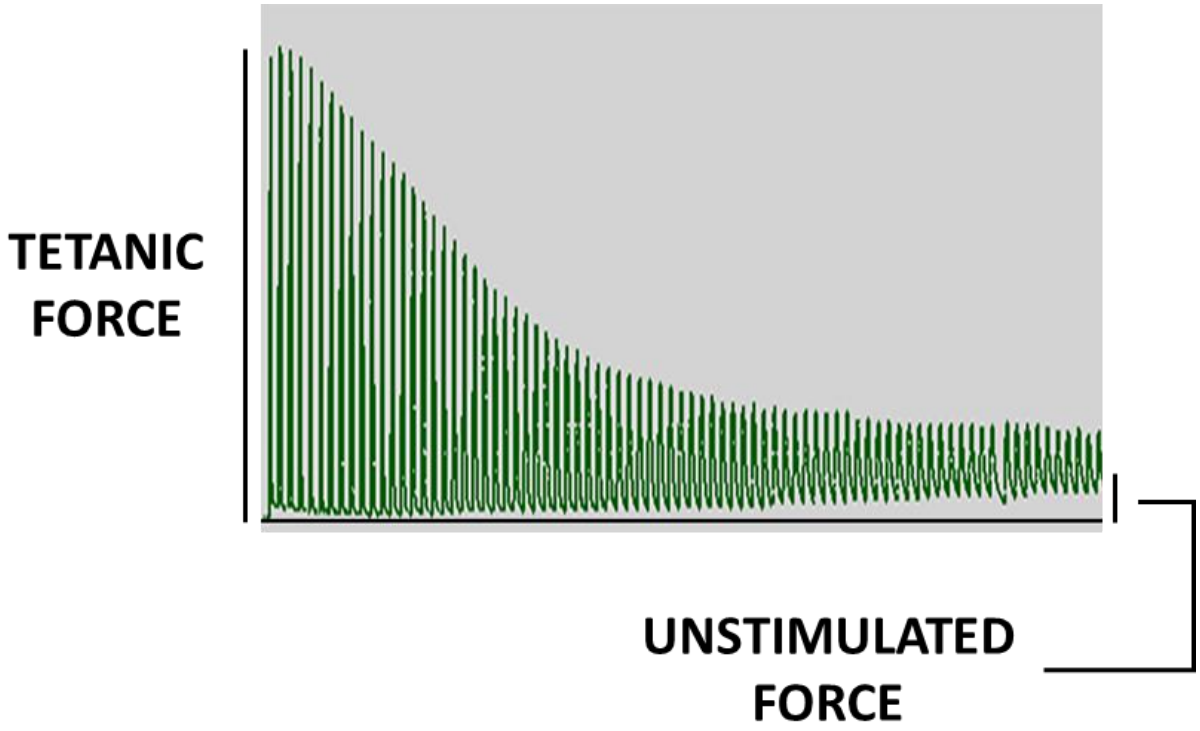

Figure 2.1: Example of a fatigue bout triggered with 1 contraction per sec in mouse FDB. The first 79 sec of the 180 sec fatigue bout is shown. Each green vertical line represents an increase in force when the FDB is stimulated. The magnitude of the first tetanic force is shown by the vertical black line on the left and is calculated as the difference between the peak and the baseline (i.e., zero force shown with the horizontal black line). During the fatigue bout, FDB failed to fully relax, and force did not return to baseline. The difference in force between two contractions and the baseline represents the unstimulated force as shown by the vertical black line on the right.

buffer mix. 10µL of Bovine Serum Albumin (BSA) protein standards and resuspended pellet were then pipetted into a 96 well plate and 200µL of CB-X Assay Dye was added to each well. Absorbance of protein standards and samples was read at 595nm using a Plate Reader (Synergy H1 Multi-Mode, BioTek, Winooski VT, USA). All protein extracts were then diluted to 0.4µg/µL with double distilled water and stored at -20^{o}C.

SDS-PAGE AND WESTERN BLOT ANALYSES

Protein extracts were prepared in Laemmli buffer and heated for 5 min at 70^{o}C. Four µg of proteins and Benchmark pre-stained protein ladder (Thermo Fisher) was separated by SDS-PAGE at 100V for 2 hr on self-casted 8% polyacrylamide gels and transferred to nitrocellulose membrane via 2 hours wet transfer at 100V, keeping the transfer rig on ice throughout. Membranes were then placed on a rocker and total protein was stained with Ponceau Dye solution (5% Glacial Acetic Acid, 0.1% wt/vol Ponceau Red Dye) for 15 min and imaged using the ponceau channel of a ChemiDoc imager (BioRad, Hercules CA, USA). Ponceau dye was rinsed from the membranes with double-distilled water and membranes were blocked with 5% BSA in TBS-T (200mM Tris, 1.5M NaCl, 0.1% Tween 20) for 2 hours at room temperature. Membranes were then washed 3 x 10 min with TBS-T and exposed to 1:1000 dilutions of primary antibodies in 2% BSA TBS-T at 4^{o}C overnight: Rabbit anti AMPKα IgG (2532) or Rabbit anti phospho-T172-AMPKα IgG (2535) from New England Bio Labs (Ipswich MA, USA). Excess antibody was removed via 3 x 10-min washes with TBS-T and membranes were exposed to a 1:5000 dilution of HRP-conjugated anti-rabbit IgG (New England Biolabs) in 2% milk for 1 hour at room temperature. Excess secondary antibody solution was then removed with a final 3 x 10-min wash with TBS-T.

Membranes were then exposed to Western Lightning Plus-ECL chemiluminescence substrate (PerkinElmer, Waltham MA, USA) for 1 min and imaged using the chemiluminescence channel of a ChemiDoc imager (BioRad), with exposure time kept equal between membranes exposed to the same primary antibody to allow for comparison.

Total protein, total AMPK (tAMPK), and phospho-T172-AMPK (pAMPK) band densities were calculated from Ponceau and Chemiluminescence channel images using ImageJ software. Ponceau Stain densities were used as a loading control to normalize AMPK/pAMPK band density between lanes and membranes to allow for comparison.

HISTOLOGY AND IMMUNOSTAINING

CD 1 Solei, EDL, and FDB were dissected and embedded in Optimal Cutting Temperature compound (Fisher Scientific, Hampton, NH, USA), and flash-frozen in isopentane (Sigma, St. Louis, MO, USA) pre-cooled in liquid nitrogen. Frozen tissue blocks were then trimmed to size and stored at -80^{o}C until ready for analysis. Serial 10µm thick cross-sections were cut from the muscle midbelly in a -20^{o}C cryostat (Thermo Shandon 525 MX). Sections were then mounted on SuperFrost Plus slides (Fisher Scientific, Hampton NH, USA), with each slide containing one cross section from soleus, EDL, and FDB from the same animal. Slides were kept at -80^{o}C until immunostaining.

Cross sections were thawed for 15 min at room temperature before being blocked and stained using a Mouse-on-Mouse immunostaining kit (M.O.M., Vector Laboratories, Newark, CA, USA) with some adjustments made to the manufacturer's protocol[108]. Slides were blocked for

1h in M.O.M. Mouse IgG blocking reagent, then washed 3 x 2 min with PBS. Sections were then exposed to primary antibodies at 4^{o}C overnight: 1:300 rabbit anti-Adenosine A1 Receptor Polyclonal IgG (55026-1-AP, Thermo Fisher Scientific, Waltham MA, USA), 1:500 rat anti-Laminin Polyclonal IgG (L0663, MilliporeSigma, Burlington MA, USA), and 1:500 mouse anti-myosin against Type I (IgM, A4.840), Type IIA (IgG, SC71), Type IIB (IgM, BFF3), or all but Type IIX (IgG, BF35). All anti-myosin antibodies were purchased from the Developmental Studies Hybridoma Bank (Iowa City IA, USA). Excess antibody was then removed by 3 x 2 min washes with PBS and sections were incubated for 30 min with secondary antibodies: Alexa Fluor 594-conjugated donkey anti-rabbit IgG (Thermo Fisher, A21207) and Alexa Fluor 405-conjugated goat anti-rat IgG (Thermo Fisher, A48261). Sections that had been incubated with mouse IgM primary antibodies (anti Type I and IIB myosin) were also incubated with FITC-Conjugated goat anti-mouse IgM (Cedarlane, Burlington ON, Canada, CLCC31501). Excess antibodies were then removed by washing 3 x 2 min with PBS and sections treated with mouse IgG primary antibodies (Anti Type IIA and all but Type IIX myosin) were incubated with M.O.M. Biotinylated Anti-Mouse IgG secondary antibody for 10 min, followed by a 5-min incubation with Fluorescein Avidin DCS (Vector Laboratories). Slides were then mounted with Vectashield Antifade Mounting Medium and sealed with nail polish.

FIBER TYPING AND QUANTIFICATION OF ADENOSINE RECEPTOR FLUORESCENCE INTENSITY

Images were obtained using an Axio Imager M2 Epifluorescent Microscope (Zeiss, Toronto ON, Canada). Image exposure time and binning were initially set to maximize antibody imaging and kept constant between secondary antibodies to allow for comparison of fluorescence

intensity across experiments. Fluorescence intensity was quantified using Imaris (Oxford Instruments, Abingdon, UK). The Anti-Laminin channel (AF 405) was used to segment images into individual cells, and both mean and sum fluorescence for the Anti-Adenosine A1R (AF 594) and Anti-Myosin (FITC/Fluorescein) channels as well as cross-sectional area for each individual muscle fiber was calculated. A threshold mean myosin fluorescence was then set for each image. Fibers were identified as type I, IIA or IIB when the fluorescence was greater than the threshold. Type IIX fibers were identified when the fluorescence intensity was below threshold as the BF35 stained all fibers but type IIX. A1R fluorescence/μm^2 for each muscle was then calculated by dividing the sum of all A1R fluorescence for a given fiber type by the sum of the cross-sectional area occupied by the same fiber type. Considering that A1R fluorescence for the same muscle can be different from one slide to another, a direct comparison of A1R fluorescence between fiber types could not be made as cross sections for different fiber types were on different slides. Instead, normalization was carried out to make sure that differences in A1R fluorescence between fiber types were not due to differences in staining intensity between slides. For each of the four slides stained for the four different fiber types, the A1R fluorescence/μm^2 was first calculated as described above, except that it included the fluorescence of all fibers within a muscle. An A1R fluorescence ratio was then calculated by dividing the fluorescence/μm^2 for each slide by the fluorescence/μm^2 of the slide used to identify type I fibers. For example, for type IIA the calculation was as follows:

$$Ratio_{IIA} = \frac{Fluorescence/\mu m^2_{IIA}}{Fluorescence/\mu m^2_{I}}$$

This ratio was then used to correct the A1R fluorescent intensity for Type IIA, IIB, and IIX fibers. For example, for type IIA fibers the corrected fluorescence was calculated as follow:

$$Corrected\ Fluorescence/\mu m^2_{IIA} = \frac{Calculated\ Fluorescence/\mu m^2_{IIA}}{Ratio_{IIA}}$$

STATISTICAL ANALYSIS

Data are presented as mean ± standard error (S.E.). Any usage of the term "significant" in this thesis refers solely to statistical significance at $p < 0.05$ and not physiological significance. Split-plot ANOVA was used to determine significant differences for force measurement experiments, as contractile force and resting tension was tested at all time points. For force measurement, drug treatment conditions were in the whole plot and time points were in the split plot. When a main effect or interaction was significant, the Least Square Difference (L.S.D.) method was used to locate significant differences[109]. For immunohistochemistry data, differences in A1R fluorescence between muscle types were tested using one-way ANOVA, while differences in A1R fluorescence and ratios between fiber types and muscles was tested via two-way ANOVA. For western blot data, differences in pAMPK/tAMPK ratios were tested using one-way ANOVA. Where a factor was found to be significant in an omnibus ANOVA, post-hoc comparisons were performed using the Tukey Honest Significant Difference Test. Statistical calculations were made using Version 4.2.1 of R statistical analysis software (R Foundation for Statistical Computing, Vienna, Austria)[110]. Split plot ANOVA was performed using the sp.plot function from Version 1.3-3 of the Agricolae package[111].

CHAPTER 3: RESULTS

SKELETAL MUSCLE ADENOSINE RECEPTOR EXPRESSION

The presence of adenosine A1R, A2AR, A2BR, and A3R receptor was first determined on a qualitative basis. To do this, mRNA was extracted from single soleus, EDL, and FDB muscle fibers after a collagenase digestion to avoid contamination from other non-muscle cells, such as capillary and vascular cells, which also express adenosine receptors[104]. Presence of PCR product was found for all four receptor subtypes across all three muscles (Fig. 3.1).

EFFECT OF MODULATING A1R, A2AR, AND A2BR ACTIVITY ON TETANIC FORCE DURING FATIGUE

The first aim was to determine whether adenosine receptors are involved in triggering fatigue. As explained in the Introduction, if the receptors are involved then exposing FDB bundles to receptor agonists (Table 3.1) is expected to result in faster and greater extent of tetanic force decrease compared to control; i.e., as observed when K_{ATP} channels, a component in the mechanism of muscle fatigue, are activated with pinacidil [111]. If adenosine receptors are important in preventing muscle dysfunction during fatigue as K_{ATP} channels are, then exposing FDB bundles to receptor antagonists (Table 3.1) is expected to result in muscle; i.e., faster fatigue rate, greater increase in unstimulated force and lower force recovery after fatigue as observed in K_{ATP} channel deficient muscle.

Fatigue was elicited with one contraction per sec for 3 min. In control conditions, i.e., in

FIGURE 3.1

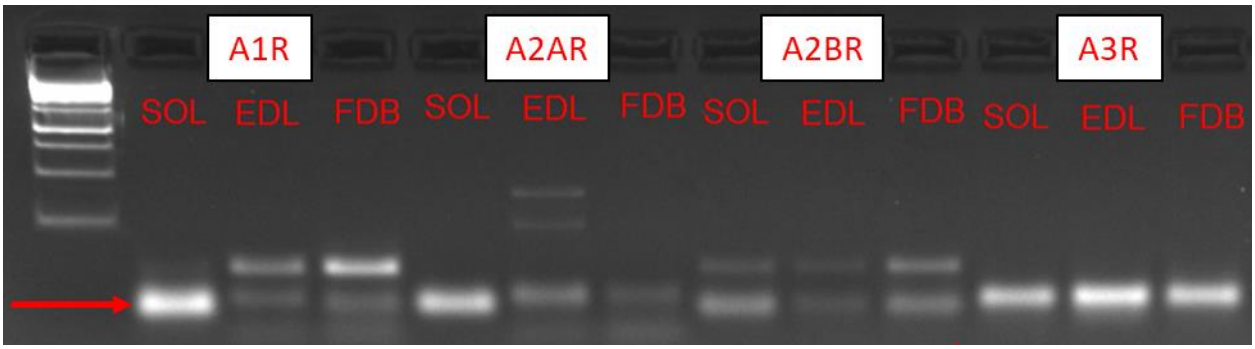

Figure 3.1: mRNA expression assay for the A1, A2A, A2B and A3 adenosine receptors determined by RT-PCR. The arrow on the left points to the bands expected to be that of a receptor.

TABLE 3.1

Agonist/Antagonist	K_D/K_i value (nM)	Receptor Subtype Target
NECA	8.5, 6.8, 6.6[112]	A1, A2A, A2B
ENBA (aka CCPA)	0.8 [113]	A1
PSB 0777 (PSB)	44.4 [114]	A2A
8-Phenyltheophylline (8-PT)	130, 126[115,116]	A1, A2A
DPCPX	3.9 [117]	A1
ZM-241385 (ZM)	0.8[118]	A2A

Table 3.1: Selective adenosine receptor agonists and antagonists used for pharmacological modulation of adenosine receptor signalling. Agonists are shown highlighted in orange and antagonists in blue. K_D values are taken from manufacturer's websites.

the absence of agonists/antagonists, FDB bundles rapidly lost approximately 80% of tetanic force over the course of 1 min of fatiguing stimulation followed by a plateau at approximately 20% of initial force that lasted the remainder of the 3-min fatigue bout. Exposing FDB muscles to 2 μM ENBA, an A1R, had no significant effect on the decrease in force during fatigue (Fig. 3.2A). The same was observed for 2 μM PSB 0777, an A2A agonist (Fig. 3.2C) and 2 μM NECA, an A1, A2A, and A2B agonist (Fig. 3.2E). At 2μM, the A1 receptor antagonist DPCPX (Fig. 3.2B), the A2A receptor antagonist ZM-241385 (Fig. 3.2D), and the A1/A2A antagonist 8-Phenyltheophylline (Fig. 3.2F) also had no significant effect on the decrease of tetanic force during fatigue. Under control conditions, unstimulated force increased by 0.3-1.3% of the pre-fatigue tetanic force over 90 s of fatiguing stimulation then plateaued for the remaining 90 s. Similar to contractile force, exposure to 2μM ENBA or DPCPX had no significant effect on the development of unstimulated force (Fig. 3.3A-B) or force recovery (Fig. 3.3C-D). Similar results were also obtained for the other agonists and antagonists (data not shown).

Although the 2 μM concentration was well above the reported K_D/K_i values, it is not uncommon to observe differences between reported values and effective concentrations in whole muscles. For example, the K_{ATP} channel blocker glibenclamide has a K_i of 63 nM under patch-clamp conditions (i.e., small patch of isolated membrane[119]) whereas 10 μM is typically used as an effective dose in whole cardiac and skeletal muscle[21,120–122]. Reported K_D/K_i values for the adenosine agonists/antagonists were primarily generated via radioligand binding assays in isolated cell membranes rather than intact whole tissues, potentially causing a similar

FIGURE 3.2

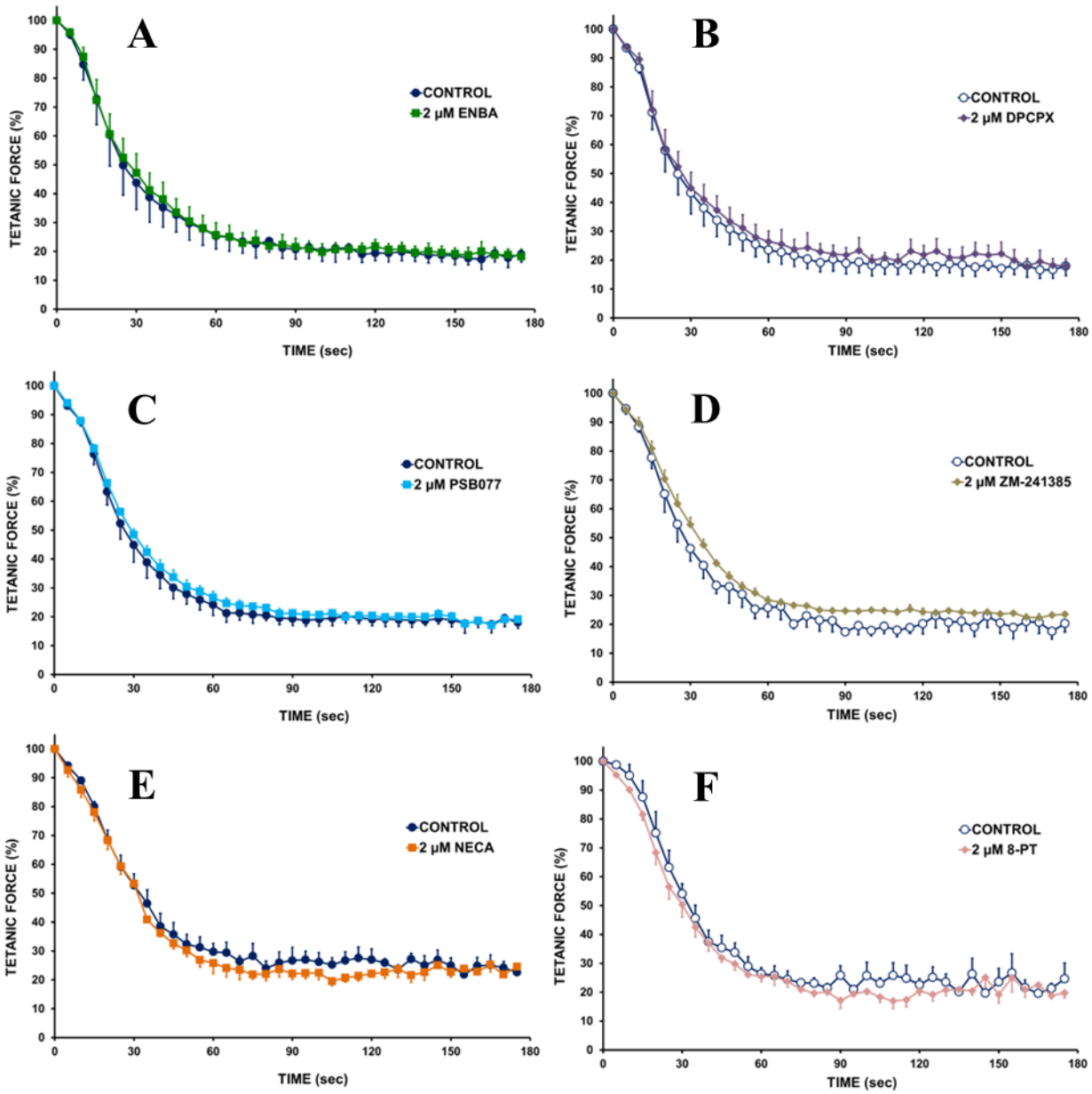

Figure 3.2: Adenosine receptor modulation using 2 µM agonists or antagonists did not alter the rate at which tetanic force decreased during 3-min fatigue elicited by one contraction every s in mouse FDB muscles. A) 2µM ENBA: A1R agonist, B) 2µM DPCPX: A1R antagonist, C) 2µM PSB: A2AR agonist, D) 2µM ZM-241385: A2A antagonist, E) 2µM NECA: A1R, A2AR, A2BR agonist, F) 2µM 8-PT: A1R, A2AR antagonist. Paired FDB were used for each drug; one used as control and the other as drug treated. Tetanic force is expressed as a percent of the pre-fatigue tetanic force. Muscles were incubated in the presence of agonists or antagonists for 30 min prior to and during fatigue. Vertical bars represent S.E. of 3 muscles. Neither agonists nor antagonists had a significant effect, ANOVA, $P > 0.05$.

FIGURE 3.3

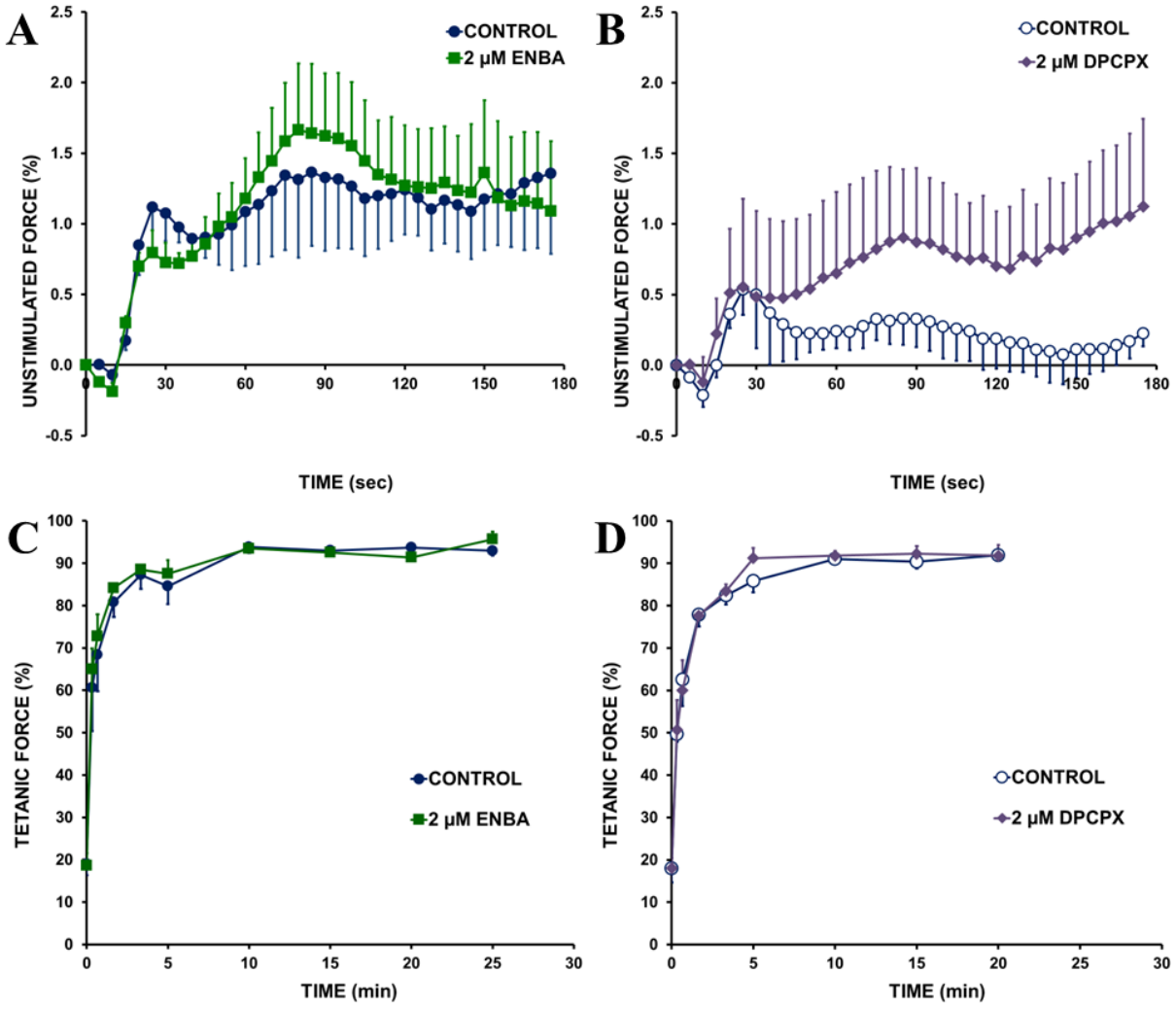

Figure 3.3: A1R receptor modulation using 2 µM ENBA or DPCPX did not alter the development of unstimulated force during 3-min fatigue elicited by one contraction every s in mouse FDB muscles or post-fatigue force recovery. Effect of 2 µM ENBA (A1R agonist) on A) unstimulated force and C) post-fatigue tetanic force recovery; effects of 2 µM DPCPX (A1R antagonist) on B) unstimulated force and D) post-fatigue tetanic force recovery. Paired FDB were used for each drug; one used as control and the other as drug treated. FDB were incubated in the presence of agonists or antagonists for 30 min prior to fatigue, during fatigue and the subsequent recovery period. Tetanic and unstimulated force are expressed as a percent of the pre-fatigue tetanic force (see Methods for more details about the calculation of unstimulated force). Vertical bars represent S.E. of 3 muscles. Neither agonists nor antagonists had a significant effect, ANOVA, $P > 0.05$.

discrepancy. Furthermore, like glibenclamide these drugs are highly hydrophobic, incorporating themselves not only in sarcolemma but also in t-tubules and sarcoplasmic reticulum membranes which are extensive in skeletal muscles.

The experiments were therefore repeated using 10 and 20 µM adenosine, NECA (A1, A2A, A3 agonist) and ENBA (A1R agonist). At 10 µM, adenosine slightly but not significantly reduced the decrease in tetanic force; the largest difference was observed at 25 s when tetanic force was 6.3% less in adenosine-exposed than in control FDB (Fig. 3.4A). Contrary to adenosine, NECA increased the rate of fatigue resulting in 4.5% lower tetanic force compared to control FDB upon reaching plateau around 90 s (Fig. 3.4B). Although the ANOVA main effect was significant for NECA, the effect was not always consistent; i.e., it was only observed in 50% of the NECA-treated FDB. ENBA, on the other hand, had the greatest effect consistently increasing tetanic force loss starting after 15 s of stimulation, culminating in a 4.8% reduction in tetanic force compared to controls by 90 s (Fig 3.4C). At 20 µM, adenosine resulted in a small but not significant reduction in the extent of tetanic force loss for the first 25 s of stimulation; the difference between control and adenosine treated FDB decreasing over time (Fig. 3.5A). NECA again was inconsistent at increasing tetanic force loss compared to controls. Although the final extent of tetanic force loss was 4.3% greater in the presence of NECA, the effect was not significant due to a high variability (Fig. 3.5B). ENBA had the greatest impact and significantly increased the final extent of tetanic force by 7.0% compared to control FDB (Fig. 3.5C). The effects of 20 µM ENBA were completely blocked by the presence of 5 µM DPCPX (A1R antagonist) (Fig. 3.5D). Neither, adenosine, NECA nor ENBA had an effect on the increased in unstimulated force during fatigue or the tetanic force recovery after fatigue (data not shown).

FIGURE 3.4

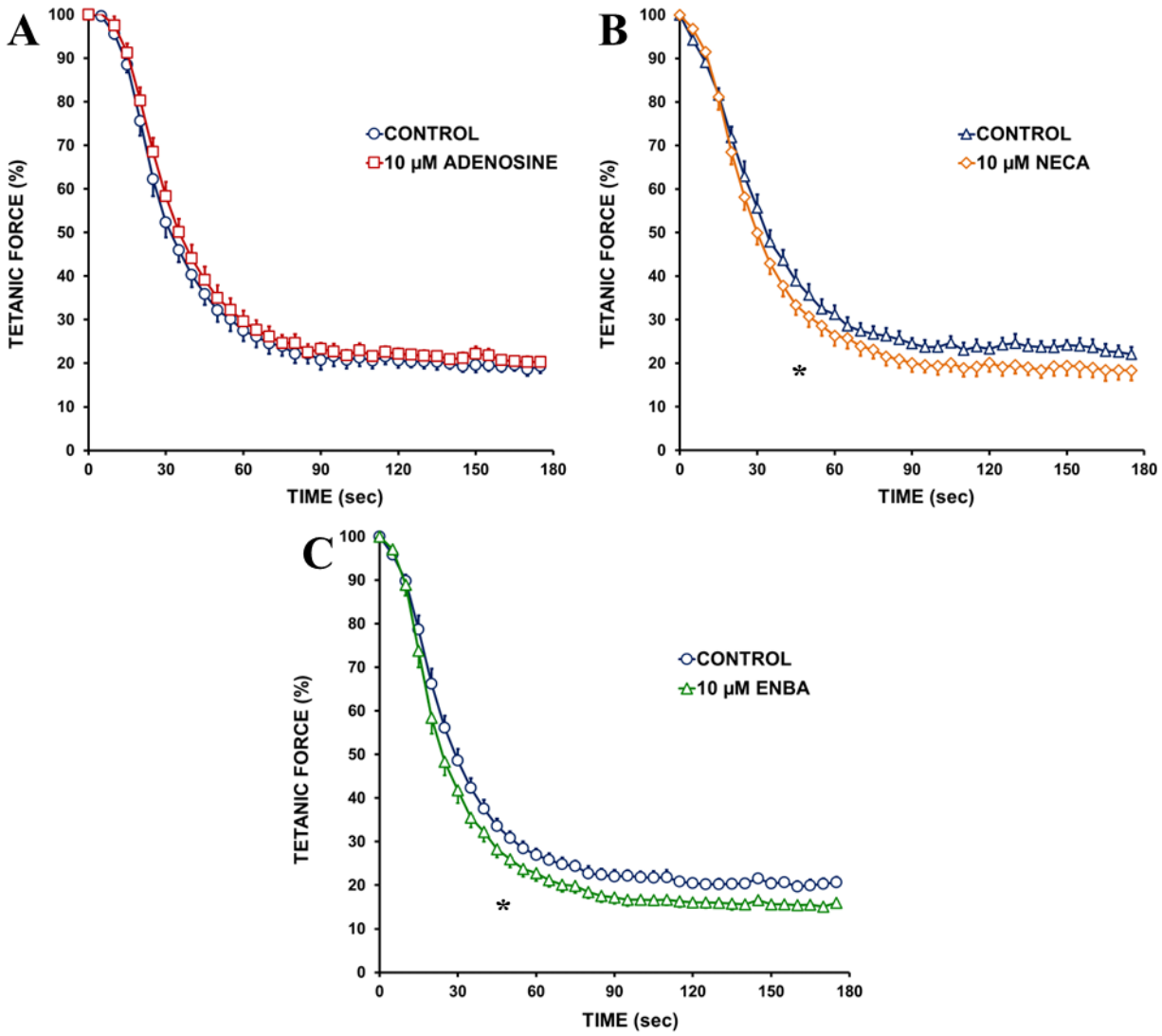

Figure 3.4: At 10 µM, NECA and ENBA but not adenosine significantly increased tetanic force loss in mouse FDB muscles during fatigue, elicited by one contraction every s for 3 min. A) 10 µM adenosine (pan-AR agonist), B) 10 µM NECA (pan A1R, A2AR, A2BR agonist), C) 10 µM ENBA (A1R agonist). Tetanic force is expressed as a percent of maximum force at the onset of fatiguing stimulation. Paired FDB were used for each drug; one used as control and the other as drug treated. FDB were incubated in the presence of agonists or antagonists for 30 min prior to and during fatigue. All experiments were carried out using paired FDB; one FDB as control and the other drug treated. Vertical bars represent S.E. of 5-6 muscles. * Indicates significant differences between control and drug condition; ANOVA, $P < 0.05$ (main effect).

FIGURE 3.5

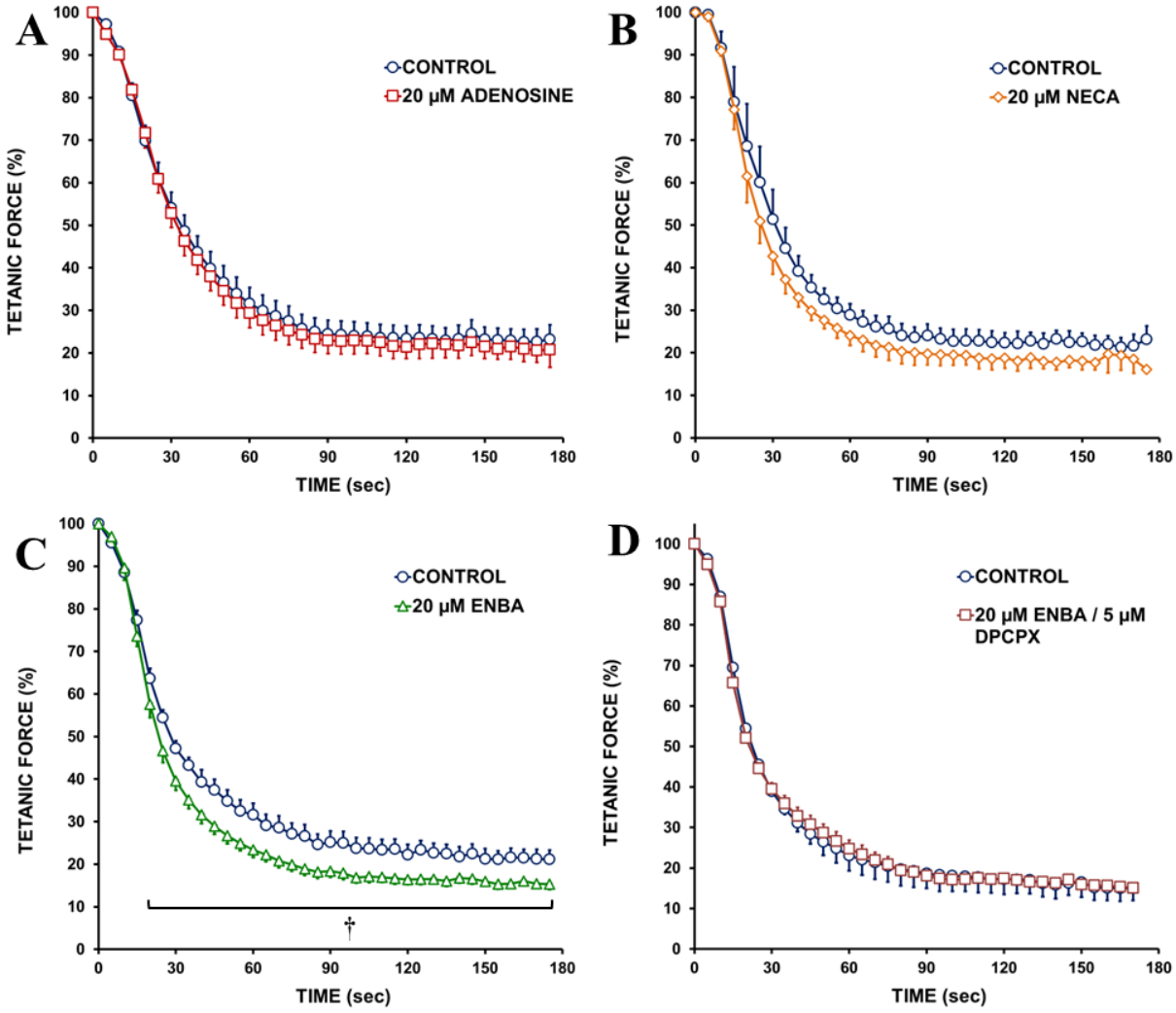

Figure 3.5: At 20 µM, ENBA, but not adenosine or NECA, significantly increased tetanic force loss in mouse FDB muscles during fatigue, elicited with one contraction every s for 3 min an effect blocked by DPCPX. A) 20 µM adenosine (pan-AR agonist), B) 20 µM NECA (pan A1R, A2AR, A2BR agonist), C) 20 µM ENBA (A1R agonist), D) co-20 µM ENBA (A1R agonist) / 5 µM DPCPX (A1R antagonist). Tetanic force is expressed as a percent of maximum force at the onset of fatiguing stimulation. Paired FDB were used for each drug; one used as control and the other as drug treated. FDB were incubated in the presence of agonists or antagonists for 30 min prior to and during fatigue. All experiments were carried out using paired FDB; one FDB as control and the other drug treated. Vertical bars represent S.E. of 3-6 muscles. † Indicates the time period during which there were significant differences between control and drug conditions; ANOVA, LSD $P < 0.05$ (interactive effect).

THE EFFECT OF ADENOSINE RECEPTOR ACTIVATION ON AMPK PHOSPHORYLATION

As discussed in the Introduction, both AMPK and adenosine receptor signalling play a role in cardioprotective ischemic preconditioning via the activation of K_{ATP} channels to reduce excitability[54,55,57,73]. Additionally, 5'-NT knockdown was found to increase AMPK activity while overexpression was found to have the opposite effect[96,97], suggesting potential interactions between adenosine receptors and AMPK activation. It is therefore possible that the small/lack of effect from an activation of adenosine receptors on fatigue kinetics is because of lower AMPK activation, i.e., lower extent of AMPK phosphorylation. So, the effects of activating adenosine receptors on AMPK Thr-172 phosphorylation immediately after fatigue were determined.

At 10 µM, adenosine, ENBA, and NECA significantly increased AMPKα T172 phosphorylation compared to control muscles, the effects being the largest with ENBA (Fig. 3.6A-C). A similar situation was observed at 20µM with less differences between adenosine, ENBA and NECA, the pAMPK/tAMPK ratios being respectively 2.4, 2.7, and 2.9-fold greater than control (Fig. 3.6D-E). Thus, while pan-activation of A1R, A2AR, A2BR with adenosine and NECA and A1R activation with ENBA had a large impact on AMPK phosphorylation, only ENBA had a consistent and significant effect on the decrease in tetanic force during fatigue. Taking into consideration this latter result, the primary focus for the rest of this study was on A1R and AMPK, including a quantification of A1R protein content between EDL, soleus and FDB, as well as between fiber types.

FIGURE 3.6

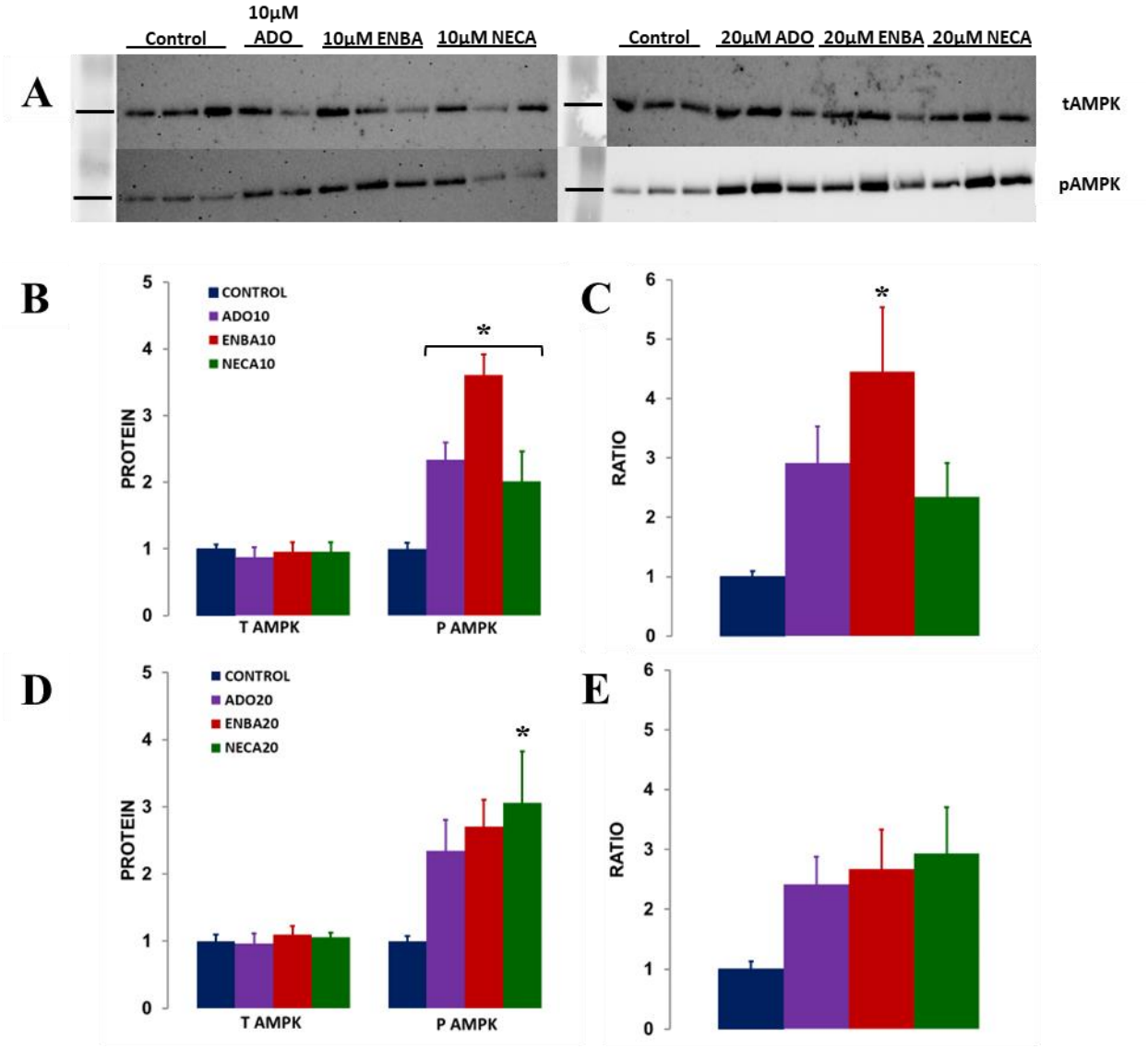

Figure 3.6: An activation of adenosine receptors prior to fatigue significantly increased the extent of AMPKα T172 phosphorylation measured after fatigue. FDB muscles were exposed to control solution, adenosine (ADO, pan-AR agonist), ENBA (A1R agonist), or NECA (A1R, A2AR, A2BR agonist) for 30 min prior to and during fatigue and were frozen immediately after fatigue (A) representative western blot images, black lines represent expected location of 62kDa bands. Densitometric analyses of protein density of total AMPK (tAMPK) and phospho-T172 AMPK (pAMPK) for the agonist concentrations of 10µM (B) and 20µM (D). pAMPK/tAMPK ratios for the 10 µM (C) and 20 µM concentrations (E). All values are expressed relative to control. Error bars represent S.E. of 4-7 FDB. *Protein content was significantly greater than control; ANOVA, Tukey Post-hoc comparison, $P < 0.05$.

ADENOSINE A1 RECEPTOR PROTEIN QUANTIFICATION IN SOLEUS, EDL, AND FDB

The protein content of K_{ATP} channels, which are crucial for preventing muscle dysfunction during fatigue, is the largest in glycolytic fatigable fibers/muscles and smallest in oxidative/fatigue resistant fibers/muscles; i.e., in the order of Type IIB > IIX > IIA > I as well as FDB ~ EDL > Soleus. So, if A1R is an important factor in fatigue and in activating K_{ATP} channels, then its expression may also correlate with the fatigability of fiber types and muscles similar to the K_{ATP} channel.

A1R is not expected to be located just in the sarcolemma but also in t-tubules. This is because PanX1 ATP transporters as well as P2X4 ATP receptors are located in t-tubules[59,63]. Additionally, β2-adrenergic receptors are present in cardiac t-tubules[123] and their activity is modulated by A1R[83]. Thus, A1R is expected to be present not only at the sarcolemmal level but also in t-tubules as observed for Cav1.1 Ca^{2+} and K_{ATP} channels[41]. As a 10 µm thick cross-section contains at least 3 layers of t-tubules, staining muscle cross-sections with anti-A1R antibody is expected to be at the sarcolemmal level as well as in the middle of the fiber allowing for a quantification of A1R protein content in t-tubules. The specificity of the A1R antibody was tested by western blot using whole FDB homogenates. Only a single band was observed at the expected molecular weight of 37kDa (Fig 3.7).

Representative images with labelled type I myosin fibers are shown in Figures 3.8 (Soleus), 3.9 (EDL), and 3.10 (FDB). Qualitatively, EDL had the greatest overall fluorescence intensity for A1R compared to solei or FDB. Another consistent observation was type I fibers having the lowest

FIGURE 3.7

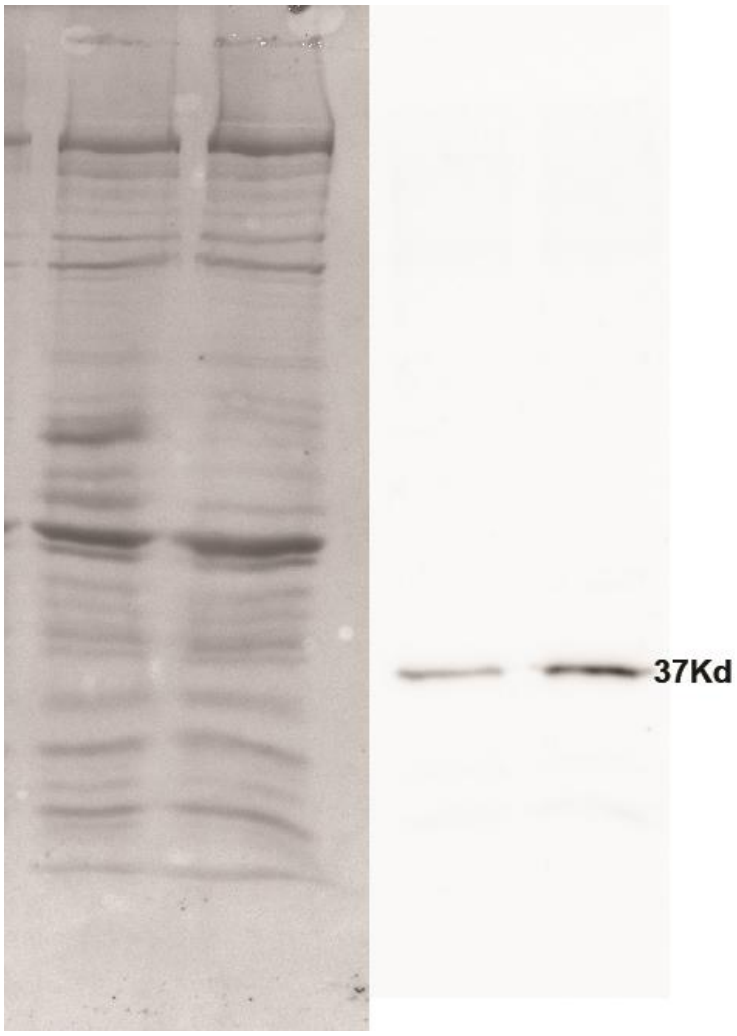

Figure 3.7: A1R antibody specificity was confirmed via Western Blot from FDB homogenates prior to immunostaining. Western blot was performed using homogenates from two FDB muscles. The ponceau staining are shown in the first two lanes on the left while staining with the A1R antibody resulted in one clear band at the expected molecular weight of 37Kd.The ponceau and A1R staining are from two separate images.

FIGURE 3.8

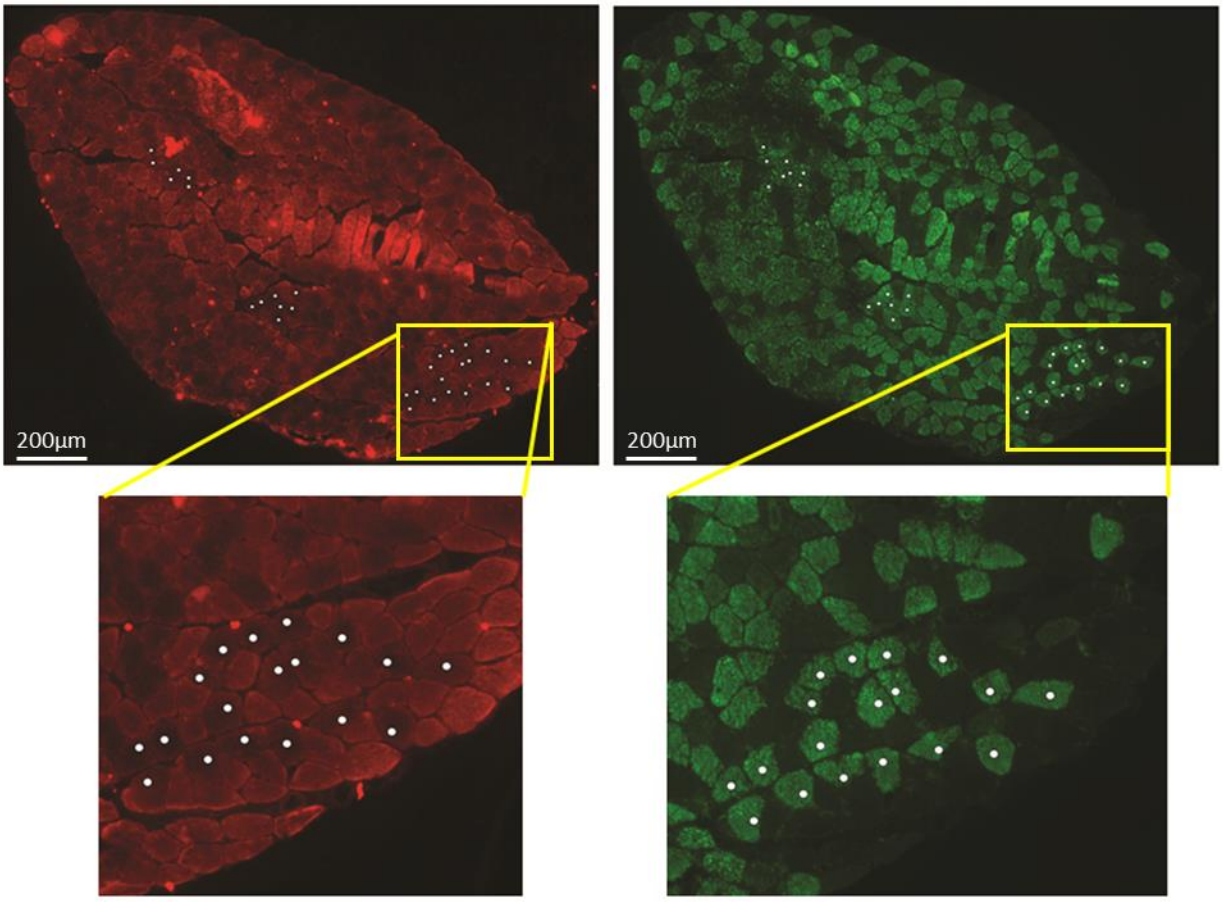

Figure 3.8: In soleus, type I fibers have less A1R protein content than type IIA fibers. Cross sections were immunostained for A1R (red) and type I myosin (green, also shown with white dots). Most of the unstained fibers are those expressing type IIA and IIX myosin[41]. Scale bar represents 200µm.

FIGURE 3.9

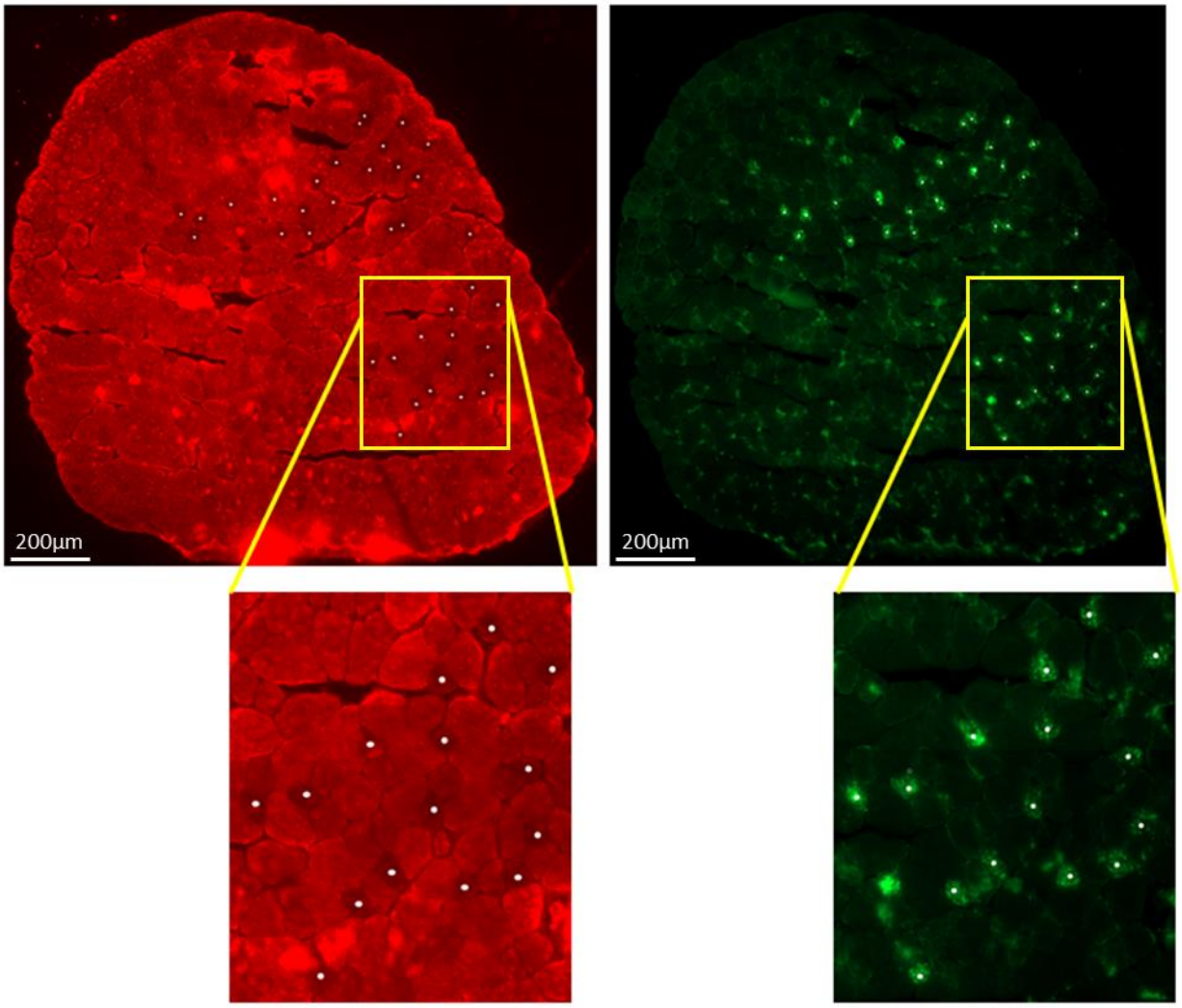

Figure 3.9: In EDL, type I fibers have less A1R content than type IIA, IIB, and IIX fibers. Cross sections were immunostained for A1R (red) and type I myosin (green, also shown with white dots). Unstained fibers expressed primarily type IIB and IIX fibers [41]. Scale bar represents 200µm.

FIGURE 3.10

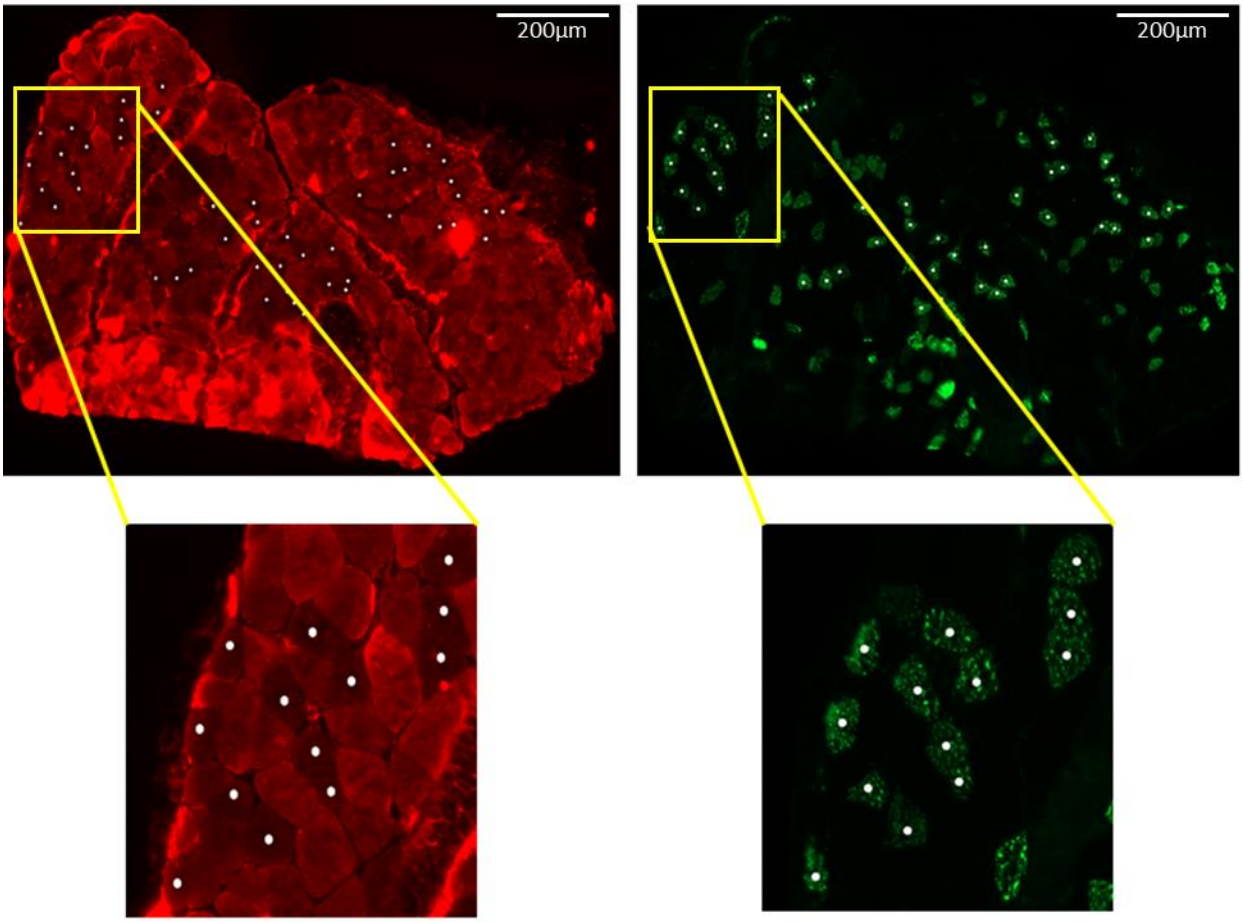

Figure 3.10: In FDB, type I fibers have less A1R protein content than type IIA, IIB, and IIX fibers. Cross sections were immunostained for A1R (red) and type I myosin (green, also shown with white dots). Scale bar represents 200µm.

fluorescence intensity for A1R compared to all other fiber types regardless of their content in soleus, EDL and FDB. On a quantitative basis, mean A1R fluorescence intensity was significantly greater in EDL muscles than in solei or FDB by 51% and 57% respectively (Fig. 3.11A). There was a small but insignificant tendency for type IIB fibers to have the highest fluorescence intensity and type I fibers the lowest intensity with little differences between type IIA and IIX fibers resulting in an order of Type IIB > IIA ≈ IIX > I fibers in EDL and soleus and IIX ≈ IIA ≈ IIB > I for FDB (Fig. 3.11B).

THE EFFECT OF MODULATING AMPK ACTIVITY ON TETANIC FORCE DURING FATIGUE

The second aim was to determine whether AMPK is involved in triggering fatigue. In a first series of experiments, CD1 mouse FDB bundles were exposed to 10 μM MK-8722, an allosteric AMPK activator, for 30 min followed by the same fatigue protocol used above. If AMPK is involved in the activation of fatigue, then allosteric AMPK activation is expected to increase fatigue rate (i.e., a faster force decrease). FDB bundles exposed to MK-8722 fatigued significantly slower than control muscles for the first 30 s of stimulation; the largest difference occurred at 15 s when the decrease in tetanic force was 8.2% greater in control than in MK-8722-treated FDB (Fig. 3.12). By 30 s, tetanic force reached approximately 40% of pre-fatigue tetanic force for both conditions. Thereafter, the decrease in tetanic force became greater in MK-8722-treated FDB. At the end of the fatigue bout mean tetanic forces were significantly different between control and MK-8722-exposed FDB, the values being 17.2% and 14.9% of pre-fatigue force, respectively. Similar to the observation for the adenosine receptors, MK-8722 had no significant effect on unstimulated force during fatigue (data not shown).

FIGURE 3.11

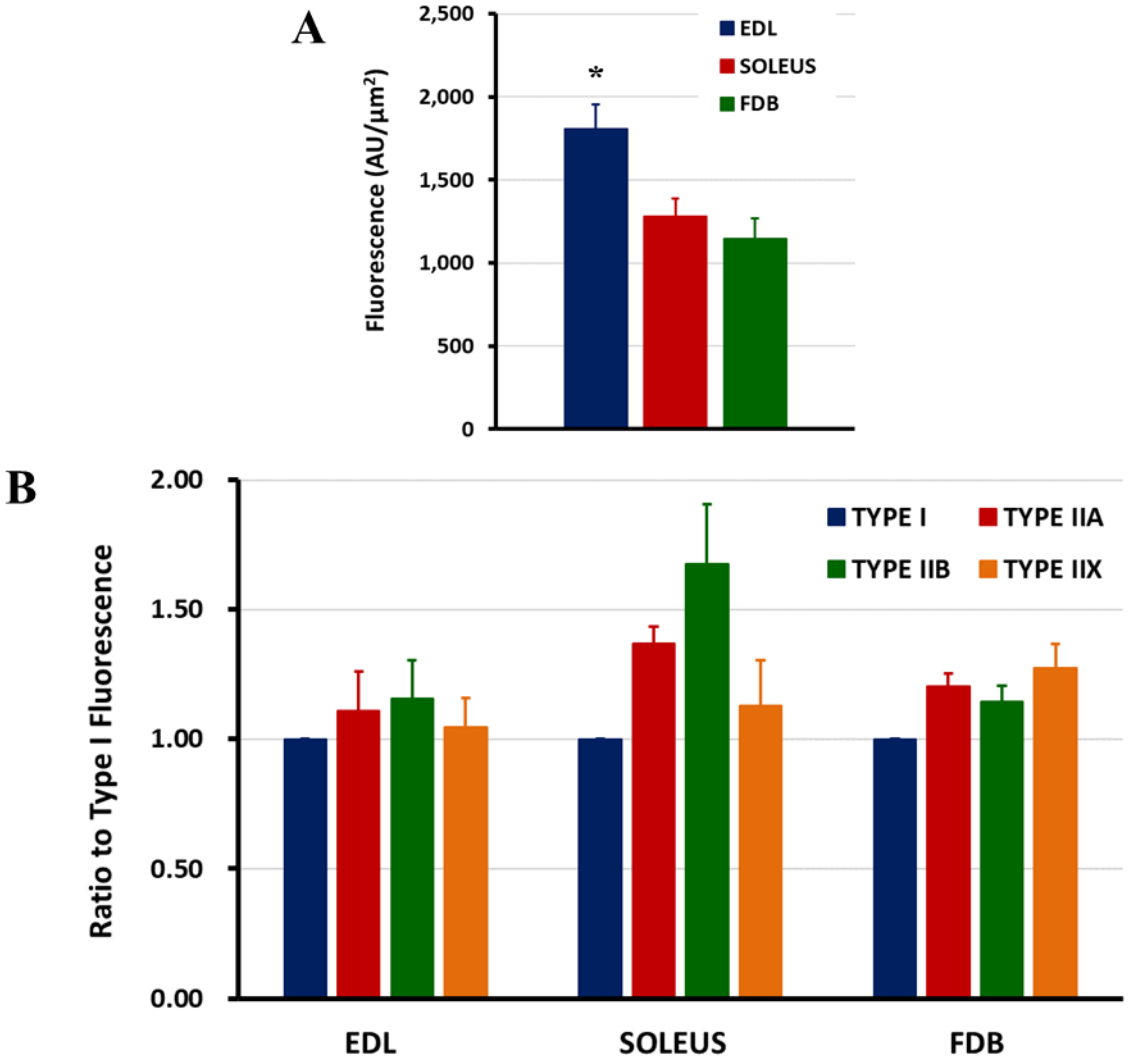

Figure 3.11: A1R fluorescence intensity is in the order of EDL > soleus ≈ FDB with a tendency for type IIB > IIA ≈ IIX > I fibers in EDL and soleus and IIX ≈ IIA ≈ IIB > I. A) Mean fluorescence intensity for A1R between EDL, soleus, and FDB muscles. For each mouse, all three muscles were put on the same slide and stained simultaneously. B) Mean fluorescence intensity for A1R between fiber types. The intensities for a given fiber type were added and then divided by the total surface area occupied by that same fiber type. Mean fluorescence intensities are expressed as a ratio to type I fiber (See Methods and Materials for the calculation). Vertical bars represent the S.E. Numbers of fibers/muscles are shown in Table 3.2. * Fluorescent intensity in EDL was significantly different from that of soleus and FDB, ANOVA $P < 0.05$. Differences in fluorescent intensities between fiber types were not significant, ANOVA $P > 0.05$.

TABLE 3.2

Muscle	Type I	Type IIA	Type IIB	Type IIX
EDL	83 / 4	920 / 4	1458 / 4	401 / 4
Soleus	1128 / 4	935 / 4	30 / 3	286 / 4
FDB	264 / 4	1221 / 4	2 / 2	661 / 4

Table 3.2: Numbers of Fibers and Muscles used for analysis in Figure 3.9. Numbers are # fibers/ # muscles.

FIGURE 3.12

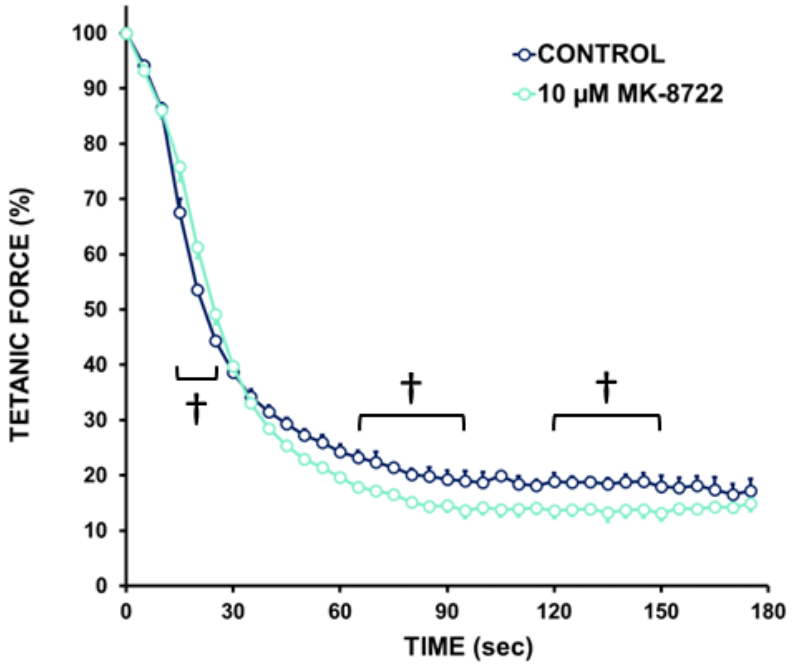

Figure 3.12: Activating AMPK with 10 µM MK-8722 initially resulted in slower decrease in tetanic force for 30 s before the loss became faster and greater compared to control mouse FDB muscles. Fatigue was triggered with one tetanic contraction every s for 3 min. Paired FDB were used; one used as control and the other as MK-8722-treated. FDB were exposed to 10 µM MK-8722 30 min prior to and during fatigue. Tetanic force is expressed as a percent of maximum force at the onset of fatiguing stimulation. Vertical bars represent the S.E. of 2-3 FDB. † Indicates the time period during which there were significant differences between control and MK-8722-treated FDB; ANOVA, LSD $P < 0.05$ (interactive effect).

As AMPK inhibitors were not available, the effect of a lack of AMPK was tested using an inducible AMPK double knockout AMPK $\alpha1^{-/-}/\alpha2^{-/-}$ IndKO mouse model triggered by tamoxifen three weeks prior to the fatigue experiments. Western blot analysis confirmed the total absence of AMPK in AMPK $\alpha1^{-/-}/\alpha2^{-/-}$ IndKO FDB (Fig. 3.13). Cre-positive AMPK $\alpha1^{fl/fl}/\alpha2^{fl/fl}$ FDB were used as control. As discussed in the Introduction and for the adenosine receptors, if AMPK triggers fatigue including an activation of K_{ATP} and ClC-1 channels, then muscle dysfunctions are expected to occur during fatigue in AMPK $\alpha1^{-/-}/\alpha2^{-/-}$ IndKO FDB bundles.

AMPK $\alpha1^{-/-}/\alpha2^{-/-}$ IndKO FDB bundles fatigued slightly but significantly faster than untreated AMPK $\alpha1^{+/+}/\alpha2^{+/+}$ FDB early in the fatigue run. After 30 sec, the force loss was 10.8% greater in AMPK $\alpha1^{-/-}/\alpha2^{-/-}$ FDB than in control. (Fig. 3.14A). The difference decreased to just 2.6% by the time force reached a plateau around 95 seconds into the fatigue bout. Unstimulated force increased similarly for AMPK $\alpha1^{-/-}/\alpha2^{-/-}$ IndKO and AMPK $\alpha1^{+/+}/\alpha2^{+/+}$ FDB bundles during the first 80 s. Thereafter, it decreased slightly for AMPK $\alpha1^{+/+}/\alpha2^{+/+}$ control FDB bundles while it continued to increase for AMPK $\alpha1^{-/-}/\alpha2^{-/-}$ IndKO FDB (Fig. 3.14B). By the end of the fatigue run, final mean unstimulated force was 10.6% of initial force for AMPK $\alpha1^{-/-}/\alpha2^{-/-}$ IndKO FDB compared to 5.9% in control FDB. This difference was not found to be significant due to high variability between FDB.

THE EFFECTS OF MODULATING THE ACTIVITY OF BOTH ADENOSINE RECEPTORS AND AMPK

The third aim was to determine whether adenosine receptor-AMPK signalling crosstalk occurs during fatigue. Two sets of experiments were carried out to do this. The first experiment

FIGURE 3.13

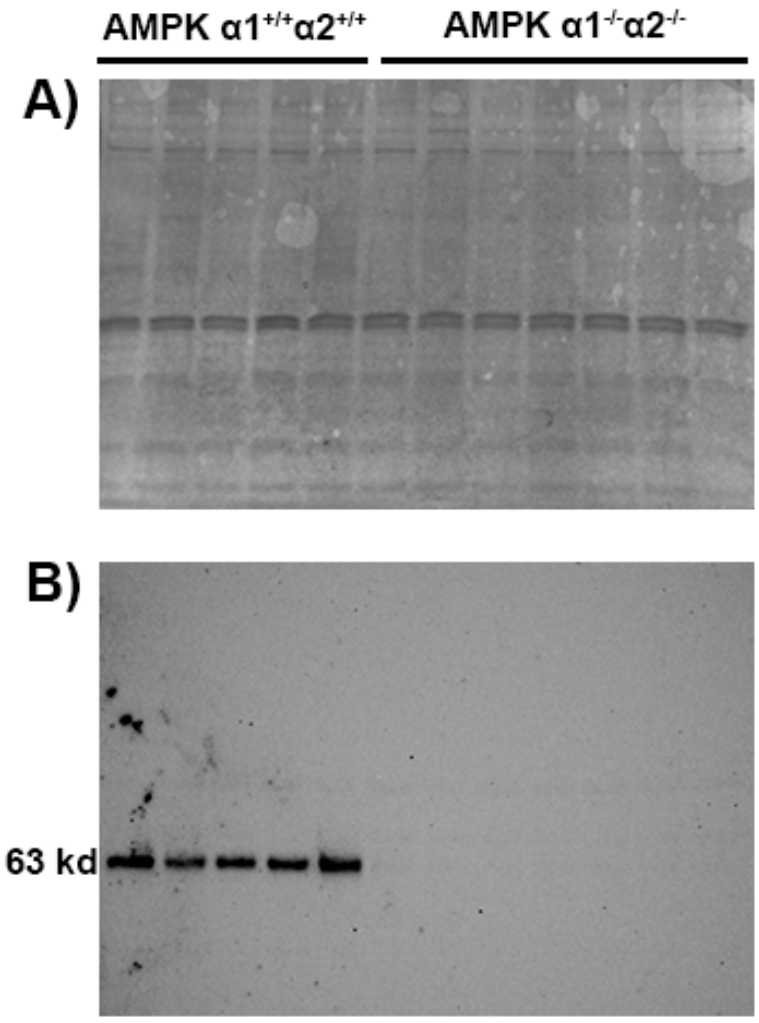

Figure 3.13: Tamoxifen treatment knocked out AMPKα expression in AMPK $\alpha1^{fl/fl}/\alpha2^{fl/fl}$ mouse FDB, generating AMPK $\alpha1^{-/-}/\alpha2^{-/-}$ indKO FDB. Representative western blot showing 5 control AMPK $\alpha1^{+/+}/\alpha2^{=/=}$ and 7 induced AMPK $\alpha1^{-/-}/\alpha2^{-/-}$ indKO FDB on the same membrane with A) Ponceau staining and B) AMPK α1/α2 immunostaining.

FIGURE 3.14

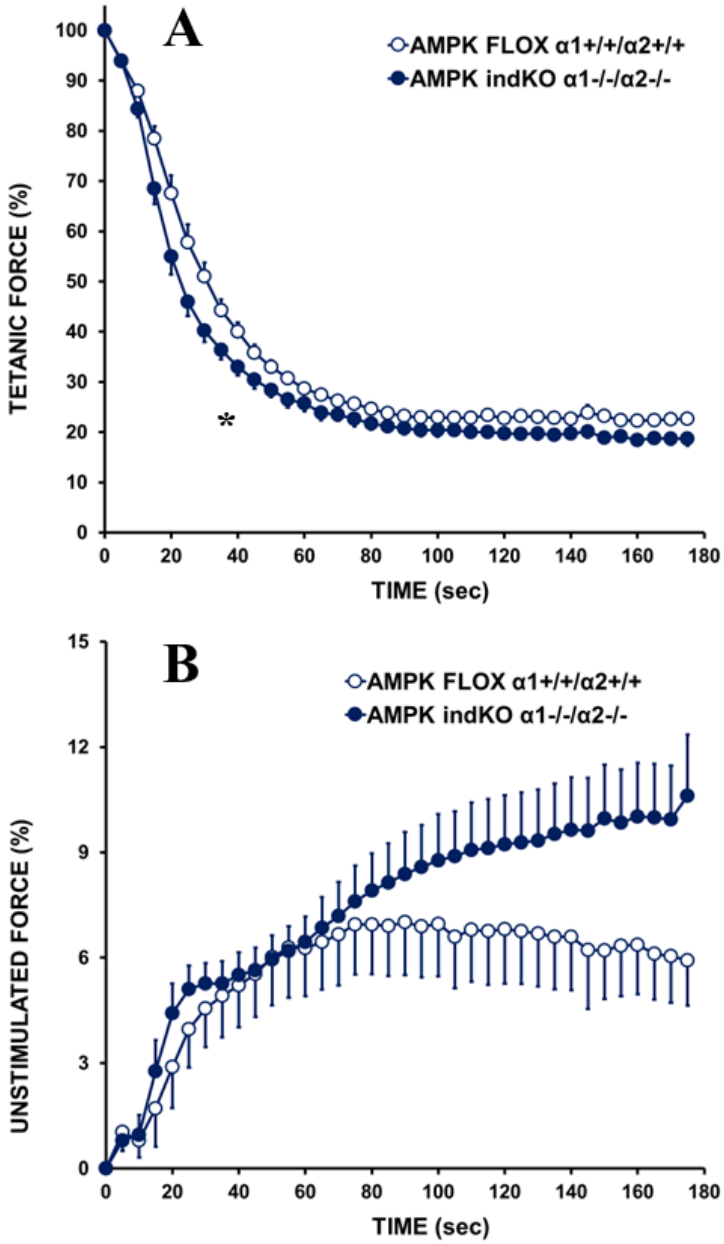

Figure 3.14: AMPK $\alpha1^{-/-}/\alpha2^{-/-}$ indKO FDB had significantly faster and greater decreases in tetanic force loss and greater increase in unstimulated force during fatigue compared to control AMPK $\alpha1^{fl/fl}/\alpha2^{fl/fl}$ FDB. A) Tetanic force and B) unstimulated force are expressed as a percent of pre-fatigue tetanic force. AMPK $\alpha1^{-/-}/\alpha2^{-/-}$ IndKO mice were injected once daily over 3 days with 100mg/Kg tamoxifen and FDB were tested 3-weeks later. Fatigue was elicited with 1 contraction every sec for 180 sec. Vertical bars are S.E. of 4-5 FDB. * indicates a significant difference between control AMPK $\alpha1^{fl/fl}/\alpha2^{fl/fl}$ and AMPK $\alpha1^{-/-}/\alpha2^{-/-}$ IndKO; ANOVA, $P < 0.05$ (main effect only).

involved co-activation of adenosine receptors and AMPK in CD-1 mouse FDB. At 10µM, MK-8722/adenosine and MK-8722/ENBA combinations did not affect the rate of fatigue (Fig. 3.15A, C) whereas the MK-8722/NECA combination slightly but not significantly increased it, causing an extra 2.7% greater decrease compared to control (Fig. 3.15B). Increasing ENBA concentration to 20µM with 10 µM MK-8722 lead to faster and greater extent of tetanic force loss, similar to that observed with either 10µM ENBA (Fig. 3.4C) or 10µM MK-8722 (Fig. 3.12); i.e., increasing tetanic force loss by 6.4% (Fig. 3.15D). However, as with MK-8722/NECA, this difference was not statistically significant due to high variability.

The second experiment involved the activation and inhibition of A1R in the absence of AMPK activity. If an interactive and compensatory relationship exists between A1R and AMPK, then A1R activation in AMPK $\alpha1^{-/-}/\alpha2^{-/-}$ indKO FDB is expected to result in a much greater effect than in control FDB. Additionally, a lack of both A1R and AMPK activity should result in severe contractile dysfunction similar to that observed in K_{ATP} channel deficient muscles, greater than with the loss of A1R or AMPK activity alone. As observed with CD-1 FDB muscles (Fig. 3.5C), 20 µM ENBA increased the extent of the tetanic force loss during fatigue in AMPK $\alpha1^{+/+/}/\alpha2^{+/+}$ FDB, albeit the difference of 4% was observed at the very end of fatigue and lacked statistical significance (Fig. 3.16A). ENBA had a greater and significant effect in AMPK $\alpha1^{-/-}/\alpha2^{-/-}$ indKO FDB. The decrease in tetanic force was faster in the presence of ENBA, the greatest difference of 7.7% being observed at 175 s (Fig. 3.16B). At 5µM, DPCPX had no effect on tetanic force loss during fatigue in AMPK $\alpha1^{+/+}/\alpha2^{+/+}$ FDB (Fig. 3.16C). DPCPX exposure did have a slight effect in indKO FDB however, where it increased tetanic force loss by 4%, albeit observed at the very end of fatigue and lacking significance (Fig. 3.16D).

FIGURE 3.15

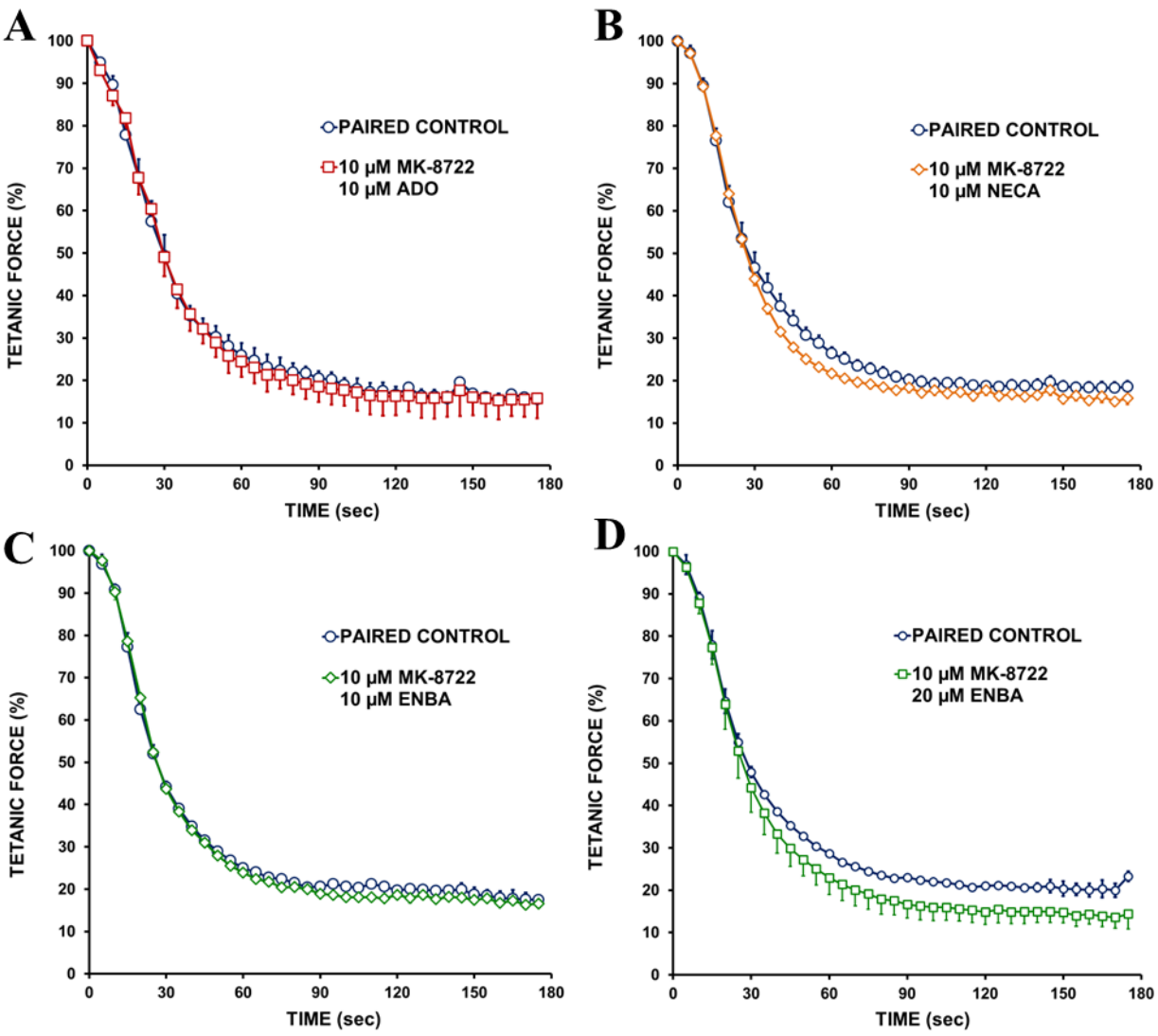

Figure 3.15: FDB co-activation of adenosine receptors with NECA (10 µM) and ENBA (20 µM) and AMPK with 10 µM MK-8722 slightly increased tetanic force loss in CD-1 mouse FDB. A) 10 µM MK-8722 (AMPK activator) + 10 µM adenosine (pan-AR agonist). B) 10 µM MK-8722 (AMPK activator) + 10 µM NECA (A1R, A2AR, A2BR agonist). C) 10 µM MK-8722 (AMPK activator) + 10 µM ENBA (A1R agonist). D) 10 µM MK-8722 (AMPK activator) + 20 µM ENBA (A1R agonist). Paired FDB were used: one as control the other as drug treated. Tetanic force is expressed as a percent of pre-fatigue tetanic force. FDB were incubated in the presence of agonists 30 min prior to and during fatigue. Vertical bars represent S.E. of 3-6 muscles. Vertical bars represent S.E. of 3-7 muscles. There was no significant difference between the various conditions, ANOVA: $P > 0.05$.

FIGURE 3.16

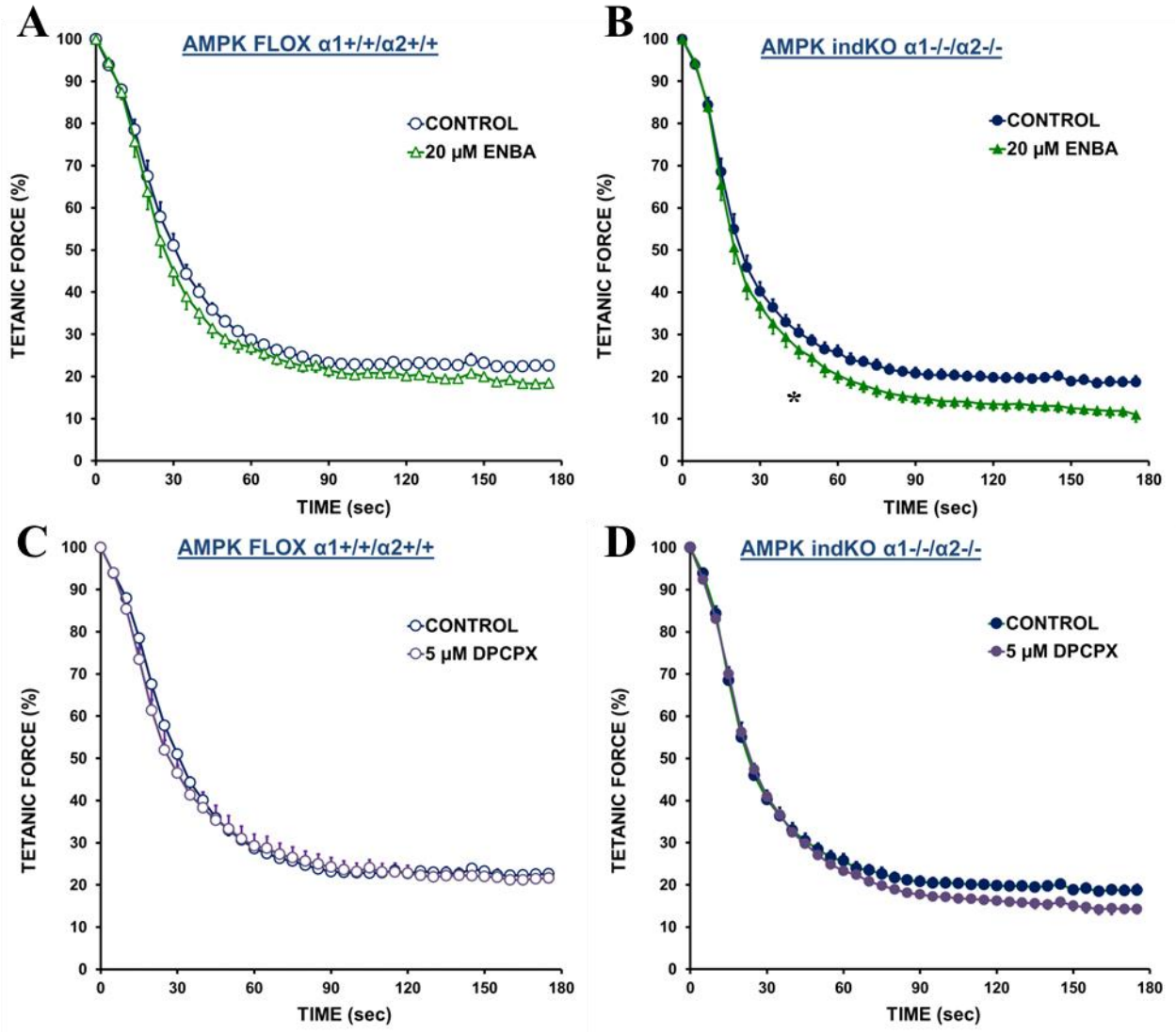

Figure 3.16: An activation or inhibition of A1R in AMPK $\alpha1^{-/-}/\alpha2^{-/-}$ indKO FDB slightly increased the extent of tetanic force loss compared to control AMPK $\alpha1^{+/+}/\alpha2^{+/+}$ FDB. A) 20 μM ENBA (A1 agonist) in AMPK $\alpha1^{+/+}/\alpha2^{+/+}$ FDB. B) 20 μM ENBA (A1 agonist) in AMPK $\alpha1^{-/-}/\alpha2^{-/-}$ indKO FDB. C) 5 μM DPCPX (A1R antagonist) in AMPK $\alpha1^{+/+}/\alpha2^{+/+}$ FDB. D) DPCPX (A1R antagonist) in AMPK $\alpha1^{-/-}/\alpha2^{-/-}$ indKO FDB. Fatigue was elicited with 1 contraction every sec for 180 sec. Tetanic force is expressed as a percent of pre-fatigue tetanic force. Vertical bars represent S.E. of 5 muscles. * indicates a significant difference between control and ENBA-treated FDB, ANOVA, $P < 0.05$ (main effect).

Unstimulated force was also analyzed to determine the extent of any potential contractile dysfunction. At 20 µM, ENBA exposure had no statistically significant effect on unstimulated force development in either AMPK $\alpha1^{+/+}/\alpha2^{+/+}$ (Fig. 3.17A) or AMPK $\alpha1^{-/-}/\alpha2^{-/-}$ indKO FDB (Fig. 3.17B). However, ENBA exposure did cause a slight decrease in unstimulated force in AMPK $\alpha1^{+/+}/\alpha2^{+/+}$ FDB starting around 30 s of stimulation and resulting in 3% lower unstimulated force compared to control FDB upon reaching a plateau around 80 s while having the opposite effect in AMPK $\alpha1^{-/-}/\alpha2^{-/-}$ indKO FDB, increasing unstimulated force for the first 25 s of activity, resulting in ~3% greater unstimulated force compared to control upon normalizing at 30 s. 5µM DPCPX exposure also had no significant effect on unstimulated force in either AMPK $\alpha1^{+/+}/\alpha2^{+/+}$ or indKO FDB (Fig. 3.17 C,D).

THE EFFECTS OF MODULATING THE ACTIVITY OF BOTH ADENOSINE RECEPTORS AND AMPK

To further understand how adenosine, NECA and ENBA affected fatigue kinetics under different conditions, i.e., drug concentrations and AMPK activity, the differences in tetanic force between paired control and drug treated FDB were calculated. At 10 µM, adenosine reduced the rate at which tetanic force decreased especially during the first 60 sec, the greatest difference occurring at 25 sec when the decrease in tetanic force of adenosine-treated (10 µM) FDB was 6.4% less than that of control FDB (Fig. 3.18A). There was a significant difference in the adenosine effect between 10 and 20 µM (ANOVA, main effect). First, the slower decrease in tetanic force during the first 60 s at 10 µM was almost inexistent at 20 µM. Second, while the decrease in tetanic force of adenosine treated FDB during the last 2 min was less than in control at 10 µM,

FIGURE 3.17

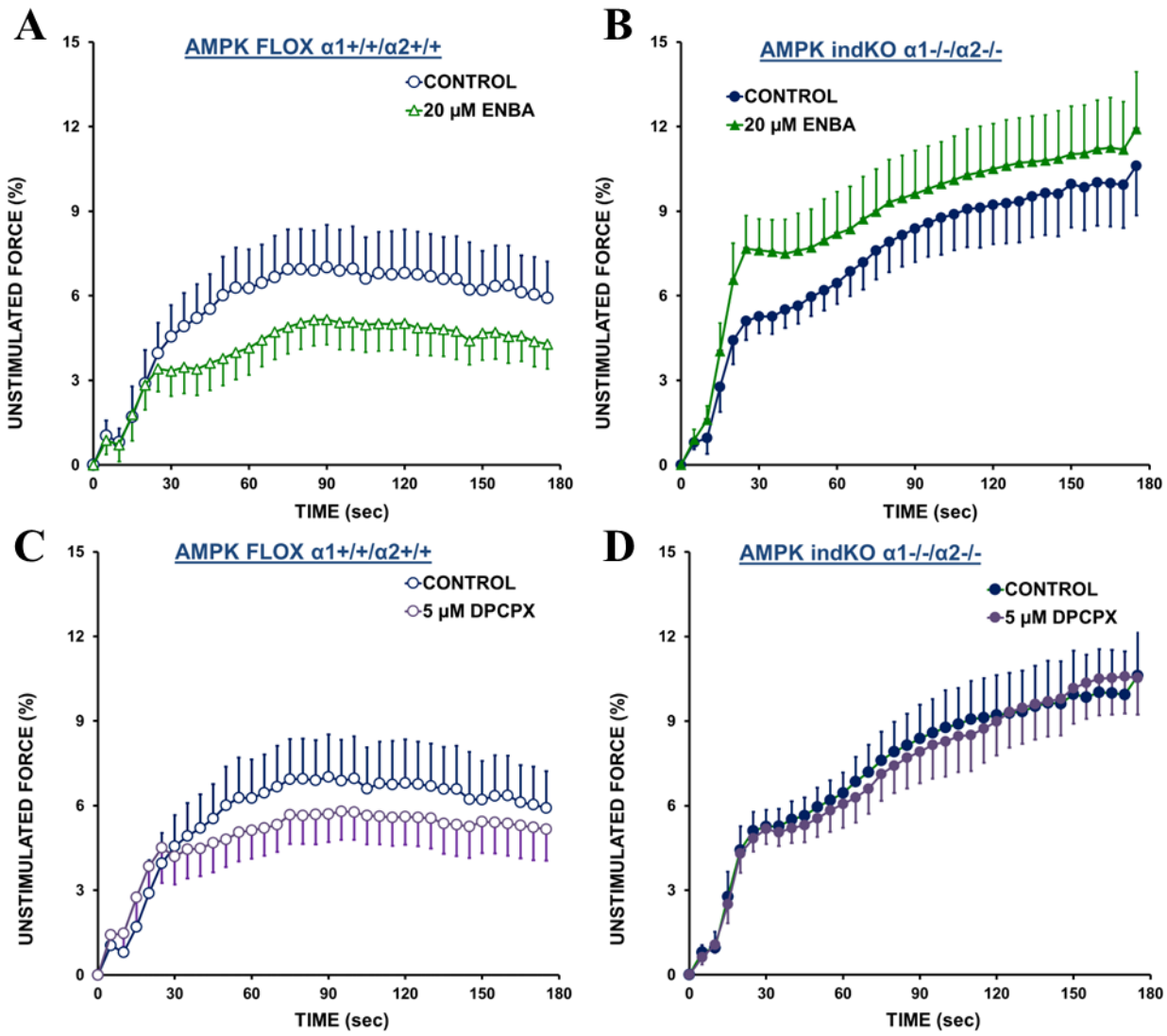

Figure 3.17: Neither ENBA nor DPCPX exposure significantly increased unstimulated force development in AMPK $\alpha1^{+/+}/\alpha2^{+/+}$ or AMPK $\alpha1^{-/-}/\alpha2^{-/-}$ indKO FDB. A) 20 μM ENBA (A1 agonist) in AMPK $\alpha1^{+/+}/\alpha2^{+/+}$ FDB. B) 20 μM ENBA (A1 agonist) in AMPK $\alpha1^{-/-}/\alpha2^{-/-}$ indKO FDB. C) 5 μM DPCPX (A1R antagonist) in AMPK $\alpha1^{+/+}/\alpha2^{+/+}$ FDB. D) DPCPX (A1R antagonist) in AMPK $\alpha1^{-/-}/\alpha2^{-/-}$ indKO FDB. Fatigue was elicited with 1 contraction every sec for 180 sec. Unstimulated force is expressed as a percent of maximum tetanic force at the onset of fatiguing stimulation. Vertical bars represent S.E. of 5 muscles. There was no significant difference between the various conditions, ANOVA: $P > 0.05$.

FIGURE 3.18

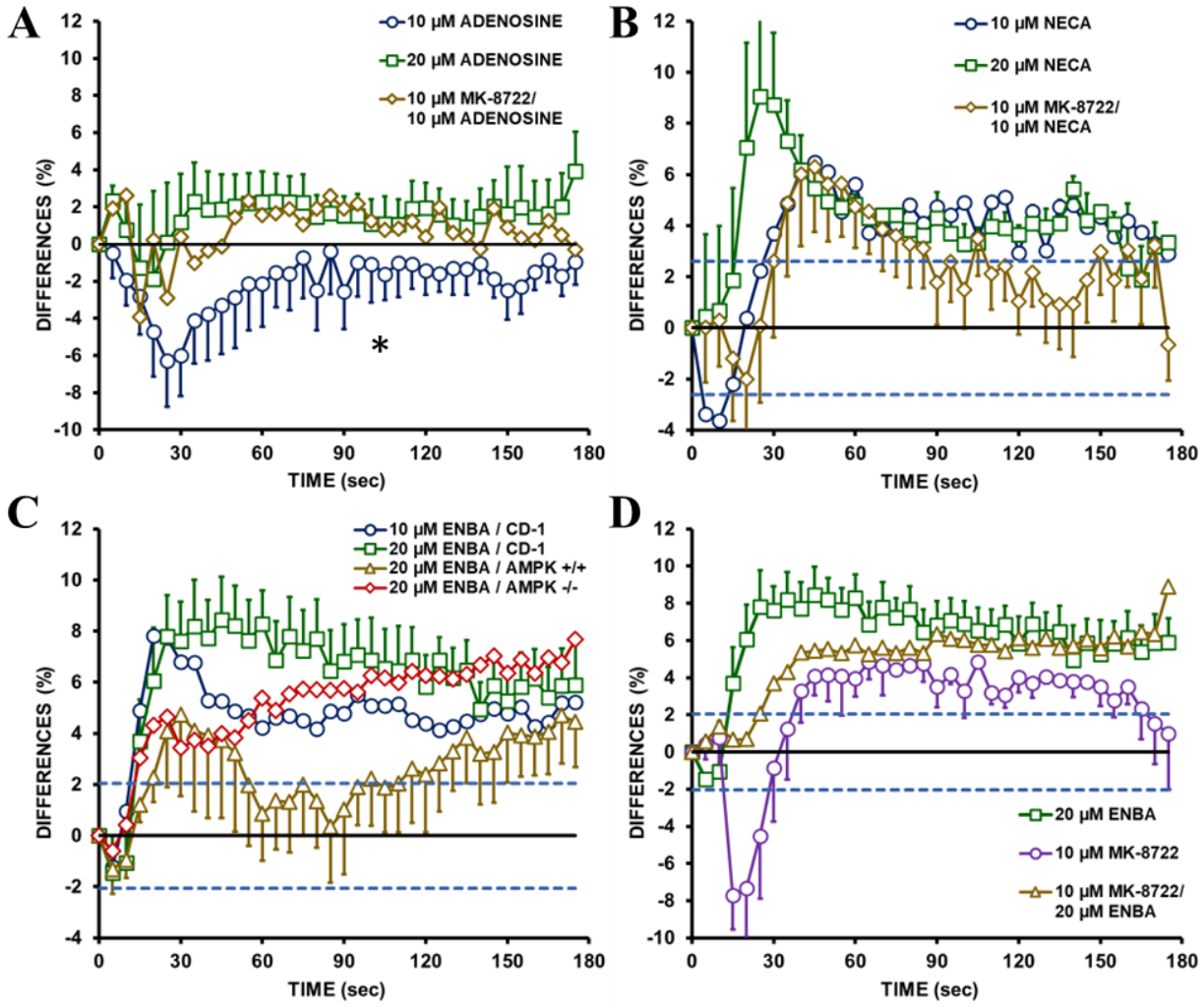

Figure 3.18: The effects of A) adenosine, B) NECA C) ENBA and D) MK-8722 by themselves and in combination on tetanic force loss during fatigue. Differences in tetanic force during fatigue were calculated by subtracting the tetanic force of drug-treated FDB from the value of the paired control FDB; i.e., positive values indicate how much more tetanic force loss occurred in drug-treated than in control FDB. Vertical bars represent the S.E. of 4-7 muscles (except 2 FDB for 10 µM MK-8722). For clarity, S.E. were removed for some conditions. * In A indicates a significant difference between 10 and 20 µM adenosine; ANOVA and L.S.D. $P < 0.05$ (drug main effect). Dashed blue horizontal lines in B-D represent the minimum difference necessary to achieve significant difference from 0% (horizontal black line); ANOVA, L.S.D. $P < 0.05$ (time main effect).

the reverse was observed at 20 µM. Co-activation of adenosine receptors with 10 µM adenosine and AMPK with 10 µM MK-8722 also resulted in an effect similar to 20 µM adenosine; i.e., no slower decrease in tetanic force during the first 60 s and slight increase in force loss during the last 2 min. NECA, which activates A1R, A2AR, and A2BR, had a similar effect on the initial slower decrease in tetanic force compared to adenosine. That is, 10 µM NECA initially reduced the decrease in tetanic force, while this effect was no longer observed at 20 µM NECA (Fig. 3.18B). There was, however, a major difference for the last 2 min as NECA increased the rate at which tetanic force decreased compared to control, an effect only observed at 20 µM adenosine. Co-activation of adenosine receptors and AMPK with 10 µM NECA and 10 µM MK-8722 resulted fatigue kinetics similar to that of 10 µM NECA.

Contrary to the adenosine and NECA effects, ENBA, which only activates A1R, did not cause the initial slower decrease in tetanic force. That is, ENBA, at 10 and 20 µM, consistently and significantly increased the rate at which tetanic force decreased during fatigue when compared to control conditions in FDB from CD-1, AMPK $a1^{+/+}$ $a2^{+/+}$ flox and AMPK $A1^{-/-}$ $a2^{-/-}$ indKO mice (Fig. 3.18C). The largest mean differences were observed with 20 µM ENBA in the FDB of CD-1 mice being 8.5% at 45 s of the fatigue bout decreasing slightly to 5.9% at the end. The peak difference between control and ENBA-treated FDB was the same with 10 µM ENBA, being 7.8% at 20 s, but thereafter became less than at 20 µM. The activation of AMPK alone with 10 µM MK-8722 resulted in significantly slower force tetanic force loss reaching a peak of 7.7% at 15 s followed by an increase in force loss after 30 s (Fig. 3.18D). Co-activation of AMPK with 10 µMK-8722 and a15 with 20 µM ENBA abolished the initial slower force loss and increased the extent of force loss when compared to 10 µM MK-8722 alone.

CHAPTER 4: DISCUSSION

The main findings of this study are as follows: 1) the presence of mRNA transcripts for all four adenosine receptor subtypes are expressed in isolated soleus, EDL, and FDB single fibers; 2) EDL muscles had significantly greater A1R protein content compared to soleus and FDB; 3) there was a small tendency for type IIB fibers to have the greatest amount of A1R protein content and type I to have the lowest, but the differences were not statistically significant; 4) at 2μM, neither AR agonists nor antagonists affected the decrease in tetanic force of FDB muscles when fatigue was triggered; 5) at 10 μM, adenosine reduced the rate of tetanic force loss while at 20 μM adenosine alone or in combination with 10 μM MK-8722 increased force loss; 6) NECA at 10 and 20 μM had the same effect on the initial slower force loss observed with adenosine, but contrary to adenosine it increased the extent of force loss during the last 2 min; 7) at 10 and 20 μM ENBA, an A1R agonist, caused a statistically significant and consistent greater force loss throughout the entire fatigue bout, an effect that was blocked by 5 μM DPCPX, an A1R antagonist; 8) activation of A1R with ENBA or A1R, A2AR, A2BR activation with NECA or adenosine prior to fatigue resulted in significant increase in AMPK phosphorylation after fatigue when compared to control; 9) compared to control, exposure to 10 μM MK-8722, an AMPK activator, gave rise to an initial slower decrease in tetanic force followed by significantly increased extent of force loss; 10) FDB muscles from a double knockout for α1 and α2 AMPK isoforms had significant greater extent of force loss compared to FDB muscles and greater unstimulated force during the last 100 sec of the fatigue bout compared to FDB expressing both AMPK isoforms; 11) co-activation of AMPK (with MK-8722) and A1R (with ENBA) or A1R, A2AR, and A3R (with NECA) increased the extent of

force loss similar to the effect of MK-or ENBA alone; 12) activation of A1R with ENBA in AMPK $\alpha1^{-/-}$ / $\alpha2^{-/-}$ indKO FDB increased force loss to a greater extent than in AMPK $\alpha1^{+/+}$ $\alpha2^{+/+}$ FDB.

ROLE OF ADENOSINE RECEPTORS IN THE MECHANISM OF MUSCLE FATIGUE

Part of the hypothesis of this study was that ARs trigger the fatigue process during muscular activity when metabolic stress occurs. To test this, t-tubular A1R protein content and the effects of modulating different adenosine isoforms on the kinetics of fatigue were determined.

A1R expression did not correlate with the fatigability of muscles and fiber types

Although the mRNA of all four adenosine receptors is expressed in skeletal muscle fibers, only the t-tubular A1R protein content was determined because activating A1R with ENBA caused a consistent and statistically significant greater loss of tetanic force throughout the entire fatigue bout, whereas a pan-activation of several adenosine receptors with either adenosine or NECA had complex effects on the fatigue kinetics. If A1R plays a major role in fatigue then the expectation was that the more fatigable a muscle or a fiber type is, the greater the t-tubular A1R protein content; i.e., in the order of FDB ~ EDL > Soleus and type IIB>IIX>IIA>I fibers. This concept was based on three facts. First, in isolated patch clamp membrane preparations from FVB muscle fibers, A1R activates K_{ATP} channels[75]. Second, the K_{ATP} channel is vital during fatigue to prevent damaging ATP depletion leading to several dysfunctions and fiber damage[45,46,49]. Third and most importantly, the distribution of t-tubular $K_{ir}6.2$ protein content, the subunit that makes up the

channel pore, correlates with fiber type fatiguability on the order of FDB ~ EDL > Soleus and Type IIB>IIX>IIA>I[41].

EDL, a muscle with low fatigue resistance, had greater t-tubular A1R protein content than soleus, a fatigue resistant muscle. However, this was the only result supporting the hypothesis for two reasons. First, although EDL and FDB muscles have similar fatigue kinetics when stimulated with one tetanic contraction per s[46,124], FDB muscles had similar A1R protein content as solei, and thus less than EDL. Second, there was a tendency for type IIB fibers to have greater t-tubular A1R content than type I fibers, but the differences were small and non-significant whereas for Kir6.2 protein content the differences between muscles and fiber types were large and significant. The lack of correlation between A1R protein content and muscle/fiber fatigability is either because A1R is not important in the mechanisms of muscle fatigue or it has other functions, such as stimulating glucose uptake (see Discussion in section entitled "SUMMING UP: THE ROLE OF ARs AND AMPK IN SKELETAL MUSCLE FATIGUE" below).

The complexity of activating adenosine receptors on fatigue kinetics in mouse FDB

This study is the first to document the impact of modulating adenosine receptor activity on contractile force during fatigue. According to the hypothesis, exposing FDB muscles to AR agonists will increase both the rate and extent of force loss during fatigue. At 2 μM, neither ENBA (A1R), PSB077 (A2AR), nor NECA (A1R, A2AR, A2BR) affected how i) tetanic force decreased and ii) how unstimulated force increased during fatigue as well as how tetanic force recovered after fatigue. These agonist concentrations were initially used as their K_D values are in the nM range; i.e., 2 μM should have been enough for maximal binding. However, much greater effective drug

concentrations are often required for in vitro muscle preparations, especially when said drugs are hydrophobic, as they incorporate themselves in the large amount of t-tubular and SR membranes present. For example, the K_i for the K_{ATP} channel blocker glibenclamide is 63 nM when measured under patch-clamp conditions, but typically requires an effective concentration of 10 μM in isolated skeletal muscles[119]. Indeed, at 10 and 20 μM adenosine, NECA, and ENBA significantly affected fatigue kinetics. It may then be argued that at 10 and 20 μM, NECA and ENBA had some non-specific effects. As discussed below, some of NECA's effects were similar to those of adenosine making it unlikely that NECA had non-specific effects. The ENBA-related effects at 20 μM, on the other hand, were completely abolished by co-exposure to 5 μM DPCPX, the A1R antagonist, suggesting that the ENBA's effects were via an activation of A1R.

The effect of pan-activation of all receptors with 10 μM adenosine was first an initial slower decrease in tetanic force during the first 60 s of the fatigue bout; an effect that was also observed with 10 μM NECA. This initial slower force decrease was not observed with 10 μM ENBA as it immediately caused greater force loss. These results suggest i) that A1R is a potential factor in the mechanism of fatigue and ii) A2AR and/or A2BR are involved in the initial slower decrease in force loss. While the increase in force loss via an activation of A1R is consistent throughout the fatigue bout, the adenosine and NECA's effects were more complex. First, the slower force loss did not occur with 20 μM adenosine and NECA as there was a tendency for faster force loss throughout the fatigue bout. Second, during the last 2 min of the fatigue bout 10 μM adenosine kept reducing force loss while 10 μM NECA eventually caused faster force loss. This suggests a concentration dependent effect for which at low concentrations of adenosine and NECA, an

activation of primarily A2AR and A2BR reduces the rate of fatigue while at higher concentrations fatigue rate is increased.

The next question is why there was a difference in the effects of adenosine and NECA exposure at 10 μM during the last 2 min of fatigue. Adenosine can be metabolized and therefore its final concentration in the interstial space from the surface fibers to those located in the muscle core depends on how fast metabolism occurs and how fast it diffuses throughout the muscle, the latter being more limited in t-tubules due to their small size. During light exercise at a work rate of 10 W, the interstitial adenosine concentration of human vastus lateralis muscle increases from 0.22 μM at rest to 1.14 μM, reaching 2.22 μM at 50 W[68]. A 50 W work load is not high enough to rapidly cause a fatigue state, which is observed at a work load of 90 W[125]. So, if at a bulk concentration of 10 μM the interstitial and especially the t-tubular adenosine concentration is within the 1-2 μM range, then its primary effect via A2AR and/or A2BR is most likely a decrease in the rate of force loss. A 28% decrease in total ATP occurs during the first 60 s when FDB is fatigued with 1 tetanic contraction per s[50]. As a metabolic stress occurs, which is associated with greater adenosine production[126], the slower rate of fatigue driven by A2AR and/or A2BR activation may switch to a faster fatigue rate driven primarily by other AR isoforms, the effect being greater with NECA because it cannot be metabolized and its concentration within the muscle is expected to remain close to 10 μM.

The next question is whether or not ARs are a major component in the mechanism of muscle fatigue, considering that none of the effects of modulating their activity caused changes exceeding 10% compared to an overall decrease in tetanic force of 80-85%. As discussed in the Introduction, there is an inverse relationship between adenosine production via the activity of

5'-nucleotidase (5'-NT), and AMPK activation. That is, 5'-NT overexpression in cultured Human Embryonic Kidney (HEK) cells results in lower oligomycin-induced AMPK activity while siRNA-mediated 5'-NT knockdown increases resting AMPK activity in cultured human myotubes[96,97]. Furthermore, AMPK activates K_{ATP} channels in cardiac muscles[57], and this channel is crucial in protecting muscle fiber function during fatigue in skeletal muscles[45,46,50]. This is why it was hypothesized that AMPK is also involved in triggering fatigue. The effects of AMPK activation during fatigue will first be discussed, followed by further discussion on the potential relationship between ARs and AMPK.

AMPK AFFECTS THE RATE OF TETANIC FORCE LOSS DURING FATIGUE

Activating AMPK with 10 µM MK-8722 initially caused a slower rate of force loss during the first 30 seconds of fatiguing stimulation. This phase was then followed by a faster decrease in tetanic force. These AMPK effects were therefore similar to the initial effects of 10 µM adenosine and full effect of 10 µM NECA, supporting a potential role for AMPK in fatigue. If this is the case and if AMPK's effects involve an activation of K_{ATP} channels, then AMPK-deficient FDB should behave like K_{ATP} channel deficient FDB during fatigue. That is, a lack of AMPK should result in contractile dysfunctions including greater fatigue rate and unstimulated. Indeed, AMPK$\alpha1^{-/-}/\alpha2^{-/-}$ FDB muscles fatigued faster and had greater increases in unstimulated force during fatigue than the control floxed AMPK$\alpha1^{+/+}/\alpha2^{+/+}$ FDB. The greater force loss and unstimulated force in AMPK$\alpha1^{-/-}/\alpha2^{-/-}$ FDB suggests that some degree of contractile dysfunction occurred, but much less than in K_{ATP} channel deficient FDB. That is, compared to control, the largest difference in tetanic force loss occurred at 20 s when the decrease in tetanic force was 13% greater in AMPK

deficient FDB compared to 30% for K_{ATP} channel deficient. Also, the difference for the increase in unstimulated force by the end of fatigue was just 5% in AMPK deficient FDB compared to 15% in K_{ATP} channel deficient FDB.

AMPK is an important factor in the regulation of mitochondrial content, glucose uptake and metabolism, glycogen content and fatty acid metabolism[91]. It is therefore possible that the faster decrease in tetanic force and greater increase in unstimulated force during fatigue in AMPK$\alpha1^{-/-}/\alpha2^{-/-}$ FDB is due to a decreased capacity to generate ATP. This is because a three-week incubation period post-tamoxifen injection was necessary to ensure complete AMPK deletion. However, using the same AMPK$\alpha1^{-/-}/\alpha2^{-/-}$ mouse model, Lantier et al. (2014)[95] reported the following major findings: i) fatigue resistance decreased in the soleus, an oxidative muscle, but not in the tibialis, a more glycolytic muscle like FDB; ii) there is no diffrence in citrate synthase activity or mitochondrial number, size, or structure in soleus and gastrocnemius muscle, albeit there was a decrease in mitochondrial maximal respiratory rate; iii) contraction-activated glucose uptake decreased in soleus muscles of male mice but not in female mice; iv) there is no decrease in glucose uptake in EDL (male and female mice), a muscle with similar fatigue kinetics to those of FDB. Furthermore, oxidative metabolism is not activated in FDB during the fatigue bout used in this study[50]. It is therefore unlikely that a decreased metabolic capacity to generate ATP in AMPK$\alpha1^{-/-}/\alpha2^{-/-}$ FDB was a major cause for the faster decrease in tetanic force and greater increase in unstimulated force observed in this study. One interesting observation from the AMPK$\alpha1^{-/-}/\alpha2^{-/-}$ mouse model is an increase in the number of tibialis and gastrocnemius muscle fibers containing centrally located nuclei[95]. This is actually another similarity to the observation of centrally located nuclei in K_{ATP} channel deficient tibialis, plantaris and EDL[49]. Thus, there are

three major similarities in the physiological response of AMPK- and K_{ATP} channel deficient muscles; i.e., faster rate of fatigue, greater increase in unstimulated force, and the presence of centrally located nuclei. This suggests that AMPK may also be important in protecting skeletal muscles against damaging ATP depletion as it has been demonstrated for K_{ATP} channels. However, future studies will be necessary to determine if AMPK is important in the activation of K_{ATP} channels.

CO-ACTIVATION OF ARs AND AMPK DOES NOT RESULT IN ADDITIVE OR SYNERGISTIC EFFECT ON THE FORCE LOSS DURING FATIGUE

The issue raised above was whether the small impact of activating ARs on the rate of fatigue was due to less AMPK activation, considering that the latter did contribute to faster fatigue rate. Three series of measurements provided evidence for the contrary. First, co-activation of AMPK and A1R as well as AMPK and A1R/A2AR/A2BR did not further increase the rate of fatigue above what was observed with an activation of ARs alone as expected if the latter lowered the extent of AMPK activation. In other words, concomitant activation of adenosine receptors and AMPK had neither an additive nor synergistic effect. Second, activating A1R in AMPK$\alpha1^{-/-}/\alpha2^{-/-}$ FDB did not result in a greater effect on the rate of fatigue. Third, and most importantly, at 10 and 20 μM, adenosine, NECA, and ENBA did not decrease, but actually increased the extent of T172 phosphorylation of the AMPKα subunit measured after fatigue. Evidence for AMPK activation via ARs has also been found in cardiomyocytes[127], liver cells[128], cartilage[129], and vascular epithelial cells[130], and this study now confirms that it also occurs in skeletal muscle. In fact, this latter result suggests that one mechanism of ARs may actually involve

an activation of AMPK, therefore explaining why co-activation of ARs and AMPK is neither additive nor synergistic. This possibility is supported by the effects of activating A1R with ENBA in AMPK$\alpha1^{-/-}/\alpha2^{-/-}$ FDB. That is, the increase in the rate of fatigue induced by ENBA occurred much slower in AMPK$\alpha1^{-/-}/\alpha2^{-/-}$ FDB than in wild type, but the final extent of force loss was the same (Fig. 3.18C). This suggests i) the initial increase in the rate of fatigue by ENBA involves an activation of AMPK via A1R and ii) other mechanisms exist by which A1R increases the rate of fatigue as it eventually became the same by the end of the fatigue bout.

SUMMING UP: THE ROLE OF ARs AND AMPK IN SKELETAL MUSCLE FATIGUE

From the results obtained in this study and above discussion, it can be proposed that i) activation of A2AR and/or A2BR at low agonist concentration leads to a slower fatigue rate while at high agonist concentration it increases the rate of fatigue; ii) activation of A1R leads to a faster fatigue rate; iii) AMPK activation increases the rate of fatigue and a AMPK deficiency results in contractile dysfunctions and fiber damage as observed in K_{ATP} channel deficient muscles; iv) co-activation of ARs and AMPK do not result in an additive or synergistic effect possibly because AR activation leads to an increased AMPK activity via an increased T172 phosphorylation of the AMPKα subunit.

An important issue as raised in the above discussion is whether ARs and AMPK are important factors in the mechanism of fatigue, considering that their effects on the rate of fatigue did not exceed 10% compared to an 80-85% overall decrease in tetanic force. It is possible that this study's use of FDB bundles masked some of the effects of AR/AMPK activation on fatigue. A study by Hesse (2019) found that removing glucose from the extracellular space increases the

rate of fatigue by about 10% in FDB bundles, suggesting a minor contribution of extracellular glucose for the ATP production during fatigue[131]. However, contrary to the large decrease in tetanic force during the first 60 s of the fatigue bout in FDB bundles [131], there is no sign of fatigue in the first 60 s when single FDB fibers are used. More importantly, removing extracellular glucose results in statistically significant greater decrease in Ca^{2+} release (and therefore reduced contractile) during fatigue, now suggesting that extracellular glucose is important in increasing fatigue resistance. The reason for the difference between FDB bundles and single fibers is that an anoxic/hypoxic condition is expected to occur in the middle core of the muscle in FDB bundles, while single fibers are completely surrounded by extracellular fluid[47,132]. It is therefore more than likely that hypoglycemia also occurs in FDB bundles, and the anoxic/hypoxic/hypoglycemic core contributes to a much faster and greater rate of fatigue in bundles than in single fibers, and possibly makes it more difficult to observe any effect of modulating ARs and AMPK activity. In other words, it is possible that the small observed impact of activating ARs and AMPK in FDB bundles will become much greater in single fibers.

Another factor to consider is the slower rate of fatigue that has been observed with low concentrations of adenosine and NECA agonists that activate ARs, as well as MK-8722 that activates AMPK. First, it suggests that there are two opposite effects, and it is possible that the mechanism responsible for the initial slower fatigue rate somehow reduces the extent of the expected increase in fatigue rate, at least for adenosine, NECA, and MK-8722. Second, the mechanism behind this slower fatigue rate may involve increased glucose uptake. A1R activation does not affect glucose uptake at rest, but it does increase both insulin- and exercise-induced glucose uptake via greater GLUT4 membrane translocation[77,78,133]. A2AR and A2BR may also

affect glucose uptake in skeletal muscle as they improve insulin sensitivity in normal mice and increase glucose uptake in skeletal muscles[134,135]. Finally, AMPK also increases glucose uptake via GLUT4 translocation in addition to ATP production[91]. Considering that i) FDB were incubated 30 min prior to the fatigue bout, ii) increasing extracellular glucose improves fatigue resistance[136] while iii) removing it has the opposite effect[131], it is therefore likely that greater glucose uptake prior to and during the initial period of the fatigue bout is responsible for the slower rate of fatigue. Then, as hypoglycemia develops the rate of fatigue increases and may be responsible for the apparent faster rate of fatigue in the presence of MK-8722 and high adenosine and NECA concentrations compared to controls.

CONCLUSION

The rate of fatigue determined from the decrease in tetanic force over time was affected by the modulation of AR and AMPK activity in mouse FDB. At low concentrations of pan-AR activators adenosine or NECA, the rate of fatigue in FDB bundles was initially slower compared to control FDB for about 60 s, before the rate of fatigue increased, with NECA exposure causing an overall greater extent of fatigue than controls. An activation of A1R with ENBA, on the other hand, resulted in a greater fatigue rate throughout the entire fatigue bout. These results suggest that the initial slower fatigue rate is related to an activation of A2AR and/or A2BR while the function of A1R is to trigger faster force loss. Interestingly, the initial slower rate of fatigue was abolished in the presence of higher concentrations of adenosine or NECA, suggesting that the effects of A2AR and/or A2BR may be physiologically dependent on adenosine concentration. An

activation of AMPK also resulted in an initial slower rate of fatigue followed by faster rate compared to control.

Co-activation of ARs and AMPK did not result in any additive or synergistic effects possibly because adenosine, NECA, and ENBA all increased AMPK activity via the phosphorylation of T172 of the α subunit. This result also raises the possibility that one mechanism of action for ARs is an activation of AMPK. Contractile dysfunction, shown by a faster rate of fatigue and greater increase in unstimulated force, occurred in AMPK-deficient FDB while another study observed the occurrence of fiber damage in AMPK-deficient skeletal muscles. The occurrence of this dysfunction and fiber damage is similar to that observed in K_{ATP} channel deficient muscles, suggesting that like K_{ATP} channels, AMPK may be important for preventing damaging ATP depletion during times of metabolic stress such as fatigue. Future studies will now be necessary to determine i) if the effects of modulating ARs and AMPK are much greater in single skeletal muscle fibers as it had been observed in a previous study on the effect of removing extracellular glucose; ii) if one mechanism for ARs during fatigue is via an activation of AMPK; iii) if the initial slow rate of fatigue observed under some conditions are related to an increased glucose uptake during the pre-fatigue incubation and/or during the first 60 s of fatigue period; and iv) if the mechanism of action for ARs and AMPK also involves the activation of Cl^- ClC-1 and K_{ATP} channels, two major components in the mechanism of fatigue.

REFERENCES

1. Sahlin K, Tonkonogi M, Söderlund K. Energy supply and muscle fatigue in humans. *Acta Physiol Scand*. 1998;162(3):261-266. doi:10.1046/J.1365-201X.1998.0298F.X

2. Fitts RH. Cellular mechanisms of muscle fatigue. *Physiol Rev*. 1994;74(1):49-94. doi:10.1152/physrev.1994.74.1.49

3. Westerblad H, Allen DG. Changes of myoplasmic calcium concentration during fatigue in single mouse muscle fibers. *J Gen Physiol*. 1991;98(3):615. doi:10.1085/JGP.98.3.615

4. Dulhunty AF. EXCITATION–CONTRACTION COUPLING FROM THE 1950s INTO THE NEW MILLENNIUM. *Clin Exp Pharmacol Physiol*. 2006;33(9):763-772. doi:10.1111/J.1440-1681.2006.04441.X

5. Allen DG, Lamb GD, Westerblad H. Skeletal muscle fatigue: Cellular mechanisms. *Physiol Rev*. 2008;88(1):287-332. doi:10.1152/physrev.00015.2007

6. Frontera WR, Ochala J. Skeletal Muscle: A Brief Review of Structure and Function. *Calcif Tissue Int*. 2015;96(3):183-195. doi:10.1007/s00223-014-9915-y

7. Romijn JA, Coyle EF, Sidossis LS, et al. Regulation of endogenous fat and carbohydrate metabolism in relation to exercise intensity and duration. *https://doi.org/101152/ajpendo19932653E380*. 1993;265(3 28-3). doi:10.1152/AJPENDO.1993.265.3.E380

8. Westerblad H, Bruton JD, Katz A. Skeletal muscle: Energy metabolism, fiber types, fatigue and adaptability. *Exp Cell Res*. 2010;316(18):3093-3099. doi:10.1016/J.YEXCR.2010.05.019

9. Hargreaves M. Skeletal muscle metabolism during exercise in humans. In: *Clinical and Experimental Pharmacology and Physiology*. Vol 27. John Wiley & Sons, Ltd; 2000:225-228. doi:10.1046/j.1440-1681.2000.03225.x

10. Schiaffino S, Sandri M, Murgia M. Activity-dependent signaling pathways controlling muscle diversity and plasticity. *Physiology*. 2007;22(4):269-278. doi:10.1152/PHYSIOL.00009.2007/ASSET/IMAGES/LARGE/Y0009-7-04.JPEG

11. Macintosh BR, Holash RJ, Renaud JM. Skeletal muscle fatigue-regulation of excitation-contraction coupling to avoid metabolic catastrophe. *J Cell Sci*. 2012;125(9):2105-2114. doi:10.1242/jcs.093674

12. Cairns SP, Leader JP, Loiselle DS, Higgins A, Lin W, Renaud JM. Extracellular Ca2+-induced force restoration in K+-depressed skeletal muscle of the mouse involves an elevation of [K+]i: Implications for fatigue. *J Appl Physiol*. 2015;118(6):662-674. doi:10.1152/japplphysiol.00705.2013

13. Bouclin R, Charbonneau E, Renaud JM. Na+ and K+ effect on contractility of frog sartorius muscle: Implication for the mechanism of fatigue. *Am J Physiol Cell Physiol*. 1995;268(6 37-6). doi:10.1152/ajpcell.1995.268.6.c1528

14. Lännergren J, Westerblad H. Force decline due to fatigue and intracellular acidification in isolated fibres from mouse skeletal muscle. *J Physiol*. 1991;434(1):307-322. doi:10.1113/jphysiol.1991.sp018471

15. Allen DG, Westerblad H. Role of phosphate and calcium stores in muscle fatigue. *J Physiol*. 2001;536(Pt 3):657. doi:10.1111/J.1469-7793.2001.T01-1-00657.X

16. Dutka TL, Cole L, Lamb GD. Calcium phosphate precipitation in the sarcoplasmic reticulum reduces action potential-mediated Ca2+ release in mammalian skeletal muscle. *Am J Physiol Cell Physiol*. 2005;289(6). doi:10.1152/AJPCELL.00273.2005

17. Fryer MW, Owen VJ, Lamb GD, Stephenson DG. Effects of creatine phosphate and P(i) on Ca2+ movements and tension development in rat skinned skeletal muscle fibres. *J Physiol*. 1995;482(Pt 1):123. doi:10.1113/JPHYSIOL.1995.SP020504

18. Laver DR, Lenz GKE, Lamb GD. Regulation of the calcium release channel from rabbit skeletal muscle by the nucleotides ATP, AMP, IMP and adenosine. *J Physiol*. 2001;537(Pt 3):763. doi:10.1111/J.1469-7793.2001.00763.X

19. Meissner G, Darling E, Eveleth J. Kinetics of rapid Ca2+ release by sarcoplasmic reticulum. Effects of Ca2+, Mg2+, and adenine nucleotides. *Biochemistry*. 1986;25(1):236-244. doi:10.1021/BI00349A033

20. Leermakers PA, Dybdahl KLT, Husted KS, et al. Depletion of ATP Limits Membrane Excitability of Skeletal Muscle by Increasing Both ClC1-Open Probability and Membrane Conductance. *Front Neurol*. 2020;11:541. doi:10.3389/FNEUR.2020.00541/BIBTEX

21. Pedersen TH, de Paoli FV, Flatman JA, Nielsen OB. Regulation of ClC-1 and KATP channels in action potential-firing fast-twitch muscle fibers. *Journal of General Physiology*. 2009;134(4):309-322. doi:10.1085/jgp.200910290

22. Pedersen TH, de Paoli F, Nielsen OB. Increased excitability of acidified skeletal muscle: Role of chloride conductance. *Journal of General Physiology*. 2005;125(2):237-246. doi:10.1085/jgp.200409173

23. Riisager A, de Paoli FV, Yu WP, Pedersen TH, Chen TY, Nielsen OB. Protein kinase C-dependent regulation of ClC-1 channels in active human muscle and its effect on fast and slow gating. *J Physiol*. 2016;594(12):3391-3406. doi:10.1113/JP271556

24. Pedersen TH, Macdonald WA, de Paoli FV, Gurung IS, Nielsen OB. Comparison of regulated passive membrane conductance in action potential-firing fast- and slow-twitch muscle. *Journal of General Physiology*. 2009;134(4):323-337. doi:10.1085/jgp.200910291

25. Wang X, Nawaz M, Dupont C, et al. The role of action potential changes in depolarization-induced failure of excitation contraction coupling in mouse skeletal muscle. *Elife*. 2022;11. doi:10.7554/ELIFE.71588

26. Pedersen TH, Riisager A, de Paoli FV, Chen TY, Nielsen OB. Role of physiological ClC-1 Cl- ion channel regulation for the excitability and function of working skeletal muscle. *J Gen Physiol*. 2016;147(4):291-308. doi:10.1085/jgp.201611582

27. Weiss DS, Magleby KL. Voltage dependence and stability of the gating kinetics of the fast chloride channel from rat skeletal muscle. *J Physiol*. 1990;426(1):145. doi:10.1113/JPHYSIOL.1990.SP018131

28. Fahlke C, Rüdel R. Chloride currents across the membrane of mammalian skeletal muscle fibres. *J Physiol*. 1995;484(Pt 2):355. doi:10.1113/JPHYSIOL.1995.SP020670

29. Hodgkin AL, Horowicz P. THE INFLUENCE OF POTASSIUM AND CHLORIDE IONS ON THE MEMBRANE POTENTIAL OF SINGLE MUSCLE FIBRES. *J Physiol (I959)*. 48:27-60.

30. Bennetts B, Rychkov GY, Ng HL, et al. Cytoplasmic ATP-sensing domains regulate gating of skeletal muscle ClC-1 chloride channels. *J Biol Chem*. 2005;280(37):32452-32458. doi:10.1074/JBC.M502890200

31. Tseng PY, Yu WP, Liu HY, Zhang XD, Zou X, Chen TY. Binding of ATP to the CBS domains in the C-terminal region of CLC-1. *J Gen Physiol*. 2011;137(4):357-368. doi:10.1085/JGP.201010495

32. Bennetts B, Rychkov GY, Ng HL, et al. Cytoplasmic ATP-sensing domains regulate gating of skeletal muscle ClC-1 chloride channels. *J Biol Chem*. 2005;280(37):32452-32458. doi:10.1074/JBC.M502890200

33. Karatzaferi C, de Haan A, Ferguson RA, van Mechelen W, Sargeant AJ. Phosphocreatine and ATP content in human single muscle fibres before and after maximum dynamic exercise. *Pflugers Arch*. 2001;442(3):467-474. doi:10.1007/s004240100552

34. McKenna MJ, Bangsbo J, Renaud JM. Muscle K+, Na+, and Cl- disturbances and Na+-K+ pump inactivation: Implications for fatigue. *J Appl Physiol*. 2008;104(1):288-295. doi:10.1152/japplphysiol.01037.2007

35. Ammar T, Lin W, Higgins A, Hayward LJ, Renaud JM. Understanding the physiology of the asymptomatic diaphragm of the M1592V hyperkalemic periodic paralysis mouse. *J Gen Physiol*. 2015;146(6):509-525. doi:10.1085/jgp.201511476

36. Uwera F, Ammar T, McRae C, Hayward LJ, Renaud JM. Lower Ca2+ enhances the K+-induced force depression in normal and HyperKPP mouse muscles. *Journal of General Physiology*. 2020;152(7). doi:10.1085/jgp.201912511

37. Fraser JA, Huang CLH, Pedersen TH. Relationships between resting conductances, excitability, and t-system ionic homeostasis in skeletal muscle. *J Gen Physiol*. 2011;138(1):95. doi:10.1085/JGP.201110617

38. Pedersen TH, Huang CLH, Fraser JA. An analysis of the relationships between subthreshold electrical properties and excitability in skeletal muscle. *J Gen Physiol*. 2011;138(1):73. doi:10.1085/JGP.201010510

39. Spruce AE, Standen NB, Stanfield PR. Voltage-dependent ATP-sensitive potassium channels of skeletal muscle membrane. *Nature*. 1985;316(6030):736-738. doi:10.1038/316736A0

40. Foster MN, Coetzee WA. KATP Channels in the Cardiovascular System. *Physiol Rev*. 2016;96(1):177-252. doi:10.1152/PHYSREV.00003.2015

41. Banas K, Clow C, Jasmin BJ, Renaud JM. The K ATP channel Kir6.2 subunit content is higher in glycolytic than oxidative skeletal muscle fibers . *American Journal of Physiology-Regulatory, Integrative and Comparative Physiology*. 2011;301(4):R916-R925. doi:10.1152/ajpregu.00663.2010

42. Gong B, Legault D, Miki T, Seino S, Renaud JM. KATP channels depress force by reducing action potential amplitude in mouse EDL and soleus muscle. *Am J Physiol Cell Physiol*. 2003;285(6 54-6). doi:10.1152/AJPCELL.00278.2003/ASSET/IMAGES/LARGE/H01231741010.JPEG

43. Zhu Z, Sierra A, Burnett CML, et al. Sarcolemmal ATP-sensitive potassium channels modulate skeletal muscle function under low-intensity workloads. *Journal of General Physiology*. 2014;143(1):119-134. doi:10.1085/jgp.201311063

44. Gong B, Legault D, Miki T, Seino S, Renaud JM. KATP channels depress force by reducing action potential amplitude in mouse EDL and soleus muscle. *Am J Physiol Cell Physiol*. 2003;285(6 54-6):1464-1474. doi:10.1152/AJPCELL.00278.2003/ASSET/IMAGES/LARGE/H01231741010.JPEG

45. Cifelli C, Boudreault L, Gong B, Bercier JP, Renaud JM. Contractile dysfunctions in ATP-dependent K+ channel-deficient mouse muscle during fatigue involve excessive depolarization and Ca2+ influx through L-type Ca2+ channels. *Exp Physiol*. 2008;93(10):1126-1138. doi:10.1113/expphysiol.2008.042572

46. Cifelli C, Bourassa F, Gariépy L, Banas K, Benkhalti M, Renaud JM. KATP channel deficiency in mouse flexor digitorum brevis causes fibre damage and impairs Ca2+ release and force development during fatigue in vitro. *Journal of Physiology*. 2007;582(2):843-857. doi:10.1113/jphysiol.2007.130955

47. Selvin D, Renaud JM. Changes in myoplasmic Ca2+ during fatigue differ between FDB fibers, between glibenclamide-exposed and Kir6.2-/- fibers and are further modulated by verapamil. *Physiol Rep*. 2015;3(3):e12303. doi:10.14814/PHY2.12303

48. Gramolini A, Renaud JM. Blocking ATP-sensitive K+ channel during metabolic inhibition impairs muscle contractility. *https://doi.org/101152/ajpcell19972726C1936*. 1997;272(6 41-6). doi:10.1152/AJPCELL.1997.272.6.C1936

49. Thabet M, Miki T, Seino S, Renaud JM. Treadmill running causes significant fiber damage in skeletal muscle of KATP channel-deficient mice. *Physiol Genomics*. 2005;22(2):204-212. doi:10.1152/physiolgenomics.00064.2005

50. Scott K, Benkhalti M, Calvert ND, et al. K ATP channel deficiency in mouse FDB causes an impairment of energy metabolism during fatigue. *Am J Physiol Cell Physiol*. 2016;311:559-571. doi:10.1152/ajpcell.00137.2015

51. Pandya JD, Nukala VN, Sullivan PG. Concentration dependent effect of calcium on brain mitochondrial bioenergetics and oxidative stress parameters. *Front Neuroenergetics*. 2013;5(DEC). doi:10.3389/FNENE.2013.00010

52. Antcliff JF, Haider S, Proks P, Sansom MSP, Ashcroft FM. Functional analysis of a structural model of the ATP-binding site of the KATP channel Kir6.2 subunit. *EMBO J*. 2005;24(2):229-239. doi:10.1038/SJ.EMBOJ.7600487

53. Karatzaferi C, De Haan A, Ferguson RA, Van Mechelen W, Sargeant AJ. Phosphocreatine and ATP content in human single muscle fibres before and after maximum dynamic exercise. *Pflugers Arch*. 2001;442(3):467-474. doi:10.1007/S004240100552/METRICS

54. Lasley RD, Narayan P, Mentzer RM. New insights into adenosine receptor modulation of myocardial ischemia-reperfusion injury. *Drug Dev Res*. 2001;52(1-2):357-365. doi:10.1002/DDR.1135

55. Lasley RD, Kristo G, Keith BJ, Mentzer RM. The A2a/A2b receptor antagonist ZM-241385 blocks the cardioprotective effect of adenosine agonist pretreatment in in vivo rat myocardium. *Am J Physiol Heart Circ Physiol*. 2007;292(1):426-431. doi:10.1152/AJPHEART.00675.2006/ASSET/IMAGES/LARGE/ZH40010771910004.JPEG

56. Yoshida H, Bao L, Kefaloyianni E, et al. AMP-activated protein kinase connects cellular energy metabolism to K ATP channel function. *J Mol Cell Cardiol*. 2012;52(2):410-418. doi:10.1016/j.yjmcc.2011.08.013

57. Sukhodub A, Jovanović S, Qingyou DU, et al. AMP-Activated Protein Kinase Mediates Preconditioning in Cardiomyocytes by Regulating Activity and Trafficking of Sarcolemmal ATP-Sensitive K+ Channels. *J Cell Physiol*. 2007;210(1):224. doi:10.1002/JCP.20862

58. Zheng J, Wang R, Zambraski E, Wu D, Jacobson KA, Liang BT. Protective roles of adenosine A1, A2A, and A3 receptors in skeletal muscle ischemia and reperfusion injury. *Am J Physiol Heart Circ Physiol*. 2007;293(6):H3685-91. doi:10.1152/ajpheart.00819.2007

59. Riquelme MA, Cea LA, Vega JL, et al. The ATP required for potentiation of skeletal muscle contraction is released via pannexin hemichannels. *Neuropharmacology*. 2013;75:594-603. doi:10.1016/j.neuropharm.2013.03.022

60. Buvinic S, Almarza G, Bustamante M, et al. ATP released by electrical stimuli elicits calcium transients and gene expression in skeletal muscle. *Journal of Biological Chemistry*. 2009;284(50):34490-34505. doi:10.1074/jbc.M109.057315

61. Bornø A, Ploug T, Bune LT, Rosenmeier JB, Thaning P. Purinergic receptors expressed in human skeletal muscle fibres. *Purinergic Signal*. 2012;8(2):255-264. doi:10.1007/s11302-011-9279-y

62. Locovei S, Wang J, Dahl G. Activation of pannexin 1 channels by ATP through P2Y receptors and by cytoplasmic calcium. *FEBS Lett*. 2006;580(1):239-244. doi:10.1016/J.FEBSLET.2005.12.004

63. Sandonà D, Danieli-Betto D, Germinario E, et al. The T-tubule membrane ATP-operated P2X4 receptor influences contractility of skeletal muscle. *The FASEB Journal*. 2005;19(9):1184-1186. doi:10.1096/FJ.04-3333FJE

64. Voss AA. Extracellular ATP inhibits chloride channels in mature mammalian skeletal muscle by activating P2Y1 receptors. *Journal of Physiology*. 2009;587(23):5739-5752. doi:10.1113/jphysiol.2009.179275

65. Zimmermann H. Extracellular metabolism of ATP and other nucleotides. *Naunyn-Schmiedeberg's Archives of Pharmacology 2000 362:4*. 2000;362(4):299-309. doi:10.1007/S002100000309

66. Hellsten Y. The effect of muscle contraction on the regulation of adenosine formation in rat skeletal muscle cells. *Journal of Physiology*. 1999;518(3):761-768. doi:10.1111/j.1469-7793.1999.0761p.x

67. Lynge J, Juel C, Hellsten Y. Extracellular formation and uptake of adenosine during skeletal muscle contraction in the rat: role of adenosine transporters. *J Physiol*. 2001;537(Pt 2):597. doi:10.1111/J.1469-7793.2001.00597.X

68. Hellsten Y, Maclean D, Rådegran G, Saltin B, Bangsbo J. Adenosine Concentrations in the Interstitium of Resting and Contracting Human Skeletal Muscle. *Circulation*. 1998;98(1):6-8. doi:10.1161/01.CIR.98.1.6

69. Mortensen SP, Nyberg M, Thaning P, Saltin B, Hellsten Y. Adenosine contributes to blood flow regulation in the exercising human leg by increasing prostaglandin and nitric oxide formation. *Hypertension*. 2009;53(6):993-999. doi:10.1161/HYPERTENSIONAHA.109.130880

70. Lynge, Hellsten. Distribution of adenosine A1, A(2A) and A(2B) receptors in human skeletal muscle. *Acta Physiol Scand*. 2000;169(4):283-290. doi:10.1046/j.1365-201X.2000.00742.x

71. Olah ME, Stiles GL. Adenosine receptor subtypes: characterization and therapeutic regulation. *Annu Rev Pharmacol Toxicol*. 1995;35(1):581-606. doi:10.1146/ANNUREV.PA.35.040195.003053

72. Murry CE, Jennings RB, Reimer KA. Preconditioning with ischemia: a delay of lethal cell injury in ischemic myocardium. *Circulation*. 1986;74(5):1124-1136. doi:10.1161/01.CIR.74.5.1124

73. Yao Z, Mizumura T, Mei DA, Gross GJ. KATP channels and memory of ischemic preconditioning in dogs: Synergism between adenosine and KATP channels. *Am J Physiol Heart Circ Physiol*. 1997;41(1). doi:10.1152/ajpheart.1997.272.1.h334

74. Mei HF, Poonit N, Zhang YC, et al. Activating adenosine A1 receptor accelerates PC12 cell injury via ADORA1/PKC/KATP pathway after intermittent hypoxia exposure. *Mol Cell Biochem*. 2018;446(1-2):161-170. doi:10.1007/s11010-018-3283-2

75. Barrett-Jolley R, Comtois A, Davies NW, Stanfield PR, Standen NB. Effect of adenosine and intracellular GTP on KATP channels of mammalian skeletal muscle. *J Membr Biol*. 1996;152(2):111-116. doi:10.1007/s002329900090

76. Clark KI, Barry SR. Aminophylline enhances resting Ca2+ concentrations and twitch tension by adenosine receptor blockade in Rana pipiens. *J Physiol*. 1994;481 (Pt 1)(Pt 1):129-137. doi:10.1113/JPHYSIOL.1994.SP020424

77. Derave W, Hespel P. Role of adenosine in regulating glucose uptake during contractions and hypoxia in rat skeletal muscle. *J Physiol*. 1999;515 (Pt 1)(Pt 1):255-263. doi:10.1111/J.1469-7793.1999.255AD.X

78. Thong FSL, Lally JSV, Dyck DJ, Greer F, Bonen A, Graham TE. Activation of the A1 adenosine receptor increases insulin-stimulated glucose transport in isolated rat soleus muscle. *Applied Physiology, Nutrition and Metabolism*. 2007;32(4):701-710. doi:10.1139/H07-039/ASSET/IMAGES/LARGE/H07-039F5.JPEG

79. Cairns SP, Borrani F. β-Adrenergic modulation of skeletal muscle contraction: key role of excitation–contraction coupling. *J Physiol*. 2015;593(21):4713-4727. doi:10.1113/JP270909

80. Calebiro D, Koszegi Z. The subcellular dynamics of GPCR signaling. *Mol Cell Endocrinol*. 2019;483:24-30. doi:10.1016/j.mce.2018.12.020

81. Bers DM, Zaccolo M. Whole-Cell cAMP and PKA Activity are Epiphenomena, Nanodomain Signaling Matters. *Physiology*. 2019;34(4):240-249. doi:10.1152/physiol.00002.2019

82. Xiao CY, Yuhki KI, Hara A, et al. Prostaglandin E2 Protects the Heart From Ischemia-Reperfusion Injury via Its Receptor Subtype EP4. *Circulation*. 2004;109(20):2462-2468. doi:10.1161/01.CIR.0000128046.54681.97

83. Duarte T, Menezes-Rodrigues FS, Godinho RO. Contribution of the extracellular cAMP-adenosine pathway to dual coupling of β 2-adrenoceptors to G s and G i proteins in mouse skeletal muscle. *Journal of Pharmacology and Experimental Therapeutics*. 2012;341(3):820-828. doi:10.1124/jpet.112.192997

84. Kjøbsted R, Hingst JR, Fentz J, et al. AMPK in skeletal muscle function and metabolism. *FASEB Journal*. 2018;32(4):1741-1777. doi:10.1096/fj.201700442R

85. Mounier R, Théret M, Lantier L, Foretz M, Viollet B. Expanding roles for AMPK in skeletal muscle plasticity. *Trends in Endocrinology & Metabolism*. 2015;26(6):275-286. doi:10.1016/J.TEM.2015.02.009

86. Birk JB, Wojtaszewski JFP. Predominant α2/β2/γ3 AMPK activation during exercise in human skeletal muscle. *J Physiol*. 2006;577(3):1021-1032. doi:10.1113/JPHYSIOL.2006.120972

87. Barnes BR, Marklund S, Steiler TL, et al. The 5'-AMP-activated Protein Kinase γ3 Isoform Has a Key Role in Carbohydrate and Lipid Metabolism in Glycolytic Skeletal Muscle. *Journal of Biological Chemistry*. 2004;279(37):38441-38447. doi:10.1074/JBC.M405533200

88. Koh HJ, Brandauer J, Goodyear LJ. LKB1 and AMPK and the regulation of skeletal muscle metabolism. *Curr Opin Clin Nutr Metab Care*. 2008;11(3):227. doi:10.1097/MCO.0B013E3282FB7B76

89. Li L, Chen Y, Gibson SB. Starvation-induced autophagy is regulated by mitochondrial reactive oxygen species leading to AMPK activation. *Cell Signal*. 2013;25(1):50-65. doi:10.1016/J.CELLSIG.2012.09.020

90. Rahman M, Mofarrahi M, Kristof AS, Nkengfac B, Harel S, Hussain SNA. Reactive oxygen species regulation of autophagy in skeletal muscles. *Antioxid Redox Signal*. 2014;20(3):443-459. doi:10.1089/ARS.2013.5410/SUPPL_FILE/SUPP_FIGURE6.PDF

91. Merrill GF, Kurth EJ, Hardie DG, Winder WW. AICA riboside increases AMP-activated protein kinase, fatty acid oxidation, and glucose uptake in rat muscle. *Am J Physiol*. 1997;273(6). doi:10.1152/AJPENDO.1997.273.6.E1107

92. Hunter RW, Treebak JT, Wojtaszewski JFP, Sakamoto K. Molecular mechanism by which AMP-activated protein kinase activation promotes glycogen accumulation in muscle. *Diabetes*. 2011;60(3):766-774. doi:10.2337/DB10-1148/-/DC1

93. Lin L, Chen K, Khalek WA, et al. Regulation of skeletal muscle oxidative capacity and muscle mass by SIRT3. *PLoS One*. 2014;9(1). doi:10.1371/JOURNAL.PONE.0085636

94. Mu J, Brozinick JT, Valladares O, Bucan M, Birnbaum MJ. A role for AMP-activated protein kinase in contraction- and hypoxia-regulated glucose transport in skeletal muscle. *Mol Cell*. 2001;7(5):1085-1094. doi:10.1016/S1097-2765(01)00251-9

95. Lantier L, Fentz J, Mounier R, et al. AMPK controls exercise endurance, mitochondrial oxidative capacity, and skeletal muscle integrity. *FASEB Journal*. 2014;28(7):3211-3224. doi:10.1096/fj.14-250449

96. Kulkarni SS, Karlsson HKR, Szekeres F, Chibalin A v., Krook A, Zierath JR. Suppression of 5'-Nucleotidase Enzymes Promotes AMP-activated Protein Kinase (AMPK) Phosphorylation and Metabolism in Human and Mouse Skeletal Muscle. *Journal of Biological Chemistry*. 2011;286(40):34567-34574. doi:10.1074/jbc.M111.268292

97. Plaideau C, Liu J, Hartleib-Geschwindner J, et al. Overexpression of AMP-metabolizing enzymes controls adenine nucleotide levels and AMPK activation in HEK293T cells. *The FASEB Journal*. 2012;26(6):2685-2694. doi:10.1096/fj.11-198168

98. Gruber HE, Hoffer ME, McAllister DR, et al. Increased adenosine concentration in blood from ischemic myocardium by AICA riboside. Effects on flow, granulocytes, and injury. *Circulation*. 1989;80(5):1400-1411. doi:10.1161/01.CIR.80.5.1400

99. Cokorinos EC, Delmore J, Reyes AR, et al. Activation of Skeletal Muscle AMPK Promotes Glucose Disposal and Glucose Lowering in Non-human Primates and Mice. *Cell Metab*. 2017;25(5):1147-1159.e10. doi:10.1016/j.cmet.2017.04.010

100. McCarthy JJ, Srikuea R, Kirby TJ, Peterson CA, Esser KA. Inducible Cre transgenic mouse strain for skeletal muscle-specific gene targeting. *Skelet Muscle*. 2012;2(1):1-7. doi:10.1186/2044-5040-2-8

101. Machery-Nagel. NucleoSpin® Tissue User Manual. Machery-Nagel. Published February 2022. Accessed August 17, 2022. https://www.mn-net.com/media/pdf/5b/d0/d9/Instruction-NucleoSpin-Tissue.pdf

102. Selvin D, Hesse E, Renaud JM. Properties of single FDB fibers following a collagenase digestion for studying contractility, fatigue, and pCa-sarcomere shortening relationship. *Am J Physiol Regul Integr Comp Physiol*. 2015;308(6):R467-R479. doi:10.1152/AJPREGU.00144.2014

103. Machery-Nagel. NucleoSpin® RNA User Manual. Machery-Nagel. Published January 2022. Accessed August 17, 2022. https://www.mn-net.com/media/pdf/b0/51/ee/Instruction-NucleoSpin-RNA.pdf

104. Dixon AK, Gubitz AK, Sirinathsinghji DJS, Richardson PJ, Freeman TC. Tissue distribution of adenosine receptor mRNAs in the rat. *Br J Pharmacol*. 1996;118(6):1461-1468. doi:10.1111/j.1476-5381.1996.tb15561.x

105. Scott K, Benkhalti M, Calvert ND, et al. KATP channel deficiency in mouse FDB causes an impairment of energy metabolism during fatigue. *Am J Physiol Cell Physiol*. 2016;311(4):C559-C571. doi:10.1152/ajpcell.00137.2015

106. Edwards JN, Macdonald WA, van der Poel C, Stephenson DG. O2.- production at 37°C plays a critical role in depressing tetanic force of isolated rat and mouse skeletal muscle. *Am J Physiol Cell Physiol*. 2007;293(2). doi:10.1152/AJPCELL.00037.2007/ASSET/IMAGES/LARGE/ZH00080753050007.JPEG

107. GBiosciences. CB-X™ Protein Assay. GBiosciences. Published March 31, 2014. Accessed August 18, 2022. https://cdn.gbiosciences.com/pdfs/protocol/786-12XT_protocol.pdf

108. Vector Laboratories. M.O.M.® (Mouse on Mouse) Immunodetection Kit User Guide. Vector Laboratories. Published 2019. Accessed August 17, 2022. https://vectorlabs.com/media/folio3/productattachments/protocol/FMK-2201.pdf

109. Steel RGD, Torrie JH. *Principles and Procedures of Statistics, a Biometrical Approach.* McGraw-Hill Kogakusha, Ltd.; 1980.

110. R Core Team. R: A Language and Environment for Statistical Computing. Published online 2022. https://www.R-project.org

111. de Mendiburu F. agricolae: Statistical Procedures for Agricultural Research. Published online 2020. https://CRAN.R-project.org/package=agricolae

112. Klotz KN, Hessling J, Hegler J, et al. Comparative pharmacology of human adenosine receptor subtypes - characterization of stably transfected receptors in CHO cells. *Naunyn Schmiedebergs Arch Pharmacol*. 1998;357(1):1-9. doi:10.1007/PL00005131

113. Franchetti P, Cappellacci L, Vita P, et al. N6-cycloalkyl- And n6-bicycloalkyl-c5'(c 2')-modified adenosine derivatives as high-affinity and selective agonists at the human A1 adenosine receptor with antinociceptive effects in mice. *J Med Chem*. 2009;52(8):2393-2406. doi:10.1021/JM801456G/SUPPL_FILE/JM801456G_SI_001.PDF

114. El-Tayeb A, Michael S, Abdelrahman A, et al. Development of Polar Adenosine A2A Receptor Agonists for Inflammatory Bowel Disease: Synergism with A2B Antagonists. *ACS Med Chem Lett*. 2011;2(12):890. doi:10.1021/ML200189U

115. Ferkany JW, Valentine HL, Stone GA, Williams M. Adenosine A1 receptors in mammalian brain: Species differences in their interactions with agonists and antagonists. *Drug Dev Res*. 1986;9(2):85-93. doi:10.1002/DDR.430090202

116. Kim YC, Karton Y, Ji XD, Melman N, Linden J, Jacobson KA. Acyl-Hydrazide Derivatives of a Xanthine Carboxylic Congener (XCC) as Selective Antagonists at Human A 2B Adenosine Receptors. *Drug Dev Res*. 1999;47:178-188. doi:10.1002/(SICI)1098-2299(199908)47:4

117. Klotz KN. Adenosine receptors and their ligands. *Naunyn Schmiedebergs Arch Pharmacol*. 2000;362(4-5):382-391. doi:10.1007/S002100000315

118. Mallo-Abreu A, Majellaro M, Jespers W, et al. Trifluorinated Pyrimidine-Based A2B Antagonists: Optimization and Evidence of Stereospecific Recognition. *J Med Chem*. 2019;62(20):9315-9330. doi:10.1021/ACS.JMEDCHEM.9B01340/SUPPL_FILE/JM9B01340_SI_002.PDF

119. Barrett-Jolley R, Davies NW. Kinetic Analysis of the Inhibitory Effect of Glibenclamide on KATP Channels of Mammalian Skeletal Muscle. *The Journal of Membrane Biology 1997 155 :3*. 1997;155(3):257-262. doi:10.1007/S002329900178

120. Boudreault L, Cifelli C, Bourassa F, Scott K, Renaud JM. Fatigue preconditioning increases fatigue resistance in mouse flexor digitorum brevis muscles with non-functioning KATP channels. *Journal of Physiology*. 2010;588(22):4549-4562. doi:10.1113/jphysiol.2010.191510

121. Venkatesh N, Lamp ST, Weiss JN. Sulfonylureas, ATP-sensitive K+ channels, and cellular K+ loss during hypoxia, ischemia, and metabolic inhibition in mammalian ventricle. *Circ Res*. 1991;69(3):623-637. doi:10.1161/01.RES.69.3.623

122. RIPOLL C, JON LEDERER W, NICHOLS CG. On the mechanism of inhibition of KATP channels by glibenclamide in rat ventricular myocytes. *J Cardiovasc Electrophysiol*. 1993;4(1):38-47. doi:10.1111/J.1540-8167.1993.TB01210.X

123. Schobesberger S, Wright P, Tokar S, et al. T-tubule remodelling disturbs localized β2-adrenergic signalling in rat ventricular myocytes during the progression of heart failure. *Cardiovasc Res*. 2017;113(7):770-782. doi:10.1093/CVR/CVX074

124. Matar W, Lunde JA, Jasmin BJ, Renaud JM. Denervation enhances the physiological effects of the K(ATP) channel during fatigue in EDL and soleus muscle. *Am J Physiol Regul Integr Comp Physiol*. 2001;281(1). doi:10.1152/AJPREGU.2001.281.1.R56

125. Nielsen JJ, Mohr M, Klarskov C, et al. Effects of high-intensity intermittent training on potassium kinetics and performance in human skeletal muscle. *J Physiol*. 2004;554(3):857-870. doi:10.1113/JPHYSIOL.2003.050658

126. Walter G, Vandenborne K, Elliott M, Leigh JS. In vivo ATP synthesis rates in single human muscles during high intensity exercise. *Journal of Physiology*. 1999;519(3):901-910. doi:10.1111/j.1469-7793.1999.0901n.x

127. Pang T, Rajapurohitam V, Cook MA, Karmazyn M. Differential AMPK phosphorylation sites associated with phenylephrine vs. antihypertrophic effects of adenosine agonists in neonatal rat ventricular myocytes. *Am J Physiol Heart Circ Physiol*. 2010;298(5):1382-1390. doi:10.1152/AJPHEART.00424.2009/ASSET/IMAGES/LARGE/ZH40051093220008.JPEG

128. Peleli M, Hezel M, Zollbrecht C, et al. In adenosine A2B knockouts acute treatment with inorganic nitrate improves glucose disposal, oxidative stress, and AMPK signaling in the liver. *Front Physiol*. 2015;6(Aug). doi:10.3389/FPHYS.2015.00222

129. Friedman B, Corciulo C, Castro CM, Cronstein BN. Adenosine A2A receptor signaling promotes FoxO associated autophagy in chondrocytes. *Sci Rep*. 2021;11(1). doi:10.1038/S41598-020-80244-X

130. Zhang J, Fan W, Neng L, et al. Adenosine improves LPS-induced ROS expression and increasing in monolayer permeability of endothelial cell via acting on A2AR. *Microvasc Res*. 2022;143. doi:10.1016/J.MVR.2022.104403

131. Hesse E. Effects of Carbohydrate Availability on Fatigue and Fatigue Pre-Conditioning in Mouse FDB Muscle. Published online August 19, 2019. doi:10.20381/RUOR-23771

132. Barclay CJ. Modelling diffusive O(2) supply to isolated preparations of mammalian skeletal and cardiac muscle. *J Muscle Res Cell Motil*. 2005;26(4-5):225-235. doi:10.1007/S10974-005-9013-X

133. Faulhaber-Walter R, Jou W, Mizel D, et al. Impaired glucose tolerance in the absence of adenosine A1 receptor signaling. *Diabetes*. 2011;60(10):2578-2587. doi:10.2337/DB11-0058

134. Gnad T, Navarro G, Lahesmaa M, et al. Adenosine/A2B Receptor Signaling Ameliorates the Effects of Aging and Counteracts Obesity. *Cell Metab*. 2020;32(1):56-70.e7. doi:10.1016/j.cmet.2020.06.006

135. Sacramento JF, Martins FO, Rodrigues T, et al. A 2 Adenosine Receptors Mediate Whole-Body Insulin Sensitivity in a Prediabetes Animal Model: Primary Effects on Skeletal Muscle. *Front Endocrinol (Lausanne)*. 2020;11. doi:10.3389/FENDO.2020.00262

136. Helander I, Westerblad H, Katz A. Effects of glucose on contractile function, [Ca2+]i, and glycogen in isolated mouse skeletal muscle. *Am J Physiol Cell Physiol*. 2002;282(6 51-6):1306-1312. doi:10.1152/AJPCELL.00490.2001/ASSET/IMAGES/LARGE/H00620976006.JPEG

APPENDIX 1

49 Spadina Ave. Suite 200
Toronto ON M5V 2J1 Canada
www.biorender.com

Confirmation of Publication and Licensing Rights

June 11th, 2023
Science Suite Inc.

Subscription:	*Student Plan*
Agreement number:	*EW25H72FEW*
Journal name:	*University of Ottawa*

To whom this may concern,

This document is to confirm that Callum Mcrae has been granted a license to use the BioRender content, including icons, templates and other original artwork, appearing in the attached completed graphic pursuant to BioRender's Academic License Terms. This license permits BioRender content to be sublicensed for use in journal publications.

All rights and ownership of BioRender content are reserved by BioRender. All completed graphics must be accompanied by the following citation: "Created with BioRender.com".

BioRender content included in the completed graphic is not licensed for any commercial uses beyond publication in a journal. For any commercial use of this figure, users may, if allowed, recreate it in BioRender under an Industry BioRender Plan.

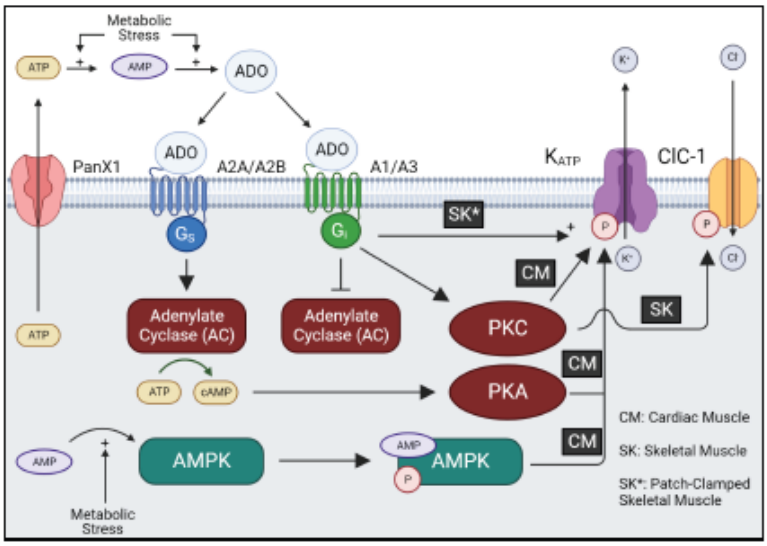

For any questions regarding this document, or other questions about publishing with BioRender refer to our BioRender Publication Guide, or contact BioRender Support at support@biorender.com.

Appendix 1: Biorender Publication License for Figure 1.1